Phenomenology of Dark Matter Annihilations in the Sun

Dissertation
zur
Erlangung des Doktorgrades (Dr. rer. nat.)
der
Mathematisch-Naturwissenschaftlichen Fakultät
der
Rheinischen Friedrich-Wilhelms-Universität Bonn

von
Raghuveer Garani Ramesh
aus
Bengaluru, India

Bonn, 14.08.2017

Dieser Forschungsbericht wurde als Dissertation von der Mathematisch-Naturwissenschaftlichen Fakultät der Universität Bonn angenommen und ist auf dem Hochschulschriftenserver der ULB Bonn http://hss.ulb.uni-bonn.de/diss_online elektronisch publiziert.

1. Gutachter:	Prof. Dr. Manuel Drees
2. Gutachter:	Prof. Dr. Sergio Palomares-Ruiz
Tag der Promotion:	06.10.2017
Erscheinungsjahr:	2018

Summary

The annihilation of dark matter (DM) particles accumulated in the Sun could produce a flux of neutrinos, which is potentially detectable with neutrino detectors/telescopes and the DM elastic scattering cross section can be constrained. Although the process of DM capture in astrophysical objects like the Sun is commonly assumed to be due to interactions only with nucleons, there are scenarios in which tree-level DM couplings to quarks are absent, and even if loop-induced interactions with nucleons are allowed, scatterings off electrons could be the dominant capture mechanism. We consider this possibility and study in detail all the ingredients necessary to compute the neutrino production rates from DM annihilations in the Sun (capture, annihilation and evaporation rates) for velocity-independent and isotropic, velocity-dependent and isotropic and momentum-dependent scattering cross sections for DM interactions with electrons and compare them with the results obtained for the case of interactions with nucleons. Moreover, we improve the usual calculations in a number of ways and provide analytical expressions. Interestingly, we find that the evaporation mass in the case of interactions with electrons could be below the GeV range, depending on the high-velocity tail of the DM distribution in the Sun, which would open a new mass window for searching for this type of scenarios.

Acknowledgments

I would like to express my deepest gratitude towards Manuel Drees for all the guidance, stimulation and support he has given me over the course of my time in Bonn. I would like to thank my collaborator and advisor Segio Palomares-Ruiz for exciting discussions and interesting projects. He has not only been a devoted and diligent supervisor, but he has been a mentor and an inspiring example. I would also like to express my great appreciation towards Nicolas who has shared with me his knowledge and experience. This thesis would not have been possible without everything that I have learned from Manuel, Sergio and Nicolas. Moreover, I am grateful to Masaki for a fruitful collaboration, and for reminding me that discipline is the key. Moreover, I thank Sudhir and Debtosh for all the encouragement and interesting collaborations. I also thank Prof. Klaus Desch and Prof. Bernd Diekkrüger for agreeing to be my third and fourth referees, respectively. I gratefully acknowledge financial support from the Bonn-Cologne Graduate School (BCGS).

For proof-reading parts of this thesis I thank Rahul and Nicolas, for their numerous suggestions. I would also like to thank many other past and present fellows in the BCTP for many memories we shared together. Thank you Toby, Stefano, Annika, Rahul, Jie, Vipin, Sadra, Swasti, Bardia and Zhongyi. Last but not the least, I thank the BCTP secretaries: Christa, Dagmar, Petra and Patricia for making bureaucracy smooth. I also thank Andreas for providing technical support, and for providing me extra disk space in the cluster.

I also thank the members of the now dissolved U. Bonn cricket team, Vishwas, Santosh, Ripunjay and Vikram; for joyful Saturdays during summer.

Finally, I'm grateful to my parents, amma, amama and my sister jinni, for the support and encouragement all through these years.

Contents

CHAPTER 1

Introduction

"It was the best of times, it was the worst of times, it was the age of wisdom, it was the age of foolishness, it was the epoch of belief, it was the epoch of incredulity, it was the season of Light, it was the season of Darkness, it was the spring of hope, it was the winter of despair, we had everything before us, we had nothing before us, we were all going direct to Heaven, we were all going direct the other way—in short, the period was so far like the present period, that some of its noisiest authorities insisted on its being received, for good or for evil, in the superlative degree of comparison only."

A Tale of Two Cities
Charles Dickens

The existence of non-luminous Dark Matter (DM) is by now well established, albeit only through gravitational interactions [1]. Nearly half a century after the acceptance of DM hypothesis, the hunt is still on to test the particle nature of DM, for a historical overview, see [2]. In some of the most plausible scenarios, the role of DM is played by a stable particle with weak scale interaction strength and mass (WIMP). The abundance of WIMPs from thermal production in the early universe naturally matches the DM abundance. While WIMP candidates are absent in the Standard Model (SM) of particle physics, they exist in some of its appealing extensions [3, 4].

Efforts to identify the particle nature of DM during the past decades have brought together the particle physics, cosmology, and astrophysics communities, and might enable us to constrain the nature of DM by combining the results of cosmological simulations, astrophysical observations, and particle DM searches. In order to detect and constrain the nature of DM, four complementary and competing strategies have been developed: Collider searches, Direct searches, Indirect searches and Astrophysical probes. Collider searches try to produce DM with energetic scattering of SM particles in the laboratory; direct and indirect searches, attempt to use the existing DM halo of the Milky-Way to either observe a rare scattering of DM off nuclei at Earth or to measure SM particles produced by annihilation or decays of DM. Obviously, direct and indirect methods depend crucially on the properties of the Milky Way DM halo. For example, direct detection experiments depend on the flux of halo DM particles streaming through the detector, which naturally depends on the local density of DM particles. Indirect detection experiments measure the flux of gamma-rays, or neutrinos, or anti-particles such as anti-protons, positrons, that are products of DM annihilation or decays in astrophysical objects. More specifically, flux of annihilation products at the detector is proportional to the product of total annihilation cross section, the branching ratio for the given process, and the energy spectra in that channel.

In this thesis, indirect detection of DM at neutrino telescopes is studied. Galactic WIMPs which stream through the galaxy can become gravitationally bound to a massive celestial object if after elastically scattering off the nuclei, they lose their kinetic energy such that their velocity becomes

smaller than the escape velocity from that body. Upon consecutive scatters, DM eventually sinks into the core of the celestial body and leads to the build up of DM over-density localized to a relatively small volume. In the core, the orbiting DM particles can annihilate to standard model particles. However, not all annihilation products can emerge from the core of the body. For example: charged particles are stopped inside the plasma of the Sun and only neutrinos can emerge practically unscathed. Detection of these neutrinos would arguably constitute one of the best signatures of DM annihilation, as there are no known astrophysical processes able to replicate it. The advantage of probing this neutrino channel is that stronger bounds on DM-proton couplings can be obtained than those inferred from direct detection methods. While the idea is rather old, there is a renewed interest in the subject since neutrino telescopes have become more sensitive and are now capable of probing interesting regions of the relevant parameter space.

Contrary to previous attempts at DM detection through neutrinos from the Sun which consider DM scattering on nucleons, we explore the possibility of DM scattering on electrons in the Sun. We consistently evaluate the capture, evaporation and annihilation rate of DM in the Sun. Since the mass of the electron ($m_e = 511\,keV$) is relatively close to the temperature in the core ($\sim 1\,keV$), electrons have larger velocity dispersion i.e. the targets are not at rest, whereas nucleons can be considered to be effectively at rest. This thermal motion of the target has several implications for the capture and evaporation rates. For example: the evaporation rate is computed assuming that the captured DM obeys a truncated Maxwell-Boltzmann velocity distribution; cut-off at the escape velocity at a given radius. However, simulations indicate that the cut-off is indeed smaller than the escape velocity. We find that the evaporation rate is very sensitive to the cut-off velocity, lowering the cut-off by only 10% can severely suppress the evaporation rate, thereby reducing the evaporation mass to around 500 MeV, which is about six times smaller than the standard case. We also improve the standard analysis by deriving capture and evaporation rates for velocity and momentum dependent scattering cross sections, including finite temperature effects. Using the above results we systematically compare the nucleon case and the electron case for various operators. We also construct simplified models for leptonically interacting DM and tabulate their resulting cross sections for DM-electron and DM-nucleon elastic scattering. The rates and cross sections could then be used to study the phenomenology of DM-electron scattering in these models.

This thesis is organized as follows: A brief overview of WIMP DM and the current status of various DM searches are presented in chapter 2. In chapter 3 we review solar models which serve as inputs for calculations that follow in the later chapters. In chapter 4, the concept of indirect DM detection where we focus on the possible neutrino signals from WIMP annihilation in the Sun is introduced along with the theoretical formalism that is required to describe thermal effects in capture and evaporation rates. Using the formalism, in chapter 5 all the relevant rates and neutrino flux at production are calculated for electrons, spin-dependent and spin-independent nucleons in the Sun. The electron and nucleon case are comprehensively compared to each other and possibly interesting regions of cross section and DM mass is identified. In chapter 6, we survey simplified models where DM or mediator field couples to leptons only at tree level. The relevant loop-level interactions with nucleons is computed and tabulated. Final remarks and conclusion is presented in chapter 7.

Parts of this thesis have been published in the following articles:

[5] Dark matter in the Sun: scattering off electrons vs nucleons
Raghuveer Garani, Sergio Palomares-Ruiz
Published in JCAP 1705 (2017) no.05, 007
ARXIV:1702.02768

[6] Dark matter in the Sun: the Leptophilic Case
Raghuveer Garani, Sergio Palomares-Ruiz
in preparation

CHAPTER 2

The Search for Dark Matter: Status

Given the success of particle physics in describing the early Universe, it is well motivated to assume that DM is a particle. Astrophysical and cosmological observations then provide a number of constraints that any reasonable DM candidate must satisfy. The well known conditions are that DM must be non-baryonic [7–9], have no electric charge [10], and be stable on cosmological time scales, i.e. it must have a lifetime large compared to the age of the Universe.

A non trivial fact is that DM is required to be non-relativistic at matter-radiation equality [11]. Relativistic DM particles wash out density perturbations at scales (small) below the free-streaming length $0.1\ \mathrm{Mpc}\,(1keV/m_\chi)$, resulting in suppression of small-scale structures, thus constrained from observations of structures today. These considerations generally rule out DM particles with $m_\chi \sim 1\ keV$ [12, 13]. Thus Standard Model (SM) neutrinos cannot be the dominant component of DM. Consequently, the SM of particle physics does not contain a viable DM candidate. Therefore, the evidence for DM strongly hints at evidence for Beyond the Standard Model (BSM) physics.

Having mentioned the known properties of DM, we turn to the description of one of the natural generation mechanism of DM in the early Universe. In Sec. 2.1, the Weakly Interacting Massive Particle (WIMP) paradigm is reviewed. Finally, in Sec. 2.2 WIMP DM detection methods are briefly discussed and their current status is reviewed.

2.1 Thermal Genesis

By observing the the Cosmic Microwave Background (CMB) and fitting it to the parameters of the concordance cosmological model ΛCDM, the DM abundance is obtained to be [11]

$$\Omega_{DM}\mathrm{h}^2 = 0.1186 \pm 0.0020. \tag{2.1}$$

Thus, any viable DM candidate should also satisfy the above condition. In this section, the standard approach to the calculation of DM relic density from thermal freeze-out is reviewed, closely following Kolb and Turner [14].
In the early Universe, WIMPs are in equilibrium with the thermal plasma. As the universe expands and the temperature drops below the WIMP's production rate, the number density of these particles are exponentially suppressed. Eventually, WIMPs "freeze out" and remains a thermal relic of the early Universe until today. Assuming WIMPs are stable particles and are already non-relativistic, their relic abundance at decoupling can be calculated by solving the Boltzmann equation (2.2) for the number density n_χ of WIMPs,

$$\frac{\mathrm{d}n_\chi}{\mathrm{d}T} + 3\mathrm{H}n_\chi = -\langle\sigma v\rangle\left(n_\chi^2 - n_{\chi,eq}^2\right), \tag{2.2}$$

where,

$$n_{\chi,\mathrm{eq}} = g_\chi \left(\frac{m_\chi T}{2\pi}\right)^{\frac{3}{2}} \cdot e^{-\frac{m_\chi}{T}}, \tag{2.3}$$

is the equilibrium number density of a WIMP dictated by Maxwell distribution, H is the Hubble constant, g_χ is the degrees of freedom of DM particle χ and T is the temperature. In the above equation, the term $3\mathrm{H}n_\chi$ stems from the fact that the universe is expanding, $-\langle\sigma v\rangle n_\chi^2$ is the annihilation term and $+\langle\sigma v\rangle n_{\chi,eq}^2$ is the term for DM production.

The entropy density is given by,

$$s(T) = g_{\mathrm{eff}}(T)\,\frac{2\pi^2}{45}T^3, \tag{2.4}$$

where g_{eff} is the effective number of relativistic degrees of freedom, which is function that depends slowly on the temperature T [15]. The assumption that entropy is conserved in a co-moving volume makes it easier to work with scaled density $Y = n_\chi/s$ rather than the number density, n_χ. The scaled density today, Y_0 can be defined as

$$Y_0 = \frac{n_{\chi,0}}{s_0}, \tag{2.5}$$

where, $s_0 = s(T_0)$ defines today's entropy to be evaluated at $T_0 = 2.726$ K, the temperature of the microwave background. Also, DM relic density today in units of the critical density is,

$$\Omega_{\chi,0} = \frac{m_\chi n_\chi}{\rho_{\mathrm{crit}}} = \frac{m_\chi s_0 Y_0}{\rho_{\mathrm{crit}}}, \tag{2.6}$$

where $H = 100h\ \mathrm{km} s^{-1} Mpc^{-1}$ is the Hubble parameter and G is the Newton's constant. Finally, using Y, Boltzmann equation (2.2) can be recast in the form

$$\frac{\mathrm{dY}}{\mathrm{dT}} = \sqrt{\frac{\pi g_*(T)}{45G}}\,\langle\sigma v\rangle\,(\mathrm{Y}^2 - \mathrm{Y}_{\mathrm{eq}}^2), \tag{2.7}$$

$g_*(T)$ is the effective number of relativistic degrees of freedom parameter derived from the thermodynamics describing the state of the Universe [15–17] and $Y_{eq} = Y_{eq}(T)$ represents the thermal equilibrium abundance.

$$Y_{eq}(T) = \frac{45}{4\pi^4 g_{\mathrm{eff}}(T)} \sum_i g_i \frac{m_i^2}{T^2} K_2\left[\frac{m_i}{T}\right], \tag{2.8}$$

where, the sum runs over all particles i with mass m_i and g_i are the degrees of freedom in the thermal plasma. K_n is the modified Bessel function of the second kind of order n. Note that Y_{eq} falls rapidly as the temperature decreases and universe expands. $\langle\sigma v\rangle$ is the total thermally averaged annihilation cross-section for the process $\chi\chi \to SM + SM$,

$$\langle\sigma v\rangle = \frac{\sum_{i,j} g_i g_j \int_{(m_i+m_j)^2} \mathrm{ds}\,\sqrt{s} K_1(\sqrt{s}/T) p_{ij}^2 \sigma_{ij}(s)}{2T[\sum_i g_i m_i^2 K_2(m_i/T)]^2}, \tag{2.9}$$

where σ_{ij} is the total cross section for annihilation of a pair of DM particles into Standard Model particles ij, and p_{ij} is the momentum of the incoming particles in their center-of-mass frame.

$$p_{ij} = \frac{1}{2}\left[\frac{(s-(m_i+m_j)^2)(s-(m_i-m_j)^2)}{s}\right]^{\frac{1}{2}}. \tag{2.10}$$

Here, $s = (p_i + p_j)^2$ is the Mandelstam variable. It should be noted that only the final form of the results are presented here, for a detailed derivation see [14]. The most complete calculation for relic abundance of WIMP were presented in [18, 19] and has the following form,

$$\Omega_\chi h^2 = 2.755 \times 10^8 \frac{m_\chi}{\text{GeV}} Y_0. \tag{2.11}$$

Thus, the problem of finding the relic abundance is reduced to evaluating $Y_0 = Y(T = T_0)$. Integrating equation (2.7) from very high energies $T \to \infty$ to $T = T_0$ yields Y_0.
In order for this process to yield a the correct relic abundance, the annihilation cross section is required to be $\sigma \approx 0.9\,\text{pb}$ or equivalently $3 \times 10^{-26}\ \text{cm}^3/\text{s}$. Astonishingly, this is quite similar to the value obtained for a generic electroweak mass particle annihilating through the exchange of the electroweak gauge bosons, with $\langle\sigma v\rangle \sim \alpha^2/m_\chi^2$. Here, α is equal to $g_w^2/4\pi$ with g_w being the weak interaction gauge coupling. In particular one might notice that this leads us to a WIMP mass of the order of 100 GeV. This is called the "WIMP miracle" and independently provides a strong motivation for the existence of new particles at the weak scale.

Thus, the WIMP miracle leads to testable prediction that dark matter has weak-scale interactions with SM particles. To this end, the past few decades has seen major undertaking in constructing experiments that search for these non-gravitational interactions of dark matter. The idea behind these approaches as well as the current experimental status is discussed briefly in the next section.

2.2 Detecting WIMP DM

Assuming DM is comprised of WIMPs, a diverse set of experiments is required to probe all possible types of masses and couplings. DM may have interactions with one or more of four categories of particles: nuclear matter, leptons, photons and other bosons, and other dark particles. These interactions may then be probed by four complementary approaches: direct detection, indirect detection, particle colliders, and astrophysical probes as shown in Fig. 2.1.

2.2.1 Astrophysical Probes

Interactions of DM can affect a variety of astrophysical observables such as the number density and internal structure of galaxies. The most important effect is that of CMB spectral distortions due to DM annihilation or decay during the early stages of matter domination [20, 21]. We do not discuss this probe any further.

2.2.2 Collider search

DM can be produced in high-energy particle collisions. If dark matter has substantial couplings to quarks and gluons, it can be created in proton-proton collisions at the Large Hadron Collider (LHC). If DM particles are produced, they are likely to pass through the constituent detectors without a trace, but their existence may be deduced by calculating the missing momentum, similar to the case of neutrinos. Searches for DM at the LHC are therefore classified by missing momentum, and by the nature of the visible particles that accompany the DM production. Collider searches for DM are highly complementary to direct and indirect DM detection methods. The main advantage of collider searches is that they do not suffer from astrophysical uncertainties.

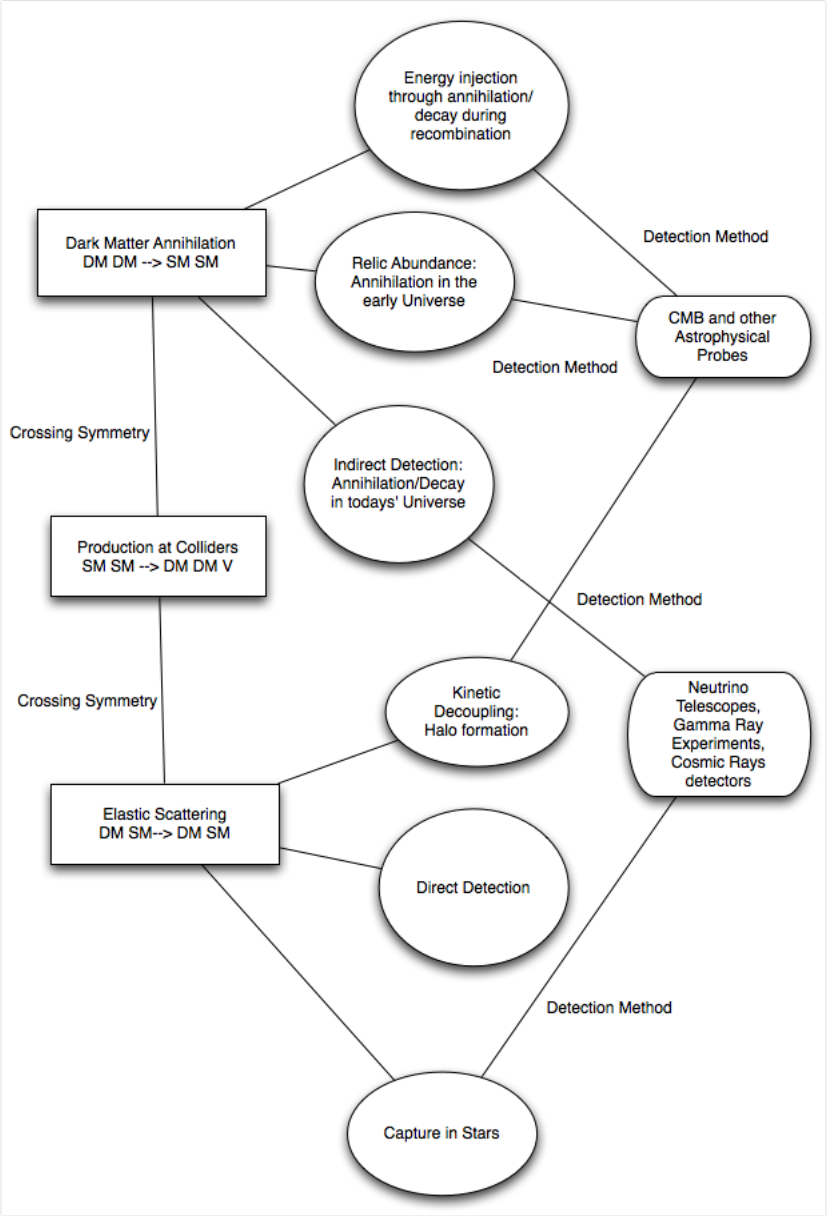

Figure 2.1: At present, DM detection experiments may be grouped into four categories: direct detection, indirect detection, particle colliders and astrophysical probes. The lines connect the experimental approaches and the characteristic cross section which they probe.

Moreover, they provide the playground to study DM in a controlled laboratory environment. This may be used to precisely constrain many DM particle properties.

Current Status:

DM has to interact sufficiently strongly with the SM particles to yield observable signatures at colliders. The efforts to search for DM in collider experiments are mainly focused on traditional WIMPs, such as the neutralino. These are searched for, in model-dependent scenarios that constrain the parameter space of UV-complete models, effective field theories and simplified models [22–27], as well as in more model-independent searches for missing energy accompanied by a monophoton [28], a mono-Z [29, 30], a monojet [31, 32] or a mono-Higgs [33, 34]. Recently, the use of simplified models, that typically contain a mediator particle connecting

the DM sector to the SM, has been under intense study in DM collider searches, as opposed to the use of effective field theories, containing non-renormalizable effective operators that are obtained in the limit of integrating out the heavy mediator particle. The contact interaction limit of effective non-renormalizable operators is only valid when the mediator mass is safely above the center of mass energy of the hard scattering event, and this assumption does not generally hold in the 13 TeV LHC. This observation has three consequences: First, the presence of the mediator propagator has to be taken into account in predictions for the DM production signal, as it can affect the kinematic characteristics of the events compared to the contact interaction limit. Second, the production of the mediator particle may also result in final states other than a DM particle pair, and these visible decay modes can be used to constrain such models. Finally, they can alter the interplay between cosmological and collider constraints.

2.2.3 Direct Detection

If the Milky Way halo is made of WIMPs, one would expect thousands of WIMPs to stream through the surface of Earth every second. In view of this, experiments are designed to detect DM particles through their scattering with nuclei. This class of techniques is collectively known as direct detection. Direct detection experiments measure the number of DM nucleus scattering events per day per kilogram of detection material, the event rate R. The number of scattering events is extracted by measuring the recoil energy deposited by rare WIMP-nuclei scattering event and distinguishing them from the background interactions. This approach requires control of low-energy backgrounds. Generally, R depends on the local density $\rho_\odot$ of DM in the solar neighborhood, the velocity distribution of DM in the galactic halo near Earth and the mass of DM m_χ. Qualitatively, the event rate R, is given as follows [35],

$$R \approx \frac{n_\chi \sigma \langle v \rangle}{m_N}, \tag{2.12}$$

where, DM number density is $n_\chi = \rho_\odot / m_\chi$, σ is the elastic cross section, $\langle v \rangle$ is the average relative speed of DM with respect to the target and m_N is the mass of the target nuclei. One should notice that the event rate is directly proportional to the local DM density $\rho_\odot$. Given a particle physics model, the cross section can be evaluated. However, variables such as $\rho_\odot$ and $\langle v \rangle$ are estimated using dynamical observations such as rotational curve of the Milky-Way. These quantities depend on the DM distribution in the halo. This distribution is often quantified by some analytical function $\rho(r)$, which depends on the distance from the galactic center and it is commonly known as the DM halo density profile. The density of DM in the local solar neighborhood is inferred by fitting observations to models of the galactic halo. These observations include the rotational speed of stars at the solar distance and other locations, the total projected surface density, estimated by considering the motion of stars perpendicular to the galactic disk and microlensing. The uncertainties involved in direct detection are likely to be significantly smaller than in most indirect detection channels, the main contributions to systematic uncertainties come from local DM density and velocity distribution of DM in the halo. The main disadvantage of this technique is that the low cross section of WIMP-SM particle scattering makes the interactions quite rare, resulting in low event rates. Despite the disadvantage, direct detection is by far the most straightforward method of detection and discovering WIMPs.

Current Status:

The current status of direct detection searches is ambiguous with a few experiments reporting hints for a DM signal like DAMA/LIBRA [36, 37], CoGent [38–42] and CDMS-II [43]. However, such observations seem inconsistent among each other and are typically in conflict with the null results of many other experiments [44–50]. Currently the XENON1T experiment [50] places

the strongest exclusion limit in the plane of spin-independent DM-nucleon cross section and WIMP mass for large DM masses, while LUX [48] and PandaX-II [47] have recently reported competitive null results. The most stringent direct detection constraint to date on the WIMP-proton spin-dependent cross section comes from the PICO-60 [51] and the LUX [52] experiments (and below ~ 4 GeV from the PICASSO experiment [53]). A new generation of direct detection DM experiments includes LZ [54, 55], DARWIN [56], DarkSide-20k [57, 58], PICO-250 [59] and SuperCDMS [60].
In light of null results from WIMP direct detection experiments, there is considerable interest in exploring new regions of DM parameter space with a variety of different techniques [61]. Multiple directions have recently been suggested for the detection of elastic and inelastic scatterings of DM in the mass range from keV to MeV: recently proposed experiments with sensitivity to DM-electron scattering include Refs. [5, 62–66]. Additional possible methods for detecting sub-GeV DM include semiconductors [67, 68], superconductors [69–71], scintillating targets [72], superfluid helium [73, 74], chemical-bond breaking [75], two-dimensional targets [76–78], color center production in crystals [79], as well as search for bremsstrahlung radiation from a recoiling nucleus [80, 81].

2.2.4 Indirect Detection

Among the techniques available, indirect detection is an attractive prospect to learn about the properties of yet undiscovered WIMP DM. The strategy here is to detect signatures of annihilation/decay of DM particles in cosmic rays. If DM is made out of WIMPs, their self-annihilation in the early Universe would explain the observed DM abundance. Today, the same annihilation process could contribute to the measured cosmic-ray fluxes; a clear detection of the annihilation products would reveal information about the DM particle's mass and interactions. Similar signatures could be produced if dark matter is unstable and decays, providing us with information on the lifetime of the DM particle. Indirect searches for DM aim at seeing such annihilation or decay signals above the astrophysical backgrounds. The advantage of this method is that while DM might be difficult to detect directly, the annihilation products of DM particles can be easily detected. Indirect detection is sensitive to DM interactions with all standard model particles and directly probes the annihilation process suggested by the WIMP miracle. As an addendum, indirect searches have the potential to shed light on DM distribution beyond our local neighbourhood. For example, the flux of gamma-rays or neutrinos from DM annihilations in the Milky Way DM halo coming from a given direction subtending a solid angle $\Delta\Omega$ is written as,

$$\frac{\mathrm{d}\Phi_\gamma}{\mathrm{d}E_\gamma}(E_\gamma, \Delta\Omega) = \frac{\langle\sigma v\rangle}{2\, m_\chi^2} \sum_i \mathrm{BR}_i \frac{\mathrm{d}N_\gamma^i}{\mathrm{d}E_\gamma} J(\Omega) \frac{\Delta\Omega}{4\pi}\,, \tag{2.13}$$

where, $\langle\sigma v\rangle$ is the thermal average of the total annihilation cross section times the relative velocity, m_χ is the DM mass, the discrete sum is over all DM annihilation channels, BR_i is the branching ratio of DM annihilation into the i-th final state and $\mathrm{d}N_\gamma^i/\mathrm{d}E_\gamma$ is the differential gamma–ray yield of SM particles into photons for the i^{th} channel. The quantity $J(\Omega)$, also called the J-factor, depends crucially on the DM distribution in the halo, is as follows,

$$J(\Omega)\Delta\Omega = \int_{\Delta\Omega} \mathrm{d}\Omega \int_{\mathrm{los}} \mathrm{d}s\, \rho(r(s,\Omega))^2\,, \tag{2.14}$$

where the spatial integration of the square of the DM density profile $\rho(r)$ is performed along the line of sight s, for the region of observation which subtends a solid angle of $\Delta\Omega$ in the sky. Discovery through indirect detection requires understanding of astrophysical backgrounds if it involves the study of charged particles from annihilation/decay, and the signal strength is typically subject to uncertainties in halo profiles.

Similar to annihilations in the galactic center, DM captured in the Sun can also lead to observable neutrino spectrum at neutrino detectors [82–88]. The fluxes of electron neutrinos and antineutrinos at the detector are given by

$$\begin{aligned}
\frac{d\Phi^{\nu_e}}{dE_{\nu_e}}(E_{\nu_e}) &= \frac{1}{4\pi d_\odot^2}\,\Gamma(m_\chi,\sigma_\chi)\left(P(\nu_e\to\nu_e)\,\frac{dF}{dE_{\nu_e}}(E_{\nu_e}) + P(\nu_\mu\to\nu_e)\,\frac{dF}{dE_{\nu_\mu}}(E_{\nu_\mu})\right)\\
\frac{d\Phi^{\bar\nu_e}}{dE_{\bar\nu_e}}(E_{\bar\nu_e}) &= \frac{1}{4\pi d_\odot^2}\,\Gamma(m_\chi,\sigma_\chi)\left(P(\bar\nu_e\to\bar\nu_e)\,\frac{dF}{dE_{\bar\nu_e}}(E_{\bar\nu_e}) + P(\bar\nu_\mu\to\bar\nu_e)\,\frac{dF}{dE_{\bar\nu_\mu}}(E_{\bar\nu_\mu})\right), \qquad (2.15)
\end{aligned}$$

where, Γ is the total annihilation rate, $d_\odot$ is the average distance Sun-Earth and dF/dE_{ν_e} and $dF/dE_{\bar\nu_e}$ (dF/dE_{ν_μ} and $dF/dE_{\bar\nu_\mu}$) are the electron (muon) neutrino and antineutrino spectra per WIMP annihilation in the Sun. The computation of Γ is the main subject of the thesis, details are described in chapters 4 and 5.

Current Status:

Several potential signals have appeared in indirect DM searches over the past few years. Most notably, in the case of the Galactic center gamma ray excess in the GeV energy range [89, 90], an anomalous emission of gamma rays coming from the inner region of the Galaxy has been reported. Various interpretations of this excess have been put forward, from astrophysical processes (e.g. Refs. [91–95]) to DM annihilation (e.g. Refs. [96, 97]). Although there is strong support for the GeV excess to arise from a population of faint, unresolved point sources, DM interpretation has not been yet robustly excluded. However, this interpretation is challenged by the latest constraints from dwarf spheroidal galaxies [98].

An anomalous emission line at the 3.55 keV energy from X-ray images taken by the telescope XMM-Newton [99, 100] has been found in a stacked analysis of the Perseus cluster, Coma-Centaurus-Ophiuchus clusters and 69 other clusters [101]. Further evidence has been gathered also from other galaxy clusters [102, 103]. However, the status of this line is controversial. In fact, these results are in tension with the Suzaku data [104], which show no indication of a 3.55 keV line in the Coma, Virgo and Ophiuchus clusters. On top of that, these findings are in tension with the Hitomi observations of the Perseus cluster, which do not support an excess in this cluster [105]. Nevertheless, the line has been recently confirmed in the summed data from deep Chandra blank fields, the Chandra Deep Field South and COSMOS [106]. This spectral feature can have a DM related origin, but it also may have no connection with the DM sector and come from some atomic transition (of a potassium origin [107]) or from some systematic errors. However, while the DM interpretation has been challenged by many independent studies it is not in contradiction with observations of dwarf galaxies or the galactic center.
The AMS-02 experiment on board the international space station has measured the fluxes of various charged particles in cosmic rays. The ratio of antiproton and proton fluxes exhibits an excess over the estimated background, that has been interpreted as a signal of DM annihilations. Intriguingly, some of the above references report good agreement with DM annihilations as an explanation for both the AMS antiproton data and the galactic center gamma ray excess discussed above. However, within systematic errors, secondary astrophysical production alone can account for the data. Furthermore, a high-energy cosmic positron excess has been discovered by PAMELA [108] and confirmed by AMS-02 [109]. While it can be produced by astrophysical objects like pulsars or supernova remnants (see e.g. Refs. [110]).

CHAPTER 3

Solar Models

The Sun is a natural astronomical laboratory. We are able to obtain information about the Sun that is not accessible for other stars, due to its proximity to Earth. Precise determination of values for mass, radius, geometric shape, luminosity , chemical composition and photon/neutrino spectrum is shown to be possible [111]. Furthermore, measurement of acoustic oscillation modes observed at the solar surface contain information about the solar interior, at least up to the convective zone. Geological records, comets and meteorites provide information about the solar history as well. Combining all the observations provides possibilities to test not only theories of stellar evolution but also new physics, in the sense of beyond the SM.

The Sun is in quasi-static main sequence phase of stellar evolution. Much of what we know about our Sun comes from spectroscopic methods and helioseismology, for the latest review see Ref. [112], and a compendium of results related to solar physics in Ref. [113]. This chapter describes how a Standard Solar Model (SSM) is derived. Important inputs include chemical abundances, opacities, equation of state and nuclear reaction rates. Much of the methodology is not truly relevant for the calculations that follow. Hence technical details are not discussed in detail. However, it is presented here for the completeness of the narrative. We begin with the global description of the Sun in Sec. 3.1. We then move on to the question "how much do we know about the solar interior ?" and the relevant physics/astrophysics behind it in Sec. 3.2; followed by a brief description of the SSM used in the calculations that are relevant to the theme of this thesis in Sec. 3.3.

3.1 The Sun and its Chemical Composition

The solar structure and operational definitions are briefly introduced in the section, starting from the outside and going inwards. First, the solar wind, then the corona, followed by chromosphere, photosphere, interior and the deep interior where nuclear reactions takes place. Distinction between some of these layers are sometimes artificial, we do not discuss them here. The interior of the Sun is theorized to be radiative and the intermediate regions are observed to be convective [113].

The determination of the abundance of chemical elements in the Sun is performed primarily through spectroscopy of the photosphere. Such analysis often involve modeling of the solar atmosphere to determine its temperature and density profile, and detailed radiation transfer calculations that connect elemental abundances with spectral line intensities and features [112]. With the introduction of full three-dimensional radiation hydrodynamic modeling of the solar atmosphere reasonable agreement exists among various studies [114, 115].

In Tab. 3.1 we show the relative isotope abundances used in this work, obtained from the

solar model AGSS09 [114]. The first column is the chemical name of the element, the second and third columns show the atomic number and atomic mass. The fourth column shows the relative isotope abundance and column 5 is the atomic mass in units of *amu*. Column six and seven show the average spin expectation value of protons, neutrons in the nuclei and the total angular momentum of the atomic nucleus in column 6. The spin expectation values is calculated using expressions provided in Ref. [116]. Refractory elements such as Si, Fe play an important role in contributing to the radiative opacity in the solar interior. The mass fraction of such metals amount to about 20% of the total metal mass fraction. Interestingly, abundances for refractories can be determined very precisely from chondritic meteorites [117]. As it turns out the spectroscopic abundances evolve towards meteoritic ones [114].

Name	Z	A	Isotope abundance	Mass (amu)	$\langle S_p \rangle$	$\langle S_n \rangle$	J
H	1	1	1.0	1.00782503223	0.5	0.0	0.5
^{4}He	2	4	1.0	4.00260325413	0.0	0.0	0.0
^{3}He	2	3	1.0	3.0160293201	-0.081	0.552	0.5
^{12}C	6	12	0.92	12.000000000	0.0	0.0	0.0
^{13}C	6	13	0.08	13.00335483507	-0.009	-0.172	0.5
^{14}N	7	14	0.99636	14.00307400443	-0.130	-0.106	1.0
^{15}N	7	15	0.00364	15.0001088989	-0.145	0.037	0.5
^{16}O	8	16	0.9976	15.99491461957	0.0	0.0	0.0
^{17}O	8	17	0.0004	16.9991317565	-0.036	0.508	2.5
^{18}O	8	18	0.0020	17.9991596129	0.0	0.0	0.0
^{20}Ne	10	20	0.9048	19.9924401762	0.0	0.0	0.0
^{21}Ne	10	21	0.0027	20.99384669	0.020	0.294	1.5
^{22}Ne	10	22	0.0925	21.991385115	0.0	0.0	0.0
^{23}Na	11	23	1.0	22.9897692820	0.2477	0.0199	1.5
^{24}Mg	12	24	0.7899	23.985041698	0.0	0.0	0.0
^{25}Mg	12	25	0.10	24.98583698	0.040	0.376	2.5
^{26}Mg	12	26	0.1101	25.98259297	0.0	0.0	0.0
^{27}Al	13	27	1.0	26.98153853	0.333	0.043	2.5
^{28}Si	14	28	0.9223	27.9769265346	0.0	0.0	0.0
^{29}Si	14	29	0.04685	28.9764946649	0.054	0.204	0.5
^{30}Ne	14	30	0.03092	29.973770136	0.0	0.0	0.0
^{31}P	15	31	1.0	30.9737619984	0.181	0.032	0.5
^{32}S	16	32	0.9499	31.9720711744	0.0	0.0	0.0
^{33}S	16	33	0.0075	32.9714589098	0.0	-0.3	1.5
^{34}S	16	34	0.0425	33.96786700	0.0	0.0	0.0
^{36}S	16	36	0.0001	35.96708071	0.0	0.0	0.0
^{35}Cl	17	35	0.7576	34.96885268	-0.094	0.014	1.5
^{37}Cl	17	37	0.2424	36.96590260	-0.178	0.0	1.5
^{36}Ar	18	36	0.003365	35.967545105	0.0	0.0	0.0
^{38}Ar	18	38	0.000632	37.96273211	0.0	0.0	0.0
^{40}Ar	18	40	0.996003	39.9623831237	0.0	0.0	0.0
^{39}K	19	39	0.932581	38.963706486	-0.196	0.055	1.5
^{40}K	19	40	0.000117	39.96399817	-0.3	-0.3	4.0
^{41}K	19	41	0.067302	40.961825258	-0.3	0.0	1.5
^{40}Ca	20	40	0.96941	39.962590864	0.0	0.0	0.0
^{42}Ca	20	42	0.00647	41.95861783	0.0	0.0	0.0
^{43}Ca	20	43	0.00135	42.95876644	0.0	0.5	3.5

^{44}Ca	20	44	0.02086	43.9554816	0.0	0.0	0.0
^{46}Ca	20	46	0.00004	45.9536890	0.0	0.0	0.0
^{48}Ca	20	48	0.00187	47.95252277	0.0	0.0	0.0
^{45}Sc	21	45	1.0	44.9559083	0.5	0.0	1.5
^{46}Ti	22	46	0.0825	45.9526277	0.0	0.0	0.0
^{47}Ti	22	47	0.0744	46.9517588	0.0	0.21	2.5
^{48}Ti	22	48	0.7372	47.9479420	0.0	0.0	0.0
^{49}Ti	22	49	0.0541	48.9478657	0.0	0.29	3.5
^{50}Ti	22	50	0.0518	49.9447869	0.0	0.0	0.0
^{50}V	23	50	0.0025	49.947156	0.36	0.36	6.0
^{51}V	23	51	0.9975	50.9439570	0.36	0.0	3.5
^{50}Cr	24	50	0.04345	49.9460418	0.0	0.0	0.0
^{52}Cr	24	52	0.83789	51.9405062	0.0	0.0	0.0
^{53}Cr	24	53	0.09501	52.9406481	0.0	0.5	1.5
^{54}Cr	24	54	0.02365	53.9388792	0.0	0.0	0.0
^{55}Mn	25	55	1.0	54.9380439	0.264	0.0	2.5
^{54}Fe	26	54	0.05845	53.9396090	0.0	0.0	0.0
^{56}Fe	26	56	0.91754	55.9349363	0.0	0.0	0.0
^{57}Fe	26	57	0.02119	56.9353928	0.0	-0.167	0.5
^{58}Fe	26	58	0.00282	57.9332744	0.0	0.0	0.0
^{59}Co	27	59	1.0	58.9331943	0.25	0.0	3.5
^{58}Ni	28	58	0.680769	57.9353424	0.0	0.0	0.0
^{60}Ni	28	60	0.262231	59.9307859	0.0	0.0	0.0
^{61}Ni	28	61	0.011399	60.9310556	0.0	0.5	1.5
^{62}Ni	28	62	0.036345	61.9283454	0.0	0.0	0.0
^{64}Ni	28	64	0.009256	63.9279668	0.0	0.0	0.0

Table 3.1: ***Relative isotope abundances***: The first column is the chemical name of the element, the second and third columns show the atomic number and atomic mass. The fourth column shows the relative isotope abundance and column 5 is the atomic mass in units of *amu*. Column six and seven show the average spin expectation value of protons, neutrons in the nuclei and the total angular momentum of the atomic nucleus in column 6.

3.2 Probing the inner Sun

Analogous to terrestrial seismology, helioseismology provides information about the interior of Sun by observing perturbations on the surface. Solar oscillations were first discovered while studying velocity shifts in absorption lines on the surface by Leighton et.al. [118] in 1962. It was found that the surface was filled with oscillatory patches of spatial coherence of a few percent of the solar diameter. A theoretical understanding of oscillations was finally formulated a decade later by Stein and Leibacher [119], and Ulrich [120], by modeling the Sun as a gigantic resonant cavity, where sound waves known as pressure modes (p-modes) that are trapped between the surface and the core oscillate.

The measurement of frequencies of thousands of global acoustic eigenmodes (or p-modes), with angular degrees from $l = 0$ up to several hundred and with precisions of the order of 1 part in 10^5 , has allowed us to reconstruct the interior structure of the Sun very precisely. This is possible because modes with different angular degree and frequencies have different turn over

points and therefore probe different regions of the Sun. Moreover, low degree modes, those with $l = 0, 1, 2$ play an important role as they reach the innermost solar regions and help probe the solar core, where solar neutrinos are produced. For two decades now, helioseismology has provided a wealth of information on the interior structure of the Sun [111].

3.3 Standard Solar Models

A Standard Solar Model (SSM) is the final product of a sequence of other models. Primary inputs to the solar models include chemical abundances of elements, radiative opacities and the equation of state. Since solar models are computed with the state of the art physics of the time and input parameters, the results of the computation vary with time, getting closer to the actual or true solar model [121, 122]. The original motivation for computing more precise SSMs was the solar neutrino problem. For an account of the historic overview of the development of solar neutrino experiments and the solar abundance problem see [123] and references therein.

The underlying assumptions involved in constructing a solar model are

- Hydrostatic equilibrium: The sun is assumed to be spherically symmetric, homogeneous, and in hydrostatic equilibrium, i.e., radiative pressure balances the forces of gravity. Phenomena such as pulsation and rotation due to magnetic fields inside are estimated to be negligible for computing neutrino fluxes [113].
- Energy transport is by photons: Energy transport in the deep interior is due to diffusive transport by photons described by Rosseland mean opacities [113]. The diffusive process strongly depends on the temperature at a given radial distance from the core. Neutrino flux is very sensitive to the core temperature [113].
- Assumptions about energy generation: Primary production of photons and neutrinos occur only through nuclear fusion.
- Changes in chemical abundance is only due to nuclear reactions: Changes in the local abundance of elements occur through nuclear reactions in regions that are convectively stable [113].

Procedure and Results

SSM is the result of the evolution of an initially fully homogeneous stellar model of one $M_\odot$, starting from the pre-main sequence, up to the present solar system age $t_\odot$. The SSM is required to match all observed properties of the Sun at $t_\odot$; such as the solar luminosity $L_\odot$, the solar radius $R_\odot$, and the surface heavy metal to hydrogen mass fraction $(Z/X)_\odot$. Stellar evolution models are constructed by integrating from the core outwards and from the surface inwards, with the requirement that the two solutions match at some mass fraction (typically, 0.1-0.2 $M_\odot$). The three adjustable quantities in the model are the initial helium and metal mass fractions Y_{ini} and Z_{ini} respectively, and the parameter of the mixing length in the theory (α_{MLT}) that describes diffusive processes. Although they are adjustable quantities, they depend on observational constraints and are therefore correlated with each other [113].

The physics input in the SSM is rather simple and it accounts for convective and radiative transport of energy, chemical evolution that is driven by nuclear reactions and gravitational settling. Over the past two decades, since the modern version of the SSM was established there has been the continuous improvements of the microscopic physics, particularly theoretical progress in computing nuclear reaction rates; which has brought about some changes in the evolution SSMs [114]. We conclude by mentioning that modeling dynamical effects in solar models from

first principle is unlikely to provide an accurate physical picture of the Sun's interior. It seems unavoidable that one has to rely on sophisticated multi-dimensional simulations designed to tackle specific problems [112].

Some results of SSM AGSS09 [114], which are potentially important for dark matter dynamics in the Sun is presented in Fig. 3.1. The upper left panel shows the mean density $\rho_{\odot}(r)$ in g/cm^3 as a function of radius fraction (r). The upper right panel depicts the solar mass fraction ($m(r)$) as a function of radius fraction. The middle left panel depicts solar temperature ($T_{\odot}$) as a function of radius fraction. The middle right panel depicts electron number density n_e as function of radius fraction. The bottom left panel shows hydrostatic pressure (P) inside the sun as function of radius fraction. The bottom right panel shows the luminosity function ($L_{\odot}$) as a function of radius fraction. Once the chemical abundances are fixed, the solar models also generate radial profiles for each of the elements. This is shown in Fig. 3.2, the kink in the outer most regions (corresponding to $r = 0.8$) is due to uncertainties in modeling the boundary of the convective envelope [114].

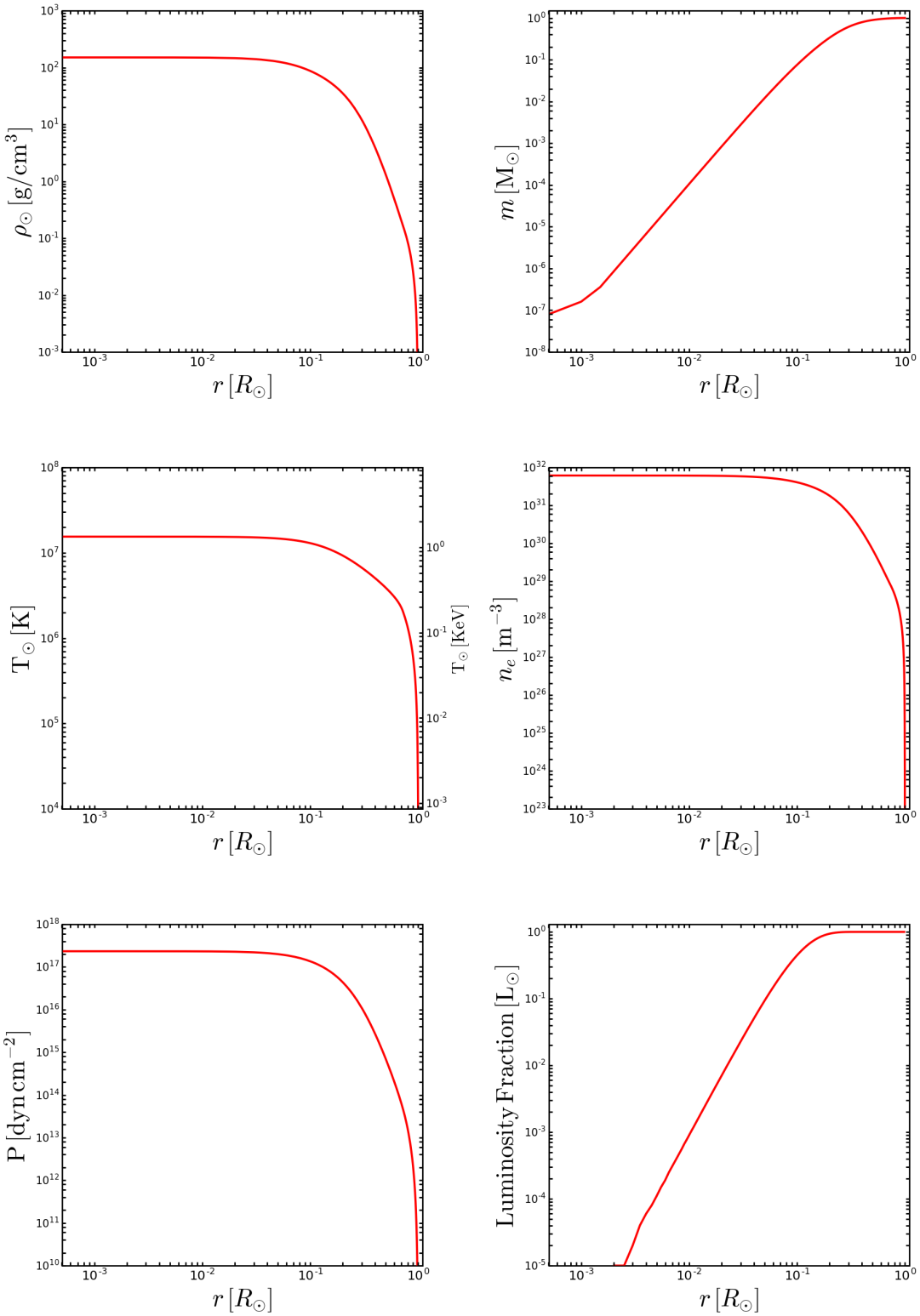

Figure 3.1: ***Characteristics of a solar model:*** The upper left panel shows the mean density $\rho_\odot(r)$ in g/cm^3 as a function of radius fraction (r). The upper right panel depicts the solar mass fraction ($m(r)$) as a function of radius fraction. The middle left column depicts solar temperature ($T_\odot$) as a function of radius fraction. The middle right column depicts electron number density n_e as function of radius fraction. The bottom left panel shows hydrostatic pressure (P) inside the sun as function of radius fraction. The bottom right panel shows the luminosity function ($L_\odot$) as a function of radius fraction.

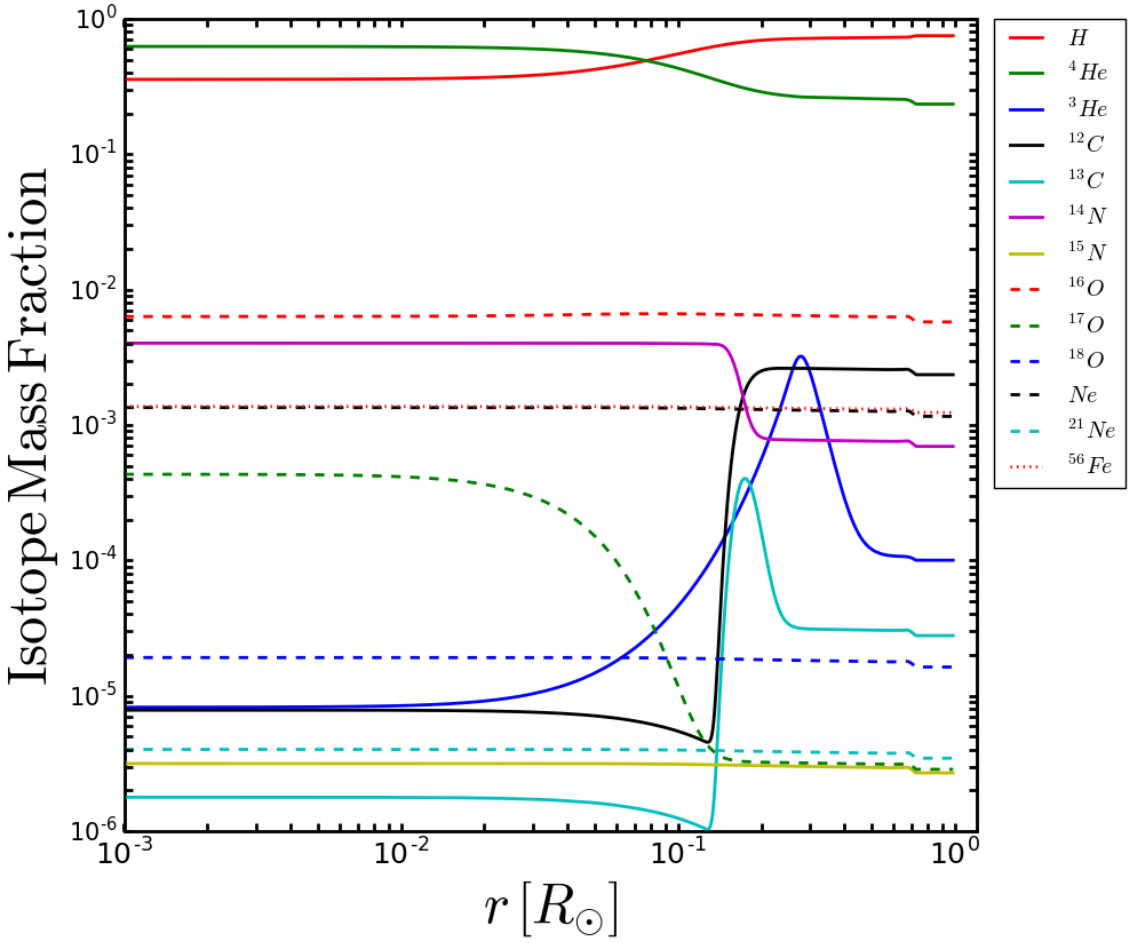

Figure 3.2: ***Isotope Mass Fraction as a function of solar radius:*** The isotope Mass Fraction as a function of solar radius of some important elements is shown. Only those elements with fraction above 10^{-6} is depicted.

CHAPTER 4

Dark Matter Annihilations in the Sun: Analytics

Dark matter (DM) particles in the galactic halo could be brought into close orbits around the Sun after scattering off solar nuclei. Subsequent scatterings could finally capture those DM particles inside the Sun and thermalize them. It has been three decades since the effects of DM particles accumulated in the Sun were originally considered to solve the *solar neutrino problem* by modifying the energy transfer in the Sun [124–126]. However, these first papers did not attempt to explain the physical origin of the required DM concentration, i.e., how solar capture of galactic DM particles would proceed, which was studied for the first time in Ref. [127] and later refined in Refs. [128, 129]. Soon after those seminal works, it was realized that annihilations of DM particles accumulated in the Sun would give rise to a neutrino flux, potentially detectable at neutrino detectors [82–88]. Since then, this is one of the existing strategies to indirectly detect DM, which is in turn complementary to DM direct searches, given that in both cases the signal would be proportional to the DM elastic scattering cross section. Indeed, numerous studies have evaluated the prospects of detection of the potential high-energy neutrino flux [130–187] and of that of neutrinos in the O(10-100) MeV range [188–191] using neutrino detectors/telescopes [192–205].

Estimating the neutrino flux arising from DM annihilations in the Sun requires inputs from both particle physics and astrophysics. The physical description of a celestial body such as the Sun, required for accurate estimates of neutrino fluxes at production, is encoded in Standard Solar Models (SSM) and obtained through astrophysical analysis and methods described in chapter 3. Whereas, the dynamics of "how" DM interacts with the solar medium is entirely controlled by principles of particle physics and statistical physics.

Often there are three processes for which the respective rates need to be computed. Namely, Capture (rate of down scattering), Annihilation (rate of depletion) and Evaporation (rate of up scattering). In order to keep the problem tractable, each of the above mentioned processes are treated independent of the others. In this chapter the formalism required to compute the above quantities is discussed, some of which is analytically tractable. Physically, the problem at hand can be classified as a double Maxwell-Boltzmann (M-B) distribution scattering problem, i.e. we are interested in the rate at which a particle at a given velocity (ω) in an ensemble that obeys M-B distribution elastically scatters off a different particle species which are also described by M-B distribution, to a velocity (v) which can either be greater or smaller than the initial velocity ω . Evaluating the capture rate is relatively simple when compared with that of the evaporation rate. The rate of capture depends on the properties of DM halo in the solar neighbourhood. However, the evaporation rate is proportional to the properties of DM velocity distribution inside the Sun. This means that we need at least a qualitative understanding of the possible DM velocity distribution inside the Sun. The most widely used approach is to assume a M-B distribution for the already trapped DM. Non-relativistic M-B distribution is characterized by just the mass and the temperature of the concerned particle. Since mass is an input to the

problem at hand, we still need to know the effective DM temperature (after successful capture). The analytical expressions required to evaluate DM temperature for untruncated and truncated M-B distribution is derived and presented in section 4.2, not only for velocity independent isotropic cross sections but also for velocity-dependent isotropic cross sections and momentum dependent cross sections. Depending on the strength of DM-target interaction, certain subtleties arise in the computation of evaporation rate which mostly suppress the evaporation rate (and allow for large total annihilation rate), this discussion is deferred to the last part of this chapter in section 4.3. Furthermore, general behavior of the results are discussed. This discussion is consequently relevant and useful to describe various results presented in the Chapter 5.

Before evaluating the scattering rates in section 4.1, the differential equation which governs the time evolution of number density of DM in the Sun (of course, its also applicable to any celestial body of interest) for different "types" of DM particles is discussed. Here, "types" refer to particle properties of DM, in order to keep the discussion complete, we consider DM which is self conjugate, asymmetric and DM with large self-interactions.

4.0.1 Variations on a Theme

The integro-differential equation for the evolution of DM number density can be derived from detailed balance arguments, as follows:

Self-Conjugate Particles

The rate of accumulation of DM particles in the Sun is simply governed by the Boltzmann equation; which implies that the time evolution of the total number of DM particles is proportional to the sum of rate of capture ($C_\odot$) from the DM halo of the galaxy, the rate of annihilation ($A_\odot$) and the rate of evaporation ($E_\odot$). The Boltzmann equation for the number density (N_χ) for self conjugate DM particles then reads [86, 88]

$$\frac{\mathrm{dN}_\chi}{\mathrm{dt}} = C_\odot - A_\odot \mathrm{N}_\chi^2 - E_\odot \mathrm{N}_\chi \,. \tag{4.1}$$

The solution to the above first order differential equation is [86, 88]

$$N_\chi(t) = \sqrt{\frac{C_\odot}{A_\odot}} \frac{\tanh(\kappa\, t/\tau_{eq})}{\kappa + \frac{1}{2}\, E_\odot\, \tau_{eq}\, \tanh(\kappa\, t/\tau_{eq})} \,, \tag{4.2}$$

where $\tau_{eq} = 1/\sqrt{A_\odot C_\odot}$ is the equilibration time scale in the absence of evaporation and $\kappa = \sqrt{1 + (E_\odot\, \tau_{eq}/2)^2}$, with the total annihilation rate is given by $\Gamma = A_\odot\, N_\chi^2/2$. General behavior of the total annihilation rate can be discerned by considering certain analytical limits of the above equation:

- When the rate of evaporation is negligible, $\kappa \to 1$, $E_\odot \tau_{eq} \to 0$, then $\Gamma = C_\odot/2$. Implying that the total annihilation rate is proportional to the elastic scattering cross section.

- In the limit of equilibration being attained, $\kappa t \gg \tau_{eq}$, then the annihilation rate reads

$$\Gamma = \frac{1}{2} \frac{C_\odot}{\left(\kappa + \frac{1}{2} E_\odot \tau_{eq}\right)^2}. \tag{4.3}$$

- When the mass of DM is $\mathcal{O}(1GeV)$

$$\Gamma = \frac{1}{2} A_{\odot} \left(\frac{C_{\odot}}{E_{\odot}} \right)^2 . \tag{4.4}$$

Asymmetric DM

The idea of asymmetric DM (ADM) is based on the observation that $\Omega_{DM} \sim 5\Omega_b$, are similar in magnitude, and cannot be explained if DM is a self-conjugate WIMP. To explain the above relation, the ideas of thermal freeze-out and baryon asymmetry were unified by invoking dynamical mechanism where DM can share the asymmetry with baryons. Thus naturally relating the baryon and DM asymmetries [206, 207]. If the DM particles stay in thermal equilibrium sufficiently long, the symmetric part can be efficiently annihilated away, whereas the anti-symmetric part yields DM number density which is exponentially suppressed, which leads to the following relation between Ω_{DM}, Ω_b, m_χ, proton mass m_p, baryon asymmetry η_b, and DM asymmetry η_χ

$$\frac{\Omega_\chi}{\Omega_b} = \frac{m_\chi}{m_p} \frac{\eta_\chi}{\eta_b}. \tag{4.5}$$

Generally, Candidates for ADM can arise in SUSY models [208] and models which call for strong dynamics [209]. Leptophilic ADM has also been considered [210]. ADM models typically predict light dark matter of mass in MeV – GeV range.

When the DM candidate under consideration is not self conjugate, DM (χ) and anti-DM ($\bar{\chi}$) should be treated seperately. This leads to the following set of coupled Boltzmann equation for DM and anti-DM reads

$$\frac{\mathrm{dN}_\chi}{\mathrm{dt}} = C_{\odot}^{\chi} - A_{\odot} \mathrm{N}_\chi \mathrm{N}_{\bar{\chi}} - E_{\odot}^{\chi} \mathrm{N}_\chi, \tag{4.6}$$

$$\frac{\mathrm{dN}_{\bar{\chi}}}{\mathrm{dt}} = C_{\odot}^{\bar{\chi}} - A_{\odot} \mathrm{N}_\chi \mathrm{N}_{\bar{\chi}} - E_{\odot}^{\bar{\chi}} \mathrm{N}_{\bar{\chi}}. \tag{4.7}$$

Similar to the notation used in the case of self conjugate DM, $C_{\odot}^{\chi}(C_{\odot}^{\bar{\chi}})$ is the capture rate of DM (anti-DM) by scattering off particles in the Sun, $A_{\odot}$ is the annihilation rate, $E_{\odot}^{\chi}(E_{\odot}^{\bar{\chi}})$ is the evaporation rate of DM (anti-DM) by scattering off particles in the celestial body. If the elastic scattering cross section of $\chi\bar{\chi} \rightarrow \chi\bar{\chi}$ is significant then, χ can get captured by scattering off the already captured χ ($\bar{\chi}$), the dynamics is reflected by the inclusion of term $C_{\bar{\chi}}^{\cdot} N_\chi$ ($C_{\chi}^{\cdot} N_{\bar{\chi}}$) to the above expressions. Similarly, term $E_{\bar{\chi}}^{\cdot} N_\chi$ ($E_{\chi}^{\cdot} N_{\bar{\chi}}$) indicates χ can be ejected out of the body (evaporation) by scattering off the already captured χ ($\bar{\chi}$). However, we work in the limit of small self interactions for the sake of simplicity.

Of particular phenomenological interest is the completely anti-symmetric case, i.e. $A_{\odot} = 0$ or when only χs or $\bar{\chi}s$ are present in the solar neigbhourhood. The above equations simplify to

$$\frac{\mathrm{dN}_\chi}{\mathrm{dt}} = C_{\odot}^{\chi} - E_{\odot}^{\chi} \mathrm{N}_\chi, \tag{4.8}$$

the solution for N_χ reads

$$N_\chi(t_{\odot}) = C_{\odot}^{\chi} t_{\odot} \left(\frac{1 - e^{-E_{\odot}^{\chi} t_{\odot}}}{E_{\odot}^{\chi} t_{\odot}} \right), \tag{4.9}$$

where $t_\odot$ is the age of the Sun. In the limit of evaporation being negligible, $N_\chi(t_\odot) = C_\odot^\chi t_\odot$. It has been noted that asymmetric DM in the Sun could alleviate tension between solar modeling and helioseismology [211].

Self Interacting DM case

When DM has large self interactions such that $\sigma(\chi\chi \to \chi\chi)$ is of the order of several hundred *mb*, the time evolution of number density of DM reads

$$\frac{\mathrm{dN}_\chi}{\mathrm{dt}} = C_\odot - \left(A_\odot + E_\odot^{self}\right)\mathrm{N}_\chi^2 - \left(E_\odot - C_\odot^{self}\right)\mathrm{N}_\chi \,, \tag{4.10}$$

again, the notation used is the same as the above cases. The last term $C_\odot^{self}$ is the rate at which χ is captured from the halo by scattering off the previously captured χ in the core; also referred to as the self capture rate. The term $E_\odot^{self}$ is the self evaporation rate, due to the process $\chi\chi \to \chi\chi$ that leads to the final state χ to be completely ejected. The solution to the above equation reads [176]

$$\mathrm{N}_\chi = \frac{C_\odot \tanh\left(t/\tau_s\right)}{\tau_s^{-1} - \left(C_\odot^{self} - E_\odot\right)\tanh\left(t/\tau_s\right)/2}, \tag{4.11}$$

with the effective time constant given by

$$\tau_s = \left(C_\odot\left(A_\odot + E_\odot^{self}\right) + \left(C_\odot^{self} - E_\odot\right)^2/4\right)^{-1/2}. \tag{4.12}$$

The total annihilation rate is $\Gamma = A_\odot/2N_\chi^2$. Some phenomenological implications of this scenario at neutrino telescopes is discussed in [154] in the limit when evaporation can be neglected (conservatively, when $m_\chi > 10\,GeV$), and [176] for a general discussion [1].

Common to all the above cases are the general expressions for capture, evaporation and annihilation rates.

Capture

When the DM mean free path $\lambda = 1/(n_\odot\sigma) \sim R_\odot$, also known as "weak" regime, the capture rate then reads

$$C_\odot = \sum_i \int_0^{R_\odot} 4\pi r^2 \mathrm{d}r \int_0^\infty \mathrm{d}u_\chi \left(\frac{\rho_\chi}{m_\chi}\right)\frac{f_{v_\odot}(u_\chi)}{u_\chi}\, w(r) \int_0^{v_e(r)} R_i^-(w \to v)\,|F_i(q)|^2\,\mathrm{d}v \,, \tag{4.13}$$

here the sum is over all the target particles i which can interact with DM. Here, $F_i(q)$ is the nuclear form factor corresponding to a given element i, $f_{v_\odot}$ is the velocity distribution of DM in the solar neighbhourhood, and ρ_χ is the local DM density [3]. The calculation of capture rate proceeds in three steps. The first step is to integrate the differential scattering rate $R_i^-(w \to v)$ (the rate of scattering to a lower velocity v, for a given w such that $w > v$). The derivation of $R_i^-(w \to v)$ is presented in the next section.The second step involves integrating over the initial DM velocities (u_χ) and in the last step we integrate over the entire volume of the Sun in the last step.

[1] Remark: At this point it is unclear whether DM with large self interactions can impact the process of stellar evolution and the present properties of the Sun significantly [2]. There are dedicated codes [212] and *DarkSTEC* which have already incorporated the leading effects of DM in any stellar body, however, the case of DM with large self interactions are not included yet.

[3] Details about these quantities are discussed in chapter 5.

Evaporation

Assuming the captured DM is sufficiently thermalized with the solar medium, the radial number density of DM $n_\chi(r,t)$, can be assumed to have an isothermal profile defined by its effective temperature T_χ ($\neq T_\odot$) and m_χ, in the "weak" regime. The velocity distribution is encoded in $f_\chi(w,r)$, which is assumed to be M-B distribution truncated to a velocity less than or equal to the escape velocity at a given radius. Therefore, $f_\chi(w,r)$ is parameterized by T_χ, m_χ and cut-off velocity $v_c(r)$. General method to estimate T_χ is outlined in section 4.2. Using the definitions above, the evaporation rate is

$$E_\odot = \sum_i \int_0^{R_\odot} s(r)\, n_\chi(r,t)\, 4\pi r^2\, \mathrm{d}r \int_0^{v_c(r)} f_\chi(\boldsymbol{w},r)\, 4\pi w^2\, \mathrm{d}w \int_{v_e(r)}^{\infty} R_i^+(w\to v)\mathrm{d}v\,, \tag{4.14}$$

the sum is over all the target particles i which can interact with DM and the factor $s(r)$ accounts for the suppression, relevant only when $\lambda << R_\odot$ [4]. Analogous to the capture, the calculation proceeds in three steps. The first step is to integrate the differential scattering rate $R_i^+(w\to v)$ (the rate of scattering to a higher velocity v, for a given w such that $w<v$). The derivation of $R_i^+(w\to v)$ is presented in the next section. The second step involves integrating over the initial DM velocities (w) and finally we integrate over the entire volume of the Sun in the last step.

Annihilation

Annihilation rate reads

$$A_\odot = \langle \sigma_A v_{\chi\chi}\rangle \frac{\int_0^{R_\odot} n_\chi^2(r,t)\, 4\pi r^2\, \mathrm{d}r}{\left(\int_0^{R_\odot} n_\chi(r,t)\, 4\pi r^2\, \mathrm{d}r\right)^2}\,, \tag{4.15}$$

where $\langle \sigma_A v_{\chi\chi}\rangle$ is the thermally averaged annihilation cross section. σ_A is the annihilation cross section and $v_{\chi\chi}$ is the relative velocity between the two annihilating DM particles.

Note that the rate of self capture and self evaporation, relevant for DM with large self interactions, is easily obtained by making suitable replacements in the expressions for $R_i^\pm(w\to v)$.

4.1 Differential Scattering Cross Sections and Rates

In the past few decades, WIMP DM with primarily spin dependent and spin independent interactions have been extensively probed at various direct detection experiments, and in the context of DM annihilation in the Sun. Such interactions in the non relativistic limit result in elastic scattering cross sections with no non trivial dependencies on velocity and momentum. In light of null results in the search for DM at direct and indirect detection experiments, and in the spirit of exploration, more possibilities have been considered [213–227].

Before we compute the rates in a particular model, it is helpful to understand their behavior independent of Lagrangian parameters by phenomenologically parametrizing the differential scattering cross section for a DM particle elastically scattering of a target i, as follows

[4] The discussion is relegated to section 4.3.2.

$$\frac{\mathrm{d}\sigma_{i,const}(v_{rel},\cos\theta_{cm})}{\mathrm{d}\cos\theta_{cm}} = \frac{\sigma_{i,0}}{2}\,, \tag{4.16}$$

$$\frac{\mathrm{d}\sigma_{i,v_{rel}^2}(v_{rel},\cos\theta_{cm})}{\mathrm{d}\cos\theta_{cm}} = \frac{\sigma_{i,0}}{2}\left(\frac{v_{rel}}{v_0}\right)^{2n}\,, \tag{4.17}$$

$$\frac{\mathrm{d}\sigma_{i,q^2}(v_{rel},\cos\theta_{cm})}{\mathrm{d}\cos\theta_{cm}} = \frac{\sigma_{i,0}}{2}\,\frac{(1+m_\chi/m_i)^2}{2}\left(\frac{q}{q_0}\right)^{2n}\,, \tag{4.18}$$

where, $n = 1, 2, -1$; v_0 and q_0 are reference velocity and momentum. In the context of simplified models, the possible Lorentz structures that lead to the above parrameterization is discussed in chapter 6. Such parameterizations have been previously considered in the context of neutrino signals from the sun and to alleviate tensions between helioseismology and solar models. Its worth a mention that contrary to the previous studies we provide general closed form analytical expressions for the differential scattering rates for all the cases considered above, including thermal motion of the target particles. Later, we apply this formalism to case when the target particles are electrons, where it is known that thermal effects play an important role for capture[5], but had not been analyzed thoroughly. As expected such analytical expressions greatly optimizes computational time and provides a good analytical handle for the problem. Hereafter we focus on the case of $n = 1$.

We consider DM particles with mass m_χ interacting with a thermal distribution of targets with mass m_i, such that we can work on the non-relativistic limit. Assuming the target particles follow a Maxwell-Boltzmann velocity distribution, $f_i(\boldsymbol{u}, r)$, with density $n_i(r)$ and temperature $T_\odot(r)$, the differential rate at which a DM particle with velocity w scatters off a target i with velocity u and relative angle θ, in the laboratory frame, to a final velocity v is given by

$$\begin{aligned} R_i(w\to v) &= \int n_i(r)\,\frac{\mathrm{d}\sigma_i}{\mathrm{d}v}\,|\boldsymbol{w}-\boldsymbol{u}|\,f_i(\boldsymbol{u},r)\,\mathrm{d}^3\boldsymbol{u} \\ &= \frac{2}{\sqrt{\pi}}\,\frac{n_i(r)}{u_i^3(r)}\int_0^\infty \mathrm{d}u\,u^2\int_{-1}^{1}\mathrm{d}\cos\theta\,\frac{\mathrm{d}\sigma_i}{\mathrm{d}v}\,|\boldsymbol{w}-\boldsymbol{u}|\,e^{-u^2/u_i^2(r)}\,, \end{aligned} \tag{4.19}$$

where $\mathrm{d}\sigma_i/\mathrm{d}v$ is the differential scattering cross section,

$$u_i(r) \equiv \sqrt{\frac{2\,T_\odot(r)}{m_i}}\,, \tag{4.20}$$

is the most probable speed of the target particles at position r, and the relative velocity between the DM and target particles is given by

$$|\boldsymbol{w}-\boldsymbol{u}| = \sqrt{w^2+u^2-2\,w\,u\,\cos\theta}\,. \tag{4.21}$$

Now, using the notation of Refs. [128, 229], we can write the above expression in terms of the velocity of the center of mass, $\boldsymbol{s}$, and the velocity of the incoming DM particle in the

[5] Ref. [228] showed for the first time that for the case of constant cross section mean motion of the target could be important, here we generalize to velocity-dependent isotropic and momentum dependent differential cross sections.

center-of-mass frame, $\boldsymbol{t}$,

$$(1+\mu_i)\,\boldsymbol{s} = \boldsymbol{u} + \mu_i \boldsymbol{w}\,, \tag{4.22}$$
$$(1+\mu_i)\,\boldsymbol{t} = \boldsymbol{w} - \boldsymbol{u}\,, \tag{4.23}$$

where we have defined

$$\mu_i \equiv \frac{m_\chi}{m_i}\,. \tag{4.24}$$

If we substitute u and $\cos\theta$ by s and t, Eq. (4.19) can be expressed as

$$R_i(w \to v) = \frac{32}{\sqrt{\pi}} \frac{\mu_{i,+}^4}{w\, u_i^3(r)}\, n_i(r) \int_0^\infty \mathrm{d}s \int_0^\infty \mathrm{d}t\, \frac{\mathrm{d}\sigma_i}{\mathrm{d}v}\, s\, t^2\, e^{-u^2/u_i^2(r)}\, \Theta(w - |s-t|)\, \Theta(s+t-w) \tag{4.25}$$

where

$$\mu_{i,\pm} \equiv \frac{\mu_i \pm 1}{2}\,, \qquad u^2 = 2\mu_i \mu_{i,+}\, t^2 + 2\mu_{i,+}\, s^2 - \mu_i\, w^2\,. \tag{4.26}$$

On the other hand, the differential cross section $\mathrm{d}\sigma_i/\mathrm{d}v$ can be written as

$$\frac{\mathrm{d}\sigma_i}{\mathrm{d}v} = \int_0^{2\pi} \frac{1}{2\pi} \frac{\mathrm{d}\sigma_i}{\mathrm{d}\cos\theta_{cm}} \frac{\mathrm{d}\cos\theta_{st'}}{\mathrm{d}v}\, \Theta(1 - |\cos\theta_{st'}|)\, \mathrm{d}\phi_{st'}\,, \tag{4.27}$$

where θ_{cm} is the center-of-mass angle between the velocity of the outgoing DM particle, $\boldsymbol{t'}$, and the velocity of the incoming DM particle, $\boldsymbol{t}$,

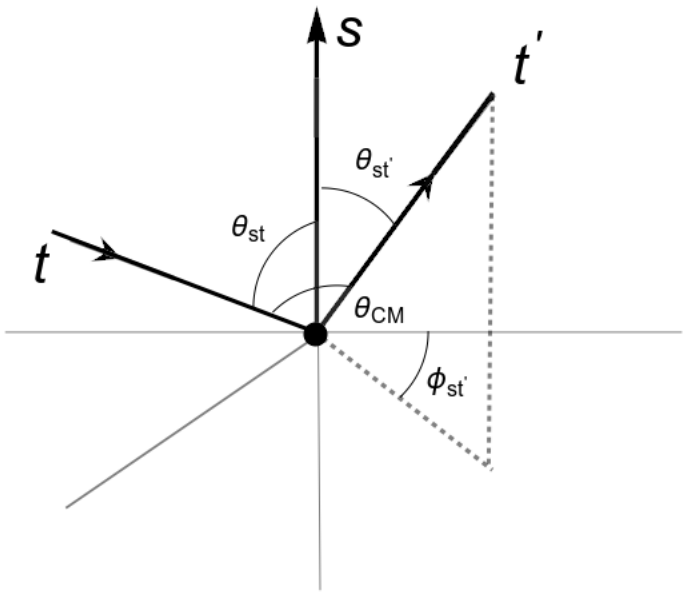

Figure 4.1: ***Relevant vectors in CM frame:*** s is the CM velocity, t is the incoming DM velocity and t' is the out-going DM velocity in the CM frame. As usually done, the angle between t, t' is θ_{CM}, the angle between s, t' is $\theta_{st'}$, the angle between s, t is θ_{st} and $\phi_{st'}$ is the azimuthal angle subtended by t', s.

$$\cos\theta_{cm} = \cos\theta_{st}\, \cos\theta_{st'} + \sin\theta_{st}\, \sin\theta_{st'}\, \cos\phi_{st'}\,, \tag{4.28}$$

and $\theta_{st'}$ and $\phi_{st'}$ are the center-of-mass angles of the outgoing DM particle with respect to $\boldsymbol{s}$ and

θ_{st} is the center-of-mass zenith angle of the incoming DM particle with respect to $\boldsymbol{s}$, see Fig. 4.1,

$$\cos\theta_{st} = \frac{w^2 - s^2 - t^2}{2\,s\,t}\,, \tag{4.29}$$

$$\cos\theta_{st'} = \frac{v^2 - s^2 - t'^2}{2\,s\,t'}\,. \tag{4.30}$$

Therefore, we can express the differential DM scattering rate off target i, Eq. (4.25), as

$$R_i(w \to v) = \frac{16}{\sqrt{\pi^3}}\,\frac{\mu_{i,+}^4}{u_i^3(r)}\,\frac{v}{w}\,n_i(r)\int_0^\infty \mathrm{d}t \int_0^\infty \mathrm{d}s\,t\,e^{-u^2/u_i^2(r)}\,H(s,t,w,v)\int_0^{2\pi}\mathrm{d}\phi_{st'}\,\frac{\mathrm{d}\sigma_i}{\mathrm{d}\cos\theta_{cm}}\,, \tag{4.31}$$

with

$$H(s,t,w,v) \equiv \Theta(w - |s-t|)\,\Theta(s+t-w)\,\Theta(v-|s-t|)\,\Theta(s+t-v)\,. \tag{4.32}$$

If one performs the s integral first, this product of Heaviside functions translates into the following integration limits for s and t:

$$\begin{aligned}
&(\text{for } v < w)\; H^-(s,t,w,v): && && (4.33)\\
&\qquad \frac{w-v}{2} \le t \le \frac{v+w}{2}\,, && w - t \le s \le v + t\,,\\
&\qquad \frac{v+w}{2} \le t \le \infty\,, && t - v \le s \le v + t\,;\\
&(\text{for } v > w)\; H^+(s,t,w,v): && && (4.34)\\
&\qquad \frac{v-w}{2} \le t \le \frac{v+w}{2}\,, && v - t \le s \le w + t\,,\\
&\qquad \frac{v+w}{2} \le t \le \infty\,, && t - w \le s \le w + t\,.
\end{aligned}$$

Finally, the full differential scattering rate is obtained by summing over all targets i, i.e, $R(w \to v) = \sum_i R_i(w \to v)$. In what follows we also use these definitions [128]:

$$\chi(a,b) \equiv \int_a^b e^{-y^2}\,\mathrm{d}y\,, \tag{4.35}$$

$$\alpha_\pm \equiv \frac{\mu_{i,+}\,v \pm \mu_{i,-}\,w}{u_i(r)}\,, \tag{4.36}$$

$$\beta_\pm \equiv \frac{\mu_{i,-}\,v \pm \mu_{i,+}\,w}{u_i(r)}\,. \tag{4.37}$$

4.1.1 Constant Cross Section: Velocity-Independent and Isotropic

We first consider velocity-independent and isotropic cross sections, which is the case usually studied in the literature,

$$\frac{\mathrm{d}\sigma_{i,const}(v_{rel},\cos\theta_{cm})}{\mathrm{d}\cos\theta_{cm}} = \frac{\sigma_{i,0}}{2}\,, \tag{4.38}$$

so that $\sigma_{i,const} = \sigma_{i,0}$. Therefore, Eq. (4.31) reads

$$R^\pm_{i,const}(w \to v) = \frac{16}{\sqrt{\pi}}\,\frac{\mu_{i,+}^4}{u_i^3(r)}\,\frac{v}{w}\,n_i(r)\,\sigma_{i,0}\int_0^\infty \mathrm{d}t \int_0^\infty \mathrm{d}s\,t\,e^{-u^2/u_i^2(r)}\,H^\pm(s,t,w,v)\,. \tag{4.39}$$

Using the conditions $v > w$ for $R^{+}_{i,const}(w \to v)$, and $v < w$ for $R^{-}_{i,const}(w \to v)$, the integrals in Eq. (4.39) can be performed analytically [128],

$$\int_0^\infty \mathrm{d}t \int_0^\infty \mathrm{d}s\, t\, e^{-u^2/u_i^2(r)}\, H^{\pm}(s,t,w,v) = \frac{u_i^3(r)}{8\,\mu_i\,\mu_{i,+}^2}\left[\chi(\pm\alpha_-,\alpha_+) + \chi(\pm\beta_-,\beta_+)\, e^{\mu_i\left(w^2-v^2\right)/u_i^2(r)}\right]. \quad (4.40)$$

Finally, the rates $R^{\pm}_{const}(w \to v)$ are given by [128]

$$R^{\pm}_{const}(w \to v) = \sum_i \frac{2}{\sqrt{\pi}}\,\frac{\mu_{i,+}^2}{\mu_i}\,\frac{v}{w}\, n_i(r)\,\sigma_{i,0}\left[\chi(\pm\alpha_-,\alpha_+) + \chi(\pm\beta_-,\beta_+)\, e^{\mu_i\left(w^2-v^2\right)/u_i^2(r)}\right]. \quad (4.41)$$

4.1.2 Velocity-Dependent Cross Section

We consider now the case of velocity-dependent and isotropic cross sections, i.e.,

$$\frac{\mathrm{d}\sigma_{i,v_{rel}^n}(v_{\rm rel},\cos\theta_{cm})}{\mathrm{d}\cos\theta_{cm}} = \frac{\sigma_{i,0}}{2}\left(\frac{v_{\rm rel}}{v_0}\right)^n, \quad (4.42)$$

so that $\sigma_{i,v_{rel}^n} = \sigma_{i,0}\,(v_{\rm rel}/v_0)^n$, and where v_{rel} is the relative velocity between the DM particle and target i,

$$v_{\rm rel} \equiv |\boldsymbol{w} - \boldsymbol{u}| = (1+\mu_i)\,t = 2\,\mu_{i,+}\,t\,, \quad (4.43)$$

and v_0 is an arbitrary reference velocity, which we set to $v_0 = 220$ km/s. Thus, for this particular case, the differential scattering rates read

$$R^{\pm}_{i,v_{rel}^n}(w \to v) = \frac{2^{4+n}}{\sqrt{\pi}}\,\frac{\mu_{i,+}^{4+n}}{u_i^3(r)}\,\frac{v}{w}\, n_i(r)\,\frac{\sigma_{i,0}}{v_0^n}\int_0^\infty \mathrm{d}t \int_0^\infty \mathrm{d}s\, t^{1+n}\, e^{-u^2/u_i^2(r)}\, H^{\pm}(s,t,w,v). \quad (4.44)$$

For the case of $n = 2$, using the conditions $v > w$ for $R^{+}_{i,v_{rel}^2}(w \to v)$, and $v < w$ for $R^{-}_{i,v_{rel}^2}(w \to v)$, the integrals in Eq. (4.44) can be performed analytically,

$$\begin{aligned}\int_0^\infty \mathrm{d}t \int_0^\infty \mathrm{d}s\, t^3\, e^{-u^2/u_i^2(r)}\, H^{\pm}(s,t,w,v) = \\ \frac{u_i^5(r)}{32\,\mu_i\,\mu_{i,+}^4}\left[\left(\mu_{i,+}+\frac{1}{2}\right)\left(\pm\frac{v-w}{u_i(r)}\,e^{-\alpha_-^2} - \frac{v+w}{u_i(r)}\,e^{-\alpha_+^2}\right)\right. \\ \left. + \left(\frac{w^2}{u_i^2(r)}+\frac{3}{2}+\frac{1}{\mu_i}\right)\chi(\pm\alpha_-,\alpha_+) + \left(\frac{v^2}{u_i^2(r)}+\frac{3}{2}+\frac{1}{\mu_i}\right)\chi(\pm\beta_-,\beta_+)\, e^{\mu_i\left(w^2-v^2\right)/u_i^2(r)}\right],\end{aligned} \quad (4.45)$$

Finally, the rates $R^{\pm}_{v_{rel}^2}(w \to v)$ are given by

$$\begin{aligned}R^{\pm}_{v_{rel}^2}(w \to v) \;=\; & \sum_i \frac{2}{\sqrt{\pi}}\,\frac{\mu_{i,+}^2}{\mu_i}\,\frac{v}{w}\, n_i(r)\,\sigma_{i,0}\left(\frac{u_i(r)}{v_0}\right)^2\left[\left(\mu_{i,+}+\frac{1}{2}\right)\left(\pm\frac{v-w}{u_i(r)}\,e^{-\alpha_-^2} - \frac{v+w}{u_i(r)}\,e^{-\alpha_+^2}\right)\right. \\ & + \left(\frac{w^2}{u_i^2(r)}+\frac{3}{2}+\frac{1}{\mu_i}\right)\chi(\pm\alpha_-,\alpha_+) \\ & \left. + \left(\frac{v^2}{u_i^2(r)}+\frac{3}{2}+\frac{1}{\mu_i}\right)\chi(\pm\beta_-,\beta_+)\, e^{\mu_i\left(w^2-v^2\right)/u_i^2(r)}\right].\end{aligned} \quad (4.46)$$

4.1.3 Momentum-Dependent Cross Section

Next, we consider the case of momentum-dependent cross sections,

$$\frac{\mathrm{d}\sigma_{i,q^n}(v_{rel},\cos\theta_{cm})}{\mathrm{d}\cos\theta_{cm}} = \frac{\sigma_{i,0}}{2}\,H_{i,n}\left(\frac{q}{q_0}\right)^n\,, \tag{4.47}$$

where

$$H_{i,n} = \frac{2^{n/2+1}\,\mu_{i,+}^n}{\int_{-1}^{1}(1-\cos\theta_{cm})^{n/2}\,\mathrm{d}\cos\theta_{cm}} = \left(1+\frac{n}{2}\right)\mu_{i,+}^n \tag{4.48}$$

is a normalization chosen so that the total momentum-dependent and velocity-dependent cross sections are equal, i.e., $\sigma_{i,q^n} = \sigma_{i,v_{rel}^n}$, if the arbitrary momentum is defined as $q_0 = m_\chi\, v_0$ and $\sigma_{i,0}$ is the same in both cases. In the non-relativistic limit, the 3-momentum transfer is given by

$$q^2 = m_\chi^2\,|\boldsymbol{w}-\boldsymbol{v}|^2 = 2\,m_\chi^2\,t^2\,(1-\cos\theta_{cm}) = \frac{m_\chi^2}{2\,\mu_{i,+}^2}\,v_{rel}^2\,(1-\cos\theta_{cm})\,. \tag{4.49}$$

Then, the differential scattering rates read

$$\begin{aligned} R^{\pm}_{i,q^n}(w\to v) \;=\; & \frac{2^{4+n/2}}{\pi^{3/2}}\,\frac{\mu_{i,+}^{4+n}}{u_i^3(r)}\,\frac{v}{w}\,n_i(r)\,\frac{\sigma_{i,0}}{v_0^n} \\ & \times\int_0^\infty \mathrm{d}t\int_0^\infty \mathrm{d}s\,t^{1+n}\,e^{-u^2/u_i^2(r)}\,H^{\pm}(s,t,w,v)\int_0^{2\pi}\mathrm{d}\phi_{st'}\,(1-\cos\theta_{cm})^{n/2}\,. \end{aligned} \tag{4.50}$$

For the case $n = 2$, using the conditions $v > w$ for $R^{+}_{i,q^2}(w\to v)$, and $w > v$ for $R^{-}_{i,q^2}(w\to v)$, the integrals in Eq. (4.50) can be performed analytically. After computing the $\phi_{st'}$ integral, one obtains

$$\begin{aligned} & 2\pi\int_0^\infty \mathrm{d}t\int_0^\infty \mathrm{d}s\left(1-\frac{(w^2-s^2-t^2)(v^2-s^2-t^2)}{4\,s^2\,t^2}\right)t^3\,e^{-u^2/u_i^2(r)}\,H^{\pm}(s,t,w,v) = \\ & \frac{\pi}{4}\,\frac{u_i^5(r)}{\mu_i^2\,\mu_{i,+}^2}\left[\pm\frac{v-w}{u_i(r)}\,e^{-\alpha_-^2} - \frac{w+v}{u_i(r)}\,e^{-\alpha_+^2}\right. \\ & \left. +\left(\frac{1}{2}\,\frac{w^2-v^2}{u_i^2(r)}+\frac{1}{\mu_i}\right)\chi(\pm\alpha_-,\alpha_+) + \left(\frac{1}{2}\,\frac{v^2-w^2}{u_i^2(r)}+\frac{1}{\mu_i}\right)\chi(\pm\beta_-,\beta_+)\,e^{\mu_i\left(w^2-v^2\right)/u_i^2(r)}\right]\,. \end{aligned} \tag{4.51}$$

Finally, the rates $R^{\pm}_{q^2}(w\to v)$ are given by

$$\begin{aligned} R^{\pm}_{q^2}(w\to v) \;=\; & \sum_i \frac{8}{\sqrt{\pi}}\,\frac{\mu_{i,+}^4}{\mu_i^2}\,\frac{v}{w}\,n_i(r)\,\sigma_{i,0}\left(\frac{u_i(r)}{v_0}\right)^2\left[\pm\frac{v-w}{u_i(r)}\,e^{-\alpha_-^2} - \frac{w+v}{u_i(r)}\,e^{-\alpha_+^2}\right. \\ & +\left(\frac{1}{2}\,\frac{w^2-v^2}{u_i^2(r)}+\frac{1}{\mu_i}\right)\chi(\pm\alpha_-,\alpha_+) \\ & \left.+\left(\frac{1}{2}\,\frac{v^2-w^2}{u_i^2(r)}+\frac{1}{\mu_i}\right)\chi(\pm\beta_-,\beta_+)\,e^{\mu_i\left(w^2-v^2\right)/u_i^2(r)}\right]\,. \end{aligned} \tag{4.52}$$

4.2 Dark Matter Temperature: in the Knudsen Limit

In the "weak" regime, after DM particles are captured by the Sun, they would thermalize non-locally by multiple interactions, with a single isothermal (iso) distribution. In this limit (Knudsen limit), their radial distribution can be written as [88, 125, 126]

$$n_{\chi,\mathrm{iso}}(r,t) = N_\chi(t)\,\frac{e^{-m_\chi\phi(r)/T_\chi}}{\int_0^{R_\odot} e^{-m_\chi\phi(r)/T_\chi}\,4\pi r^2\,\mathrm{d}r}\,, \tag{4.53}$$

which corresponds to an isothermal sphere following the law of atmospheres, with a radial dependence set by the gravitational potential $\phi(r) = \int_0^r GM_\odot(r')/r'^2\,\mathrm{d}r'$, with G the gravitational constant and $M_\odot(r)$ the solar mass at radius r, and where $N_\chi(t)$ is the total population of DM particles at a given time t.

Although a M-B distribution, Eq. (4.57), is not an exact solution of the collisional Boltzmann equation in the optically thin regime (the Knudsen limit) [128, 230, 231], one can obtain a solution for the isothermal approximation by requiring the distribution to satisfy its first energy moment and solving for T_χ. In the case of the collisionless Boltzmann equation, for a steady state equilibrium distribution without evaporation, the energy moment equation implies no net flow of energy [125], i.e.,

$$\sum_i \int_0^{R_\odot} \epsilon_i(r,T_\chi,v_c)\,4\pi r^2\,\mathrm{d}r = 0\,, \tag{4.54}$$

where

$$\epsilon_i(r,T_\chi,v_c) \equiv \int \mathrm{d}^3\boldsymbol{w}\,n_{\chi,iso}(r)\,f_{\chi,iso}(\boldsymbol{w},\boldsymbol{r}) \int \mathrm{d}^3\boldsymbol{u}\,n_i(r)\,f_i(\boldsymbol{u},r)\,\sigma_{i,0}\,|\boldsymbol{w}-\boldsymbol{u}|\,\langle\Delta E_i\rangle \tag{4.55}$$

is the energy transfer per unit volume and time, and where the velocity distribution functions are given in Eqs. (5.19) and (5.20), which we reproduce here (in the DM case, for the isothermal approximation),

$$f_i(\boldsymbol{u},r) = \frac{1}{\sqrt{\pi^3}\,u_i^3(r)}\,e^{-u^2/u_i^2(r)}\,, \tag{4.56}$$

$$f_{\chi,iso}(\boldsymbol{w},r) = \frac{e^{-w^2/v_\chi^2}\,\Theta(v_c(r)-w)}{\sqrt{\pi^3}\,v_\chi^3\left(\mathrm{Erf}\left(\frac{v_c(r)}{v_\chi}\right) - \frac{2}{\sqrt{\pi}}\frac{v_c(r)}{v_\chi}\,e^{-v_c^2(r)/v_\chi^2}\right)}\,, \tag{4.57}$$

where $u_i(r)$ is defined in Eq. (4.20),

$$v_\chi \equiv \sqrt{\frac{2\,T_\chi}{m_\chi}}\,, \tag{4.58}$$

$v_c(r)$ is the (position-dependent) cutoff velocity of the DM distribution and

$$\langle\Delta E_i\rangle = \int_{-1}^{1} \frac{\mathrm{d}\cos\theta_{cm}}{\sigma_{i,0}}\,\frac{\mathrm{d}\sigma_i}{\mathrm{d}\cos\theta_{cm}}\,\Delta E_i(\boldsymbol{w},\boldsymbol{u},\cos\theta_{cm}) \tag{4.59}$$

with ΔE_i being the energy transferred to the DM particle after one collision,

$$\Delta E_i \equiv \frac{m_\chi}{2}\left(v^2 - w^2\right)\,. \tag{4.60}$$

In terms of the incoming velocities and the scattering angle in the laboratory frame, θ, and in

terms of the scattering angle in the center-of-mass frame, θ_{cm}, Eq. (4.60) reads [125]

$$\Delta E_i(\boldsymbol{w},\boldsymbol{u},\cos\theta_{cm}) = \frac{m_\chi}{4\,\mu_{i,+}^2}\,(1-\cos\theta_{cm})\,\left(u^2-\mu_i\,w^2+2\,\mu_{i,-}\,w\,u\,\cos\theta\right)\,. \tag{4.61}$$

More explicitly, in terms of the gravitational potential $\phi(r)$ (see Eq. (5.21)), Eq. (4.54) can be written as

$$\begin{aligned}\sum_i \int_0^{R_\odot} \mathrm{d}r\, r^2\, n_i(r)\, e^{\frac{-m_\chi\,\phi(r)}{T_\chi}} \int_0^{v_c(r)} \mathrm{d}w\, w^2\, f_{\chi,iso}(\boldsymbol{w},r) \\ \times \int_0^\infty \mathrm{d}u\, u^2\, f_i(\boldsymbol{u},r) \int_{-1}^1 \mathrm{d}\cos\theta\, \sigma_{i,0}\,|\boldsymbol{w}-\boldsymbol{u}|\,\langle\Delta E_i\rangle \;=\; 0\,.\end{aligned} \tag{4.62}$$

4.2.1 Constant Cross section: Velocity-Independent and Isotropic

For the usually considered case, constant (velocity-independent and isotropic) scattering cross section, the expression for the $\cos\theta$ integral reads

$$\begin{aligned}\int_{-1}^1 \mathrm{d}\cos\theta\,|\boldsymbol{w}-\boldsymbol{u}|\,\langle\Delta E_i\rangle \;=\; \frac{m_\chi}{60\,\mu_{i,+}^2}\,\frac{1}{w\,u}\Big[\Big(\mu_i\,(4\,w+u)+(w+4\,u)\Big)\,(w-u)^3\,|w-u| \\ -\Big((4\,\mu_i+1)\,w-(\mu_i+4)\Big)\,(w+u)^4)\Big]\,.\end{aligned} \tag{4.63}$$

One can also perform analytically the velocity integrals. If there is no cutoff in the DM velocity distribution, i.e., $v_c(r)=\infty$, the equation to be solved to obtain the solution for T_χ can be written as [125]

$$\sum_i \int_0^{R_\odot} \sigma_{i,0}\; n_i(r)\,\frac{m_\chi m_i}{(m_i+m_\chi)^2}\left(\frac{m_i T_\chi + m_\chi T_\odot(r)}{m_\chi m_i}\right)^{1/2}\,\Big(T_\odot(r)-T_\chi\Big)\,e^{\frac{-m_\chi\,\phi(r)}{T_\chi}}\,r^2\,\mathrm{d}r = 0\,. \tag{4.64}$$

On the other hand, if there is a (position-dependent) cutoff on the DM velocity distribution at $v_c(r)$ and we define $T_c(r)\equiv m_\chi v_c^2(r)/2$, then

$$\begin{aligned}\epsilon_{i,const}(r,T_\chi,T_c) \;=\; & \frac{N_\chi\,e^{-m_\chi\,\phi(r)/T_\chi}}{\left(\mathrm{Erf}\left(\sqrt{\frac{T_c(r)}{T_\chi}}\right)-\sqrt{\frac{4\,T_c(r)}{\pi\,T_\chi}}\,e^{-T_c(r)/T_\chi}\right)\,4\pi\int_0^{R_\odot}\mathrm{d}r\,r^2\,e^{-m_\chi\phi(r)/T_\chi}} \\ & \times\frac{2}{\sqrt{\pi}}\,\frac{\mu_i}{\mu_{i,+}^2}\,\sqrt{\frac{2}{m_\chi}}\,n_i(r)\,\sigma_{i,0}\Big\{ \\ & \mathrm{Erf}\left(\sqrt{\frac{T_c(r)}{\mu_i\,T_\odot(r)}}\right)\frac{e^{-T_c(r)/T_\chi}}{\sqrt{T_\chi}}\left[\frac{1}{2}\left(\frac{\mu_i}{2}\,T_\odot(r)+T_c(r)\right)^2\right. \\ & \left.-\left(\frac{\mu_i}{2}\,T_\odot(r)\right)^2-\left(\frac{\mu_i}{2}\,T_\odot(r)+T_\chi+T_c(r)\right)\Big(T_\odot(r)-T_\chi\Big)\right] \\ & +\sqrt{\frac{\mu_i\,T_c(r)\,T_\odot(r)}{\pi\,T_\chi}}\,e^{-\left(\frac{T_c(r)}{T_\chi}+\frac{T_c(r)}{\mu_i T_\odot(r)}\right)}\left[\frac{1}{2}\left(\frac{\mu_i}{2}\,T_\odot(r)+T_c(r)\right)-\Big(T_\odot(r)-T_\chi\Big)\right] \\ & +\Big(\mu_i\,T_\odot(r)+T_\chi\Big)^{1/2}\,\Big(T_\odot(r)-T_\chi\Big)\,\mathrm{Erf}\left(\sqrt{\frac{T_c(r)}{T_\chi}+\frac{T_c(r)}{\mu_i\,T_\odot(r)}}\right)\Big\}\,.\end{aligned} \tag{4.65}$$

4.2.2 Velocity-Dependent Cross Section: $v_{\rm rel}^2$

In a similar way, for $\sigma_{i,v_{\rm rel}^2} \propto v_{\rm rel}^2$, the expression for the $\cos\theta$ integral reads

$$\int_{-1}^{1} \mathrm{d}\cos\theta\, |\boldsymbol{w}-\boldsymbol{u}|\,\langle \Delta E_i\rangle = \frac{m_\chi}{140\,\mu_{i,+}^2\,v_0^2}\,\frac{1}{w\,u}\Big[\Big(\mu_i\,(6\,w+u)+(w+6\,u)\Big)\,(w-u)^5\,|w-u| - \Big((6\,\mu_i+1)\,w-(\mu_i+6)\Big)\,(w+u)^6\Big)\Big]\,. \tag{4.66}$$

Again, the velocity integrals can be performed analytically. In the case with no cutoff in the DM velocity distribution, the equivalent equation to Eq. (4.64) is

$$\sum_i \int_0^{\mathrm{R}_\odot} \sigma_{i,0}\; n_i(r)\,\frac{m_\chi m_i}{(m_i+m_\chi)^2}\left(\frac{m_i T_\chi + m_\chi T_\odot(r)}{m_\chi m_i}\right)^{3/2}\left(T_\odot(r)-T_\chi\right)\,e^{\frac{-m_\chi\,\phi(r)}{T_\chi}}\,r^2\,\mathrm{d}r = 0\,. \tag{4.67}$$

The expression for $\epsilon_{i,v_{\rm rel}^2}$ with cutoff at a velocity $v_c(r)$ reads

$$\begin{aligned}
\epsilon_{i,v_{\rm rel}^2}(r,T_\chi,T_c) = {} & \frac{N_\chi\,e^{-m_\chi\,\phi(r)/T_\chi}}{\left(\mathrm{Erf}\left(\sqrt{\frac{T_c(r)}{T_\chi}}\right)-\sqrt{\frac{4\,T_c(r)}{\pi\,T_\chi}}\,e^{-T_c(r)/T_\chi}\right)4\pi\int_0^{R_\odot}\mathrm{d}r\,r^2\,e^{-m_\chi\phi(r)/T_\chi}} \\
& \times\frac{12}{m_\chi}\sqrt{\frac{2}{\pi\,m_\chi}}\,\frac{\mu_i}{\mu_{i,+}^2}\,n_i(r)\,\frac{\sigma_{i,0}}{v_0^2}\left\{\mathrm{Erf}\left(\sqrt{\frac{T_c(r)}{\mu_i\,T_\odot(r)}}\right)\frac{e^{-T_c(r)/T_\chi}}{\sqrt{T_\chi}}\right. \\
& \times\left[3\left(\frac{3\,\mu_i^2}{4}T_\odot^2(r)-2\,T_c^2(r)-\left(2\,T_\chi+\frac{3\,\mu_i}{2}\,T_\odot(r)\right)^2\right)\left(T_\odot(r)-T_\chi-T_c(r)\right)\right. \\
& \left.+\left(9\,\mu_i\,T_c(r)\,T_\odot(r)-12\,T_\chi\,T_\odot(r)-18\,\mu_i\,T_\odot^2(r)-4\,T_c^2(r)-\frac{3\,\mu_i^3}{4}\,\frac{T_\odot^3(r)}{T_c(r)}\right)T_c(r)\right] \\
& +\sqrt{\frac{\mu_i\,T_c(r)\,T_\odot(r)}{\pi\,T_\chi}}\,e^{-\left(\frac{T_c(r)}{T_\chi}+\frac{T_c(r)}{\mu_i T_\odot(r)}\right)}\left[\left(\frac{\mu_i\,m_\chi}{16}\,\frac{T_\odot(r)}{T_c(r)}+\frac{\mu_i}{30}\,T_\odot(r)+\frac{T_c(r)}{6}\right)T_c(r)\right. \\
& \left.-\left(T_\chi+\frac{5\,\mu_i}{4}\,T_\odot(r)+\frac{T_c(r)}{2}\right)\left(T_\odot(r)-T_\chi\right)\right] \\
& \left.+\left(T_\chi+\mu_i\,T_\odot(r)\right)^{3/2}\left(T_\odot(r)-T_\chi\right)\mathrm{Erf}\left(\sqrt{\frac{T_c(r)}{T_\chi}+\frac{T_c(r)}{\mu_i T_\odot(r)}}\right)\right\}
\end{aligned} \tag{4.68}$$

4.2.3 Momentum-Dependent Cross Section: q^2

For q^2-dependent cross sections, the results are the same as for the $v_{\rm rel}^2$-dependent case, except from a constant factor,

$$\epsilon_{i,q^2}(r,T_\chi,T_c) = \frac{4}{3}\left(\frac{m_\chi\,v_0}{q_0}\right)^2\,\epsilon_{i,v_{\rm rel}^2}(r,T_\chi,T_c)\,. \tag{4.69}$$

Therefore, the temperature T_χ in the isothermal approximation for the $v_{\rm rel}^2$-dependent and q^2-dependent cases, with the cross sections as defined in this work, is the same as long as condition of no net energy flow, Eq. (4.54), is applied.

4.2.4 Correction to the Temperature Calculation: Including Evaporation

So far, as done always in the literature, to compute the temperature of the isothermal distribution in the optically thin regime, we have assumed there is not net flow of energy carried away by DM particles, i.e., DM particles are assumed to be confined within the Sun. However, for low DM masses (typically below a few GeV), evaporation from the Sun is very efficient, so there is indeed a net flux of energy. Indeed, a correction becomes crucial to even find a solution in some cases. Therefore, Eq. (4.54) needs to be modified in order to take into account the energy carried out of the Sun by the evaporated DM particles, i.e.,

$$\sum_i \int_0^{R_\odot} \epsilon_i(r, T_\chi, T_c)\, 4\pi r^2\, \mathrm{d}r = \sum_i \int_0^{R_\odot} \epsilon_{evap,i}(r, T_\chi, T_c)\, 4\pi r^2\, \mathrm{d}r\,, \tag{4.70}$$

where, in general,

$$\epsilon_{evap,i}(r, T_\chi, T_c) = \int \mathrm{d}^3\boldsymbol{w}\, n_{\chi,iso}(r,t)\, f_{\chi,iso}(\boldsymbol{w}, r) \left[\int_{v_e(r)}^{w} K_i^-(w \to v)\, \mathrm{d}v + \int_w^\infty K_i^+(w \to v)\, \mathrm{d}v\right], \tag{4.71}$$

with the rates $K_i^\pm(w \to v)$ being equivalent to $R_i^\pm(w \to v)$, but including ΔE_i, i.e.,

$$\begin{aligned} K_i(w \to v) &= \int n_i(r)\, \frac{\mathrm{d}\sigma_i}{\mathrm{d}v}\, |\boldsymbol{w} - \boldsymbol{u}|\, \Delta E_i\, f_i(\boldsymbol{u}, r)\, \mathrm{d}^3\boldsymbol{u} \\ &= \Delta E_i\, R_i(w \to v) = \frac{m_\chi}{2}\left(v^2 - w^2\right) R_i(w \to v)\,. \end{aligned} \tag{4.72}$$

If there is a cutoff in the DM velocity distribution such that $w \le v_c(r) \le v_e(r)$, then Eq. (4.71) gets simplified to

$$\epsilon_{evap,i}(r, T_\chi, T_c) = \int_0^{v_c(r)} n_{\chi,iso}(r,t)\, f_{\chi,iso}(\boldsymbol{w}, r)\, 4\pi w^2\, \mathrm{d}w \int_{v_e(r)}^\infty K_i^+(w \to v)\, \mathrm{d}v\,. \tag{4.73}$$

Therefore, although the left-hand sides of Eq. (4.70) for v_{rel}^2-dependent and q^2-dependent cross sections are proportional, the right-hand sides are not, which results in slightly different temperatures for low masses, for which the right-hand side matters. Also notice that we have not included the suppression factor appearing in the general expression of the evaporation rate, Eq. (4.14), because the approximation of the isothermal distribution is only valid in the Knudsen limit, for which $s(r) = 1$.

4.3 Propagation of Dark Matter in the Sun

4.3.1 Mean Free Path

The total mean free path of DM particles in the solar medium is defined as $\ell^{-1}(r) = \sum_i \ell_i^{-1}(r)$, where $\ell_i^{-1}(r) = \langle\sigma_i\rangle(r)\, n_i(r)$ is the partial mean free path for DM interactions with a thermal averaged scattering cross section $\langle\sigma_i\rangle(r)$ off targets with density $n_i(r)$. This thermal average is performed over the two initial (DM and targets) velocity distributions, i.e.,

$$\ell_i^{-1}(r) = n_i(r)\, \langle\sigma_i\rangle(r) = n_i(r) \int \mathrm{d}^3\boldsymbol{w}\, f_\chi(\boldsymbol{w}, r) \int \mathrm{d}^3\boldsymbol{u}\, f_i(\boldsymbol{u}, r)\, \sigma(\boldsymbol{w}, \boldsymbol{u})\,. \tag{4.74}$$

For velocity-independent and isotropic cross sections, with or without velocity cutoff, trivially,

$$\langle\sigma_i\rangle(r) = \sigma_{i,0}\,. \tag{4.75}$$

For the v_{rel}^2-dependent cross sections considered in this work, $\sigma_{i,v_{\rm rel}^2} \propto v_{\rm rel}^2$, Eq. (4.42), the thermal average reads

$$\langle\sigma_{i,v_{\rm rel}^2}\rangle(r) = \frac{\sigma_{i,0}}{v_0^2}\, 6\,\mu_{i,+}\,\frac{T_\odot(r)}{m_\chi} \times\left(\frac{\Sigma_{i,LTE}(r)\,\mathfrak{f}(K)\,n_{\chi,LTE}(r,t) + \Sigma_{i,iso}(r)\left(\frac{\mu_i\,T_\odot(r)+T_\chi}{2\,\mu_{i,+}\,T_\odot(r)}\right)(1-\mathfrak{f}(K))\;n_{\chi,iso}(r,t)}{\mathfrak{f}(K)\,n_{\chi,LTE}(r,t) + (1-\mathfrak{f}(K))\;n_{\chi,iso}(r,t)}\right), \tag{4.76}$$

where the position-dependent normalizations are given by

$$\Sigma_{i,LTE}(r) = 1 - \frac{1}{6\,\sqrt{\pi}\,\mu_{i,+}}\left(\frac{v_c(r)}{\tilde{v}_\chi(r)}\right)^3 \frac{e^{-v_c^2(r)/\tilde{v}_\chi^2(r)}}{\mathrm{Erf}\left(\frac{v_c(r)}{\tilde{v}_\chi(r)}\right) - \frac{2}{\sqrt{\pi}}\frac{v_c(r)}{\tilde{v}_\chi(r)}\,e^{-v_c^2(r)/\tilde{v}_\chi^2(r)}}, \tag{4.77}$$

$$\Sigma_{i,iso}(r) = 1 - \frac{\mu_i\,T_\odot(r)}{3\,\sqrt{\pi}\,\left(\mu_i\,T_\odot(r)+T_\chi\right)}\left(\frac{v_c(r)}{u_i(r)}\right)^2\left(\frac{v_c(r)}{v_\chi}\right)\frac{e^{-v_c^2(r)/v_\chi^2}}{\mathrm{Erf}\left(\frac{v_c(r)}{v_\chi}\right) - \frac{2}{\sqrt{\pi}}\frac{v_c(r)}{v_\chi}\,e^{-v_c^2(r)/v_\chi^2}}\,, \tag{4.78}$$

with $\tilde{v}_\chi^2(r) \equiv 2\,T_\odot(r)/m_\chi$ and $v_\chi^2 = 2\,T_\chi/m_\chi$. In case of no cutoff, $\Sigma_{i,LTE}(r) = \Sigma_{i,iso}(r) = 1$. The subscript LTE indicates that DM is in local thermodynamic equilibrium, i.e. $T_\chi = T_\chi(r) = T_\odot(r)$.

The calculation of the mean free path is mainly relevant in the conduction limit (optically thick regime), i.e., when $T_\chi(r) = T_\odot(r)$ and $\mathfrak{f}(K) = 1$, in which Eq. (4.76) gets simplified as

$$\langle\sigma_{i,v_{\rm rel}^2}\rangle(r) = \frac{\sigma_{i,0}}{v_0^2}\,6\,\mu_{i,+}\,\frac{T_\odot(r)}{m_\chi}\,\Sigma_{i,LTE}\,, \tag{4.79}$$

Similarly, for q^2-dependent cross sections, $\mathrm{d}\sigma_{i,q^2}/\mathrm{d}\cos\theta_{cm} \propto q^2$, Eq. (4.47),

$$\langle\sigma_{i,q^2}\rangle(r,v_c) = \left(\frac{m_\chi\,v_0}{q_0}\right)^2\langle\sigma_{i,v_{\rm rel}^2}\rangle(r,v_c)\,, \tag{4.80}$$

and thus, the mean free paths for v_{rel}^2-dependent and q^2-dependent cross sections coincide, as long as $\sigma_{i,0}$ is the same and $q_0 = m_\chi\,v_0$, for the cross sections as defined here.

4.3.2 Suppression Factor

The suppression factor $s(r)$ that accounts for the fraction of DM particles with velocities larger than the escape velocity (after the first interaction) that escape the Sun is defined as [232]

$$s(r) = \eta_{ang}(r)\,\eta_{mult}(r)\,e^{-\tau(r)}\,, \tag{4.81}$$

where $\tau(r) = \int_r^{R_\odot}\ell^{-1}(r')\,\mathrm{d}r'$ is the optical depth in the radial direction. The optical depth in a generic direction, denoted by the angle with respect to the radial direction, θ_r, is given by

$$\tau(r,\cos\theta_r) = \int_0^{l_\odot(r,\cos\theta_r)}\ell^{-1}(r')\,\mathrm{d}l\,, \tag{4.82}$$

where $l_\odot(r,\cos\theta_r) = -r\cos\theta_r + \sqrt{R_\odot^2 - r^2\,\sin^2\theta_r}$ and $r' = \sqrt{l^2 + r^2 + 2\,l\,r\,\cos\theta_r}$.

The factor $\eta_{ang}(r)$ takes into account that DM particles move in non-radial orbits and is defined as

$$\eta_{ang}(r) = e^{\tau(r)} \int_{-1}^{1} \gamma(\theta_r)\, e^{-\tau(r,\cos\theta_r)}\, \mathrm{d}\cos\theta_r \,, \tag{4.83}$$

where $\gamma(\theta_r)$ is the DM distribution in the polar angle. This was estimated in Ref. [232] assuming an isotropic distribution ($\gamma_0(\theta_r) = 1/2$) and including an approximate correction from the dipolar contribution ($\gamma_1(\theta_r) \propto \cos\theta_r$). In order to allow for a smooth transition between the optically thin and thick regimes, the estimate of Ref. [232] can be modified as [189]

$$\eta_{ang}(r) = \frac{7}{10}\, \frac{1 - e^{-10\,\tau(r)/7}}{\tau(r)} \,. \tag{4.84}$$

Note that for $\tau \lesssim 3$, this is a better estimate of $\eta_{ang}(r)$ than that of Ref. [232]. However, also note that this factor has extra dependencies on μ_i and on the type of interaction, but we do not refine it any further here.

The factor $\eta_{mult}(r)$ takes into account the possibility of DM particles escaping even after interacting several times. Following Ref. [232], we have estimated it in the general case when the probability of one DM particle with energy E_χ loosing a fraction of energy $\hat{E}_\chi(r) \equiv \frac{E_\chi}{T_\odot(r)} - \hat{\phi}(r)$ after one interaction, with $\hat{\phi}(r) \equiv \frac{m_\chi\, v_e^2(r)}{2\, T_\odot(r)}$ the local dimensionless escape energy, is given by $1 - e^{-\hat{E}_\chi(r)/\hat{\phi}(r)}$, instead of simply $\hat{E}_\chi(r)/\hat{\phi}(r)$, the latter being valid when this probability is small. In this case [232],

$$\begin{aligned} \eta_{mult}(r) &= e^{\tau(r)} \sum_{n=0}^{\infty} \int_0^{\infty} \mathrm{d}\hat{E}_\chi(r) \left(\frac{1}{n!}\left(1 - e^{-\hat{E}_\chi(r)/\hat{\phi}(r)}\right)^n\right) \left(e^{-\tau(r)}\, \frac{\tau^n(r)}{n!}\right) e^{-\hat{E}_\chi(r)} \\ &= {}_0F_1\left(;1+\hat{\phi}(r);\tau(r)\right) \,, \end{aligned} \tag{4.85}$$

where the first term in the integral represents the probability that the DM particle looses at least an energy $\hat{E}_\chi(r)$ after n interactions, the second term is the probability of n scatterings and the third term is the initial DM distribution above the escape velocity. The result is the confluent hypergeometric limit function ${}_0F_1\,(;b;z)$. In order to correct for the fact that the probability of scattering to higher energies is finite because the medium is not at zero temperature and to correct the collision rate to take into account the targets thermal velocity in the DM-target relative velocity, in analogy with Ref. [232], finally we estimate it as

$$\eta_{mult}(r) = {}_0F_1\left(;1+\frac{2}{3}\,\hat{\phi}(r);\tau(r)\right) \,. \tag{4.86}$$

In the limit $\hat{\phi}(r) \gg 1$, which applies to most of the relevant parameter space, this factor reduces to $\eta_{mult}(r) = e^{1.5\,\tau(r)/\hat{\phi}(r)}$ [232]. In the opposite limit, $\hat{\phi}(r) \ll 1$, $\eta_{mult}(r) = I_0\left(2\,\sqrt{\tau(r)}\right)$, where $I_0(x)$ is the modified Bessel function of the first kind of order 0.

4.4 A Note on the Numerical Implementation of Erf

During the course of this study, spurious numerical results were encountered for the capture and evaporation rates at small $\mu\,(\sim 0.01)$ [6]. The origin of the inconsistent results was traced to the default intrinsic implementation of error function in standard programming language libraries (including the latest versions Fortran, Mathematica and C++). In this section, issue regarding the error function is briefly illustrated and a reasonable solution is proposed.

[6] Differential scattering rates are strictly positive definite; however, contrary numerical results were obtained

From the derivation of the differential scattering rates, it is clear that the functional form generally involves differences of two error functions, with similar but different arguments, see Eqs. (4.41), (4.46), and (4.52). To recap, consider the expression for the rate of down scattering (R^-) when the target particles are protons, for constant isotropic cross section

$$R^-_{const}(w \to v) = \frac{2}{\sqrt{\pi}} \frac{\mu_+^2}{\mu} \frac{v}{w} n(r) \sigma_0 \left[\chi(-\alpha_-, \alpha_+) + \chi(-\beta_-, \beta_+) \, e^{\mu\left(w^2 - v^2\right)/u^2(r)} \right] , \tag{4.87}$$

with $\chi(a, b)$ defined in Eq. (4.35). In practice

$$\chi(a, b) = \frac{\sqrt{\pi}}{2} \left(\text{Erf[b]} - \text{Erf[a]}\right) . \tag{4.88}$$

As discussed in the beginning of this chapter, we're often tasked with integrating Eq. (4.87) in final velocity v. Spurious functional behavior of $R^{\pm}$ translates to spurious numerical results for the capture and evaporation rate, upon integration.

General implementation of the Erf (and complimentary Erf) in most programming languages utilizes (unless otherwise specified) the following routine obtained by Chebyshev fitting [233]. Below is the routine presented in Numerical Recipes [233] for the complimentary error function:

```
FUNCTION erfcc(x)
REAL*8 erfcc,x
!Returns the complementary error function erfc(x)
! with fractional error everywhere less than 1.2d-7
REAL*8 t,z
z=abs(x)
t=1.d0/(1.d0+0.5d0*z)
erfcc=t*exp(-z*z-1.26551223d0+t*(1.00002368d0+t*(.37409196d0+
$ t*(.09678418d0+t*(-.18628806d0+t*(.27886807d0+t*(-1.13520398d0+
$ t*(1.48851587d0+t*(-.82215223d0+t*.17087277d0)))))))))
if (x.lt.0.d0) erfcc=2.d0-erfcc
return
END
```

Notice that the prescribed fractional error for this routine $\sim 10^{-7}$.

Alternatively, the integral representation of Erf can be used at arbitrary precision. Erf written in terms of incomplete Gamma functions is

$$\text{Erf}(z) = \frac{1}{\sqrt{\pi}} \gamma(\frac{1}{2}, z^2), \tag{4.89}$$

with

$$\gamma(a, x) = \int_0^x t^{a-1} e^{-t} \mathrm{d}t. \tag{4.90}$$

Now we evaluate R^-_{const} for the following set of parameters, $v \to 0.002042409$, $\omega \to 0.002314015$ and $u^{-2} \to 34932.84$; and graphically illustrate the evaluation in Fig. 4.2, blue dashed line corresponds to values of R^-_{const} obtained with the default implementation of the Erf, and solid gold when integral representation Eq. (4.89) is used. Notice that the curves coincide for large values of μ but not for small values of μ. Thus the artificial cancellations inherent in the fitting formula presented above is cured by the usage of the more exact expression Eq. (4.89).

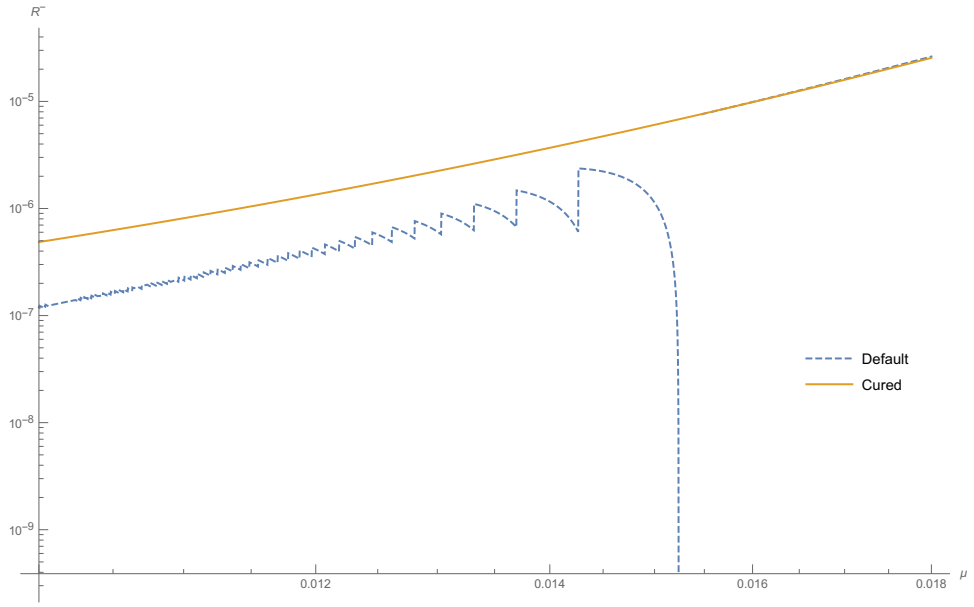

Figure 4.2: ***Differential rate R^{-}_{const} as a function μ:*** The function R^{-}_{const} evaluated at $v \to 0.002042409$, $\omega \to 0.002314015$ and $u^{-2} \to 34932.84$. Blue dashed line corresponds to values of R^{-}_{const} obtained with the default implementation of the Erf (the fitting formula), and solid gold when integral representation Eq. (4.89) is used.

CHAPTER 5

Scattering off Electrons vs Nucleons

The possibility of DM particles having no direct couplings to quarks, but only to leptons, the so-called leptophilic scenarios, has been extensively considered in the literature; to alleviate the conflict of the DM interpretation [228, 234–240] between the signal observed at the DAMA experiment [37] and the null results of other direct searches [45, 47–49, 241–245], for future strategies to search for sub-GeV DM particles with direct detection experiments [62, 246–248], within the context of cosmic-ray anomalies in order to explain the positron, but not antiproton, excess [210, 249–253] seen by different experiments [108, 254–258], to reduce the tension of the observed anomaly in the muon magnetic moment [259] or as potential signals in collider searches [260].

Even in the case of tree-level DM couplings to electrons, in general, loop-induced DM-quark couplings are also present by coupling photons to virtual leptons [228]. Therefore, DM would be captured in the Sun by both, interactions off solar electrons via tree-level processes and interactions off solar nuclei via loop processes. However, there are cases in which no loop-induced DM-quark contribution is present, such as axial vector couplings and thus, only DM capture by electrons is possible. Neutrino signals for leptophilic scenarios have been considered in Ref. [228]. In that work, a constant (velocity-independent and isotropic) cross section was assumed to compute the solar capture rate of DM particles. However, DM-electron (and DM-nucleon) interactions could have a more complicated structure and non-trivial dependencies on the relative velocity ($v_{\rm rel}$) and the scattering angle ($\theta_{\rm cm}$) do appear for various operators [213–227]. Indeed, these possibilities, assuming couplings only to quarks, have been recently considered in the context of high-energy neutrino signals from the Sun [165, 170, 174], to reduce the tension between solar models and helioseismological data [211, 261–265], and to allow for a better compatibility among different results from direct searches [266–282].

In this chapter, we present general results for the solar DM capture, annihilation and evaporation rates, as well as for the resulting neutrino fluxes from DM annihilations at production, for the cases of interactions with electrons with constant, $v_{\rm rel}^2$-dependent and transfer momentum (q^2)-dependent elastic scattering cross sections. All our results are compared to those obtained for the case of DM interactions with nucleons. We perform all computations taking into account thermal effects and study their importance. Moreover, we improve over the common calculation of the rates in a number of ways. We consistently compute the temperature in the regime of weak cross sections (Knudsen limit or optically thin regime) for each case including the effect of evaporation and the truncation of the DM velocity distribution, for which we also consider several cutoff velocities. We compute the minimum DM mass for which evaporation is not efficient enough to reduce the number of captured DM particles and find that, for the case of DM-electron scatterings, depending on the cutoff velocity, the minimum testable mass could be significantly smaller (below GeV) than the usually quoted evaporation mass in the case of DM-nucleon interactions. Finally, we compare the neutrino rates at production resulting from capture by electrons and nuclei. This is relevant to evaluate the importance of electron capture

in leptophilic scenarios, which will be studied elsewhere [6].
This chapter is organized as follows. In Section 5.2 we describe different types of interactions we consider. In Section 5.3 we review the calculation of the capture rate and compare the results of capture by solar electrons and nuclei. In Section 5.4 we describe the velocity and radial distribution of DM particles in the Sun once equilibrium is attained and show the resulting temperature in the optically thin regime for the different types of interactions and targets (electrons and nuclei). With this at hand, we write down the expression for the annihilation rate. In Section 5.5 we review the calculation of the evaporation rate and illustrate our results. In Section 5.6 we compute the minimum testable mass below which evaporation is very effective for the different cases under study, including the case of asymmetric DM. In Section 5.7 we compare the neutrino rates at production obtained for capture by electrons and by nuclei for the different cross sections we consider. Note that, some of the equations presented in chapter 4 is repeated here for clarity.

5.1 Dark Matter in the Local Neighbourhood

The differential capture rate is proportional to the the number of DM particles (n_χ) and the velocity distribution of DM in the solar neighbourhood $f_\odot(u)$ [1], hence it is of some importance to have a good understanding of the properties of the DM population in the solar neighbourhood.

Consider the spatial distribution of the DM density $\rho_\chi(r)$ in the Milky Way. Determining the rotation curve (which is directly an indicator of $\rho_\chi(r)$, since the curves simply trace the gravitational potential) of the Milky Way is a tedious task since all observations are necessarily done from within the Galactic plane. In spite of the dreadful situation, we can fairly estimate the local density of DM via indirect astrophysical methods and N-body simulations of Milky Way like halos [283–285]. According to PDG [1] the local DM density is

$$\rho_\chi(r_\odot) \equiv \rho_\chi = (0.39 \pm 0.03) \cdot (1.2 \pm 0.2) \cdot (1 \pm \delta_{\rm triax}) \, \frac{\rm GeV}{\rm cm^3}, \tag{5.1}$$

where, $\delta_{\rm triax} \leq 0.2$ accounts for the possible non-sphericity of the Milky Way halo [286]. The impact of uncertainties on direct and indirect DM searches has been extensively studied in the literature, see [287] for a recent review. In this study, we conservatively take $\rho_\chi = 0.3\,{\rm GeV/cm^3}$. Since ρ_χ is an overall normalization, the results presented here can be rescaled conveniently.

Recently, simulation of Milky Way like galaxies, including baryonic effects have become realistic and robust. Thus, we can estimate the DM velocity distribution and local density better, see [288] for a recent review on the topic. However, due to differences in hydrodynamical approach, cosmological parameters, and definitions of physical quantities, the simulations analyzed in [288] exhibit a variety of local velocity distributions. In Fig. 5.1 the local DM velocity distributions $f(v)$ in the Galactic rest frame for Miky Way-like halos in different hydrodynamical simulations (solid colored lines) which have the farthest velocity distribution from the Standard Halo Model (SHM) Maxwellian with a peak velocity of 220 km/s (dashed black line) is shown [288]. The halos shown in Fig. 5.1 are g2.79e12 from NIHAO [289], E3 from EAGLE HR [290], g1536 from MaGICC [291], and h258 from Sloane et.al. [292]. Thus, there exists a large variation in local velocity distributions between the results of different simulations.

In this study we simply consider a M-B distribution of DM in the galactic rest frame [2]. It is known

[1] The differential recoil rate is proportional to n_χ and the velocity distribution at Earth $f_\oplus(u)$ in direct detection experiments.
[2] To obtain velocity distribution at the Sun, $f(v)$ is boosted to the solar frame $f_\odot(v) = f(|v+v_\odot|)$, and for the distribution at Earth, $f(v)$ is boosted to the lab frame $f_\oplus(v) = f(|v+v_\oplus|)$.

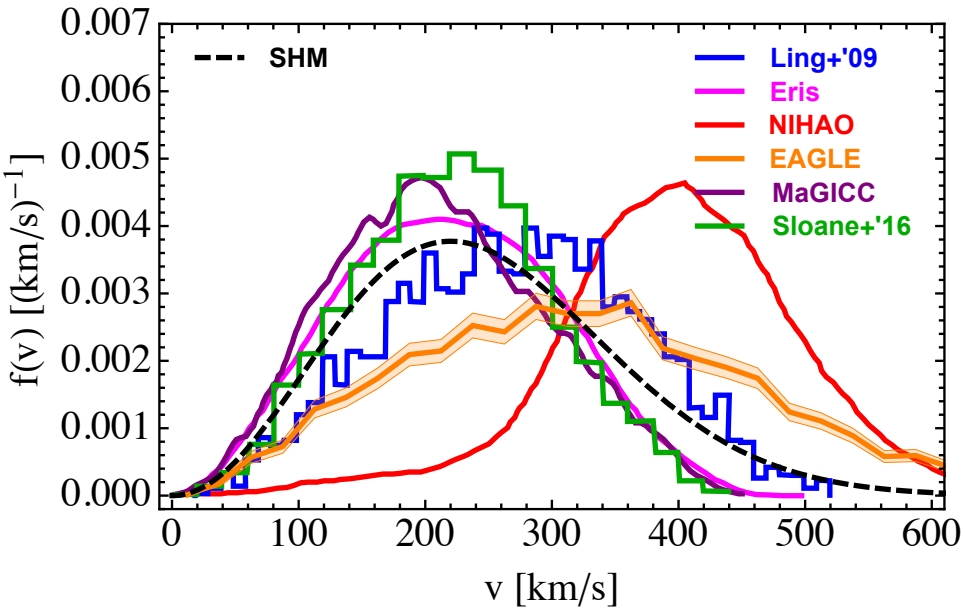

Figure 5.1: ***Predictions for DM velocity distribution in the galactic rest frame from hydrodynamic simulations:***Local DM speed distributions in the Galactic rest frame for Miky Way-like halos in different hydrodynamical simulations (solid colored lines) which have the farthest speed distribution from the SHM Maxwellian with a peak speed of 220 km/s (dashed black line) [288].

that deviation from M-B distribution does not significantly change the capture rate for constant spin dependent and independent cross sections, where the corrections are of order 10%, and $< 50\%$ for heavy DM [293]. Since the capture rate is sensitive to small DM velocities in the halo, changes to the high velocity part of the distribution does not greatly impact capture rate, but changes in the most probable DM velocity ($rms - velocity$) mostly contributes to corrections. Using a more realistic distribution such as the one shown in Fig. 5.1 is expected to yield $10 - 50\%$ correction (barring NIHAO) to the capture rates for constant spin dependent and independent cross sections, however a quantitative study on the impact on velocity and momentum dependent cross sections is lacking.

5.2 Scattering Cross Sections

The scattering rates that govern the capture and evaporation rates of DM particles in the Sun scale with the scattering cross section in the Knudsen limit (optically thin regime). For the case of interactions off free electrons, the single-particle total (constant) cross section, which appears in the scattering rates, is simply given by $\sigma_e = \sigma_{e,0}$. However, in the case of interactions off nuclei i, depending on the type of interactions, either spin-dependent (SD) or spin-independent (SI), the total (constant) DM-nucleus cross sections, at zero momentum transfer, are given, in terms of the DM-proton and DM-neutron cross sections, by

$$\sigma^{\rm SD}_{i,0} = \left(\frac{\tilde{\mu}_{A_i}}{\tilde{\mu}_p}\right)^2 \frac{4\,(J_i+1)}{3\,J_i} \left| \langle S_{p,i}\rangle + {\rm sign}(a_{\rm p}a_{\rm n}) \left(\frac{\tilde{\mu}_p}{\tilde{\mu}_n}\right) \sqrt{\frac{\sigma^{\rm SD}_{n,0}}{\sigma^{\rm SD}_{p,0}}}\, \langle S_{n,i}\rangle \right|^2 \sigma^{\rm SD}_{p,0}\,, \tag{5.2}$$

$$\sigma^{\rm SI}_{i,0} = \left(\frac{\tilde{\mu}_{A_i}}{\tilde{\mu}_p}\right)^2 \left| Z_i + (A_i - Z_i)\,{\rm sign}(f_p f_n) \left(\frac{\tilde{\mu}_p}{\tilde{\mu}_n}\right) \sqrt{\frac{\sigma^{\rm SI}_{n,0}}{\sigma^{\rm SI}_{p,0}}} \right|^2 \sigma^{\rm SI}_{p,0}\,, \tag{5.3}$$

where $\tilde{\mu}_{A_i}$ ($\tilde{\mu}_{p/n}$) is the reduced mass of the DM-nucleus i (DM-proton/neutron) system, $\sigma^{\rm SD}_{p,0}$ ($\sigma^{\rm SD}_{n,0}$) and $\sigma^{\rm SI}_{p,0}$ ($\sigma^{\rm SI}_{n,0}$) are the SD and SI elastic scattering DM cross section off protons (neutrons), respectively, Z_i, A_i and J_i are the atomic number, the mass number and the total angular momentum of the nucleus i, and $\langle S_{p,i}\rangle$ and $\langle S_{n,i}\rangle$ are the expectation values of the spins of protons and neutrons averaged over all nucleons, which we take[3] from Refs. [116, 294–297] (see Ref. [298] for a review). The quantities a_p (f_p) and a_n (f_n) are the axial (scalar) four-fermion DM-nucleon couplings. As usually done, we assume $\tilde{\mu}_n^2\,\sigma^{\rm SD}_{p,0} = \tilde{\mu}_p^2\,\sigma^{\rm SD}_{n,0}$, $\tilde{\mu}_n^2\,\sigma^{\rm SI}_{p,0} = \tilde{\mu}_p^2\,\sigma^{\rm SI}_{n,0}$ and the same sign for the couplings, so Eqs. (5.2) and (5.3) get simplified as

$$\sigma^{\rm SD}_{i,0} = \left(\frac{\tilde{\mu}_{A_i}}{\tilde{\mu}_p}\right)^2 \frac{4\,(J_i+1)}{3\,J_i}\,\left|\langle S_{p,i}\rangle + \langle S_{n,i}\rangle\right|^2\,\sigma^{\rm SD}_{p,0}\,, \tag{5.4}$$

$$\sigma^{\rm SI}_{i,0} = \left(\frac{\tilde{\mu}_{A_i}}{\tilde{\mu}_p}\right)^2 A_i^2\,\sigma^{\rm SI}_{p,0}\,. \tag{5.5}$$

In the case of SD cross sections, the coupling with protons is the one which is mainly probed because almost all DM interactions are off hydrogen.
However, only in the case of constant cross sections, the scattering rate directly depends on the total cross section. For velocity-dependent and momentum-dependent cross sections, the differential cross section enters the calculation. In addition to the usual constant (velocity-independent and isotropic) cross section case, we also consider $v_{\rm rel}^2$-dependent (isotropic) and q^2-dependent cross sections, where $v_{\rm rel}$ and q are the relative DM-target velocity and the transfer momentum, respectively. The differential cross sections (in the limit of zero transfer momentum[4]) for the constant, $v_{\rm rel}^2$-dependent and q^2-dependent cases can be written as

$$\frac{{\rm d}\sigma_{i,{\rm const}}(v_{\rm rel},\cos\theta_{\rm cm})}{{\rm d}\cos\theta_{\rm cm}} = \frac{\sigma_{i,0}}{2}\,, \tag{5.6}$$

$$\frac{{\rm d}\sigma_{i,v_{\rm rel}^2}(v_{\rm rel},\cos\theta_{\rm cm})}{{\rm d}\cos\theta_{\rm cm}} = \frac{\sigma_{i,0}}{2}\left(\frac{v_{\rm rel}}{v_0}\right)^2\,, \tag{5.7}$$

$$\frac{{\rm d}\sigma_{i,q^2}(v_{\rm rel},\cos\theta_{\rm cm})}{{\rm d}\cos\theta_{\rm cm}} = \frac{\sigma_{i,0}}{2}\,\frac{(1+m_\chi/m_i)^2}{2}\left(\frac{q}{q_0}\right)^2\,, \tag{5.8}$$

where $\theta_{\rm cm}$ is the center-of-mass scattering angle, v_0 and q_0 are a reference relative velocity and transfer momentum, and m_χ and m_i are the DM and target i masses, respectively. The mass-dependent term in Eq. (5.8) is included so that the total q^2-dependent cross section is equal to the $v_{\rm rel}^2$-dependent cross section when $q_0 = m_\chi\,v_0$ and $\sigma_{i,0}$ is the same in both cases, i.e., $\sigma_{i,v_{\rm rel}^2} = \sigma_{i,q^2} = \sigma_{i,0}\,(v_{\rm rel}/v_0)^2$. In this work, we use $v_0 = 220$ km/s. See Sec. 4.1 for further comments, definitions and for a description of how the differential cross sections enter the calculation of the differential scattering rates.

5.3 Capture of Dark Matter by the Sun

DM particles from the galactic halo could get eventually captured by the Sun if, after scattering off solar targets (nuclei and electrons), they lose energy so that their resulting velocity is lower than the Sun's escape velocity at a distance r from the center of the Sun, $v_e(r)$. The capture rate of DM particles with mass m_χ for weak cross sections, for which the probability of interaction is

[3] For ^{14}N, we take $\langle S_{p,^{14}{\rm N}}\rangle = -0.130$ and $\langle S_{n,^{14}{\rm N}}\rangle = -0.106$, which we obtain by considering the proton and neutron as if they were the only unpaired nucleon within the odd-group model [116].

[4] In the case of interactions with nuclei, when the wavelength corresponding to the transfer momentum q is small compared to the nuclear size, the cross section is suppressed with increasing q. This is taken into account by the nuclear form factor, which we discuss in the next section.

small, is (to good approximation) given by

$$C_\odot^{\rm weak} = \sum_i \int_0^{R_\odot} 4\pi r^2 {\rm d}r \int_0^\infty {\rm d}u_\chi \left(\frac{\rho_\chi}{m_\chi}\right) \frac{f_{v_\odot}(u_\chi)}{u_\chi}\, w(r) \int_0^{v_e(r)} R_i^-(w\to v)\, |F_i(q)|^2\, {\rm d}v\,, \tag{5.9}$$

where the sum is over all possible targets. We consider electrons and 29 nuclei as targets and use their density and temperature distributions as determined within the standard solar model [114, 299] (see Ref. [300] for a recent update). The factor $R_i^-(w\to v)$ (and the analogous $R_i^+(w\to v)$) is the differential scattering rate at which a DM particle with velocity w scatters off a target with mass m_i to a final velocity $v < w$ ($v > w$). They are explicitly given in Sec. 4.1 for constant, $v_{\rm rel}^2$-dependent and q^2-dependent cross sections.

The nuclear form factor for nucleus i is $|F_i(q)|^2$, which we approximate as the one corresponding to a Gaussian nuclear density distribution with root-mean-square radius r_i (i.e., equal to that of a uniform sphere of radius $\sqrt{5/3}\, r_i$), i.e.,

$$|F_i(q)|^2 = e^{-q^2 r_i^2/3}\,. \tag{5.10}$$

For SI interactions [301],

$$r_i = \left(0.89\, A_i^{1/3} + 0.3\right)\ {\rm fm}\,, \tag{5.11}$$

and given that the nuclear density distribution is different from the spin distribution [302], for SD interactions [303],

$$r_i = \frac{\sqrt{3}}{2}\left(1.7\, A_i^{1/3} - 0.28 - 0.78\left(A_i^{1/3} - 3.8 + \sqrt{\left(A_i^{1/3} - 3.8\right)^2 + 0.2}\right)\right)\ {\rm fm}\,. \tag{5.12}$$

For electrons and hydrogen, $F_e(q^2) = F_H(q^2) = 1$.

A few comments are in order. Note that a more realistic Woods-Saxon nuclear density distribution (for SI interactions) results in a form factor which is very similar to Eq. (5.10) for relatively low $q\, r_i$ values [116, 296]. Moreover, Eq. (5.9) is strictly correct if target nuclei are assumed to be at rest (for electrons and hydrogen, it is always correct as $F_e(q^2) = F_H(q^2) = 1$). In that case: $q^2 = m_i\, m_\chi\, (w^2 - v^2)$. Otherwise, up-scatterings with a final velocity below the escape velocity must also be considered (a term with the $R_i^+(w\to v)$ factor) and the nuclear form factor cannot be factored out, but has to be included in the calculation of the differential scattering rates $R_i^-(w\to v)$ and $R_i^+(w\to v)$. However, the former correction is negligible and, given the current uncertainties, the fact that we are not using more accurate nuclear response functions [215, 226, 227] and that in the end factoring out the nuclear form factor represents at most an overall 10% (much smaller in the constant case) reduction with respect to the results from Eq. (5.9) for the case of SI interactions only, we do not refine the calculation further and consider the form factor as computed in the zero-temperature limit (but not the differential scattering rates), so that it can be factored out in Eq. (5.9) and the analytical expressions in Sec. 4.1 can be used.

The local DM density is given by $\rho_\chi = 0.3$ GeV/cm^3, $R_\odot$ is the Sun radius and $f_{v_\odot}(u_\chi)$ is the halo velocity distribution seen by an observer moving at speed $v_\odot$, the speed of the Sun with respect to the DM rest frame,

$$f_{v_\odot}(u_\chi) = \frac{1}{2}\int_{-1}^{1} f_{\rm gal}\left(\sqrt{u_\chi^2 + v_\odot^2 + 2\, u_\chi\, v_\odot\, \cos\theta_\odot}\right) {\rm d}\cos\theta_\odot\,, \tag{5.13}$$

where u_χ is the DM velocity at infinity in the Sun's rest frame, $\cos\theta_\odot$ is the angle between the DM and the solar system velocities and $f_{\rm gal}(u_{\rm gal})$ is the DM velocity distribution in the galactic rest

frame, which is assumed to be a M-B distribution (the so-called standard halo model) and thus,

$$f_{v_\odot}(u_\chi) = \sqrt{\frac{3}{2\,\pi}}\,\frac{u_\chi}{v_\odot\,v_d}\left(e^{-\frac{3\,(u_\chi - v_\odot)^2}{2\,v_d^2}} - e^{-\frac{3\,(u_\chi + v_\odot)^2}{2\,v_d^2}}\right), \tag{5.14}$$

with $w^2(r) = u_\chi^2 + v_e^2(r)$, the square of the DM velocity at a distance r from the center of the Sun. We take the values $v_\odot = 220$ km/s for the velocity of the Sun with respect to the DM rest frame and thus, $v_d = 270$ km/s $\simeq \sqrt{3/2}\,v_\odot$ for the velocity dispersion. Actually, $f_{\rm gal}(u_{\rm gal})$ does not extend beyond the local galactic escape velocity, $v_{\rm esc,gal} = 533^{+54}_{-41}$ km/s at 90% confidence level [304]. However, this represents a correction on the capture rate below the percent level [293], much smaller than the very same form of the velocity distribution [162, 182, 293]. Finally, note that we are assuming the Sun to be in free space, but the presence of the planets (mainly Jupiter) could affect the solar capture rate[5], mainly for heavier DM particles for which the low-velocity tail is more important [313]. Nevertheless, it has been recently shown that planetary diffusion of DM particles in and out of the solar loss cone (orbits crossing the Sun) would result in a complete cancellation of the effect, so the free-space approximation is very accurate, as long as gravitational equilibrium has been reached (in the case of constant scattering cross sections off nucleons, for $m_\chi = 100$ GeV, this occurs for $\sigma^{\rm SD} \gtrsim 10^{-44}$ cm^2 for SD interactions and for $\sigma^{\rm SI} \gtrsim 10^{-46}$ cm^2 for SI interactions) [314].

On the other hand, Eq. (5.9) is only valid for weak scattering cross sections, such that the probability of interaction is very small: the capture rate cannot grow indefinitely with the cross section. The saturation value for the capture rate is set by the geometrical cross section of the Sun (when the probability of interaction and capture is equal to one) [189, 315],

$$C_\odot^{\rm geom} = \pi R_\odot^2\left(\frac{\rho_\chi}{m_\chi}\right)\int_0^\infty {\rm d}u_\chi\, f_{v_\odot}(u_\chi)\,\frac{\omega^2(R_\odot)}{u_\chi} = \pi R_\odot^2\left(\frac{\rho_\chi}{m_\chi}\right)\langle v\rangle_0\left(1 + \frac{3}{2}\,\frac{v_e^2(R_\odot)}{v_d^2}\right)\xi(v_\odot, v_d)\,, \tag{5.15}$$

where $\langle v\rangle_0 = \sqrt{8/(3\pi)}\,v_d$ is the average speed in the DM rest frame and the factor $\xi(v_\odot, v_d)$ takes into account the suppression due to the motion of the Sun ($\xi(v_\odot = 0, v_d) = 1$),

$$\xi(v_\odot, v_d) \equiv \frac{v_d^2\,e^{-\frac{3\,v_\odot^2}{2\,v_d^2}} + \sqrt{\frac{\pi}{6}}\,\frac{v_d}{v_\odot}\left(v_d^2 + 3\,v_e^2(R_\odot) + 3\,v_\odot^2\right){\rm Erf}\left(\sqrt{\frac{3}{2}}\,\frac{v_\odot}{v_d}\right)}{2\,v_d^2 + 3\,v_e^2(R_\odot)}\,. \tag{5.16}$$

For the chosen values of $v_\odot$ and v_d, $\xi(v_\odot = 220\,{\rm km/s}, v_d = 270\,{\rm km/s}) \simeq 0.81$. Finally, in order to allow for a smooth transition between these two regimes, we estimate the capture rate as [189]

$$C_\odot = C_\odot^{\rm weak}\left(1 - e^{-C_\odot^{\rm geom}/C_\odot^{\rm weak}}\right). \tag{5.17}$$

In the left panels of Fig. 5.2, we show the capture rates as a function of the DM mass for the case of DM-electron interactions (solid red curves), DM-nucleon SD interactions (dashed green curves) and DM-nucleon SI interactions (dot-dashed blue curves), for constant cross sections with $\sigma_{i,0} = 10^{-40}$ cm^2 (top panels), $v_{\rm rel}^2$-dependent cross sections with $\sigma_{i,0} = 10^{-42}$ cm^2 (middle panels) and for cross sections with q^2 dependence with $\sigma_{i,0} = 10^{-42}$ cm^2 (bottom panels). In each panel, we also indicate the geometric limit (dashed black curve), Eq. (5.15). We stress again that even for leptophilic DM models, in general, interactions with nucleons are possible via loop processes, so the capture rates by nuclei are relevant and need to be considered.

In the case of constant cross sections (top-left panel), for high DM masses, capture by nuclei is several orders of magnitude (up to two for SD and four for SI) larger than capture by electrons.

[5] See Refs. [305–312] for discussions about the effects of the Sun and planets on the DM capture rate by the Earth.

The differences decrease for lower masses and capture by electrons is comparable or larger for $m_\chi \lesssim 1$ GeV, which can be relevant if the DM velocity distribution has a cutoff at $v_c(r) < v_e(r)$ (see below). The results for $v_{\rm rel}^2$-dependent and q^2-dependent cross sections are similar to each other (for the normalizations used in this work). Unlike for constant cross sections, in these cases, at high masses the capture rate by electrons is a factor of a few larger than capture by nuclei via SD interactions and the differences with respect to the SI capture rate decrease, being of three orders of magnitude. These results can be understood from the even more important impact of thermal effects for these cross sections as compared to the constant case and can have important consequences in some models [6]. Moreover, the SD capture rate is much smaller than the SI case (up to four orders of magnitude). Overall, the capture rate via $v_{\rm rel}^2$-dependent and q^2-dependent cross sections is a factor of about four, three and two orders of magnitude larger than the case with constant cross sections (assuming the same $\sigma_{i,0}$ for all cases) for capture by electrons, SI and SD interactions off nucleons, respectively.

In the right panels of Fig. 5.2, we illustrate the impact of thermal effects on the capture rates. From Eq. 5.18, we see that the behavior of the ratio of the full capture rate to the capture rate at zero temperature ($C_\odot/C_\odot^{T=0}$) is driven by two competing factors: the ratio of the solar temperature to the DM escape energy, $2\,T_\odot/(m_\chi\, v_e^2(r)) = u_i^2(r)/(\mu_i\, v_e^2(r))$, where $u_i(r)$ is the most probable speed of the targets at position r, and the ratio of the targets thermal speed to the escape velocity. Whereas a larger average kinetic energy of the DM particles suppresses capture, thermal effects enlarge the range of velocities contributing to it. For the same cases of the left panels, we show the ratio of the capture rates obtained using the thermal distribution of the target particles with respect to the capture rates obtained in the limit $T_\odot(r) = 0$, i.e., when the targets are at rest.

In the case of velocity-independent and isotropic cross sections, as discussed in Ref. [228] and as can be seen in the top-right panel, thermal effects represent an order of magnitude correction if the target particles are electrons. However, the correction in the case of interactions with nucleons is very small for $m_\chi \gtrsim 1$ GeV. These differences can be explained by the larger thermal speed of electrons as compared to that for nuclei i by a factor $\sqrt{m_i/m_e}$. In the case of $v_{\rm rel}^2$-dependent and q^2-dependent cross sections, thermal effects on the capture rates by electrons are very important and represent an increase of three orders of magnitude in the range of masses we show. This can be understood from the extra $u_i^2(r)/v_0^2 \sim$ few GeV$/m_i$ factors in the differential scattering rates $R^-_{i,v_{\rm rel}^2}(w \to v)$ and $R^-_{i,q^2}(w \to v)$ (see Sec. 4.1). For these cross sections, even in the case of capture by nucleons, thermal effects cannot always be neglected. For $m_\chi \gtrsim 1$ GeV, for DM-nucleon interactions the increase in the capture rate is of a few tens of percent for both, $v_{\rm rel}^2$-dependent and q^2-dependent cross sections, although for SI interactions the correction is negligible for $v_{\rm rel}^2$-dependent cross sections. On the other hand, for $m_\chi \lesssim 1$ GeV, for all cases, thermal effects *suppress* the capture rates contrary to the results at higher masses, given that $2\,T_\odot/(m_\chi v_e^2(r)) \sim 0.1$ GeV$/m_\chi$ and $u_i^2(r)/v_e^2(r) \sim 0.1$ GeV$/m_i$. Analytically, when the target particle is either proton or electron, for a constant scattering cross section the following relation holds

$$\frac{{\rm d}C_\odot}{{\rm d}C_\odot^{T=0}} \sim e^{\frac{T_{\rm core}}{20\, m_{e/p} v_{\rm esc}^2}} - \frac{{\rm Erf}\left(\frac{m_\chi v_{\rm esc}^2}{2T_\chi}\right)}{1+\sqrt{\frac{m_\chi}{m_{e,p}}}\left(\frac{m_\chi v_{\rm esc}^2}{2T_\chi}\right)}. \tag{5.18}$$

This explains the dip in the ratios for the case of DM-nucleon interactions at $m_\chi \sim 0.1$ GeV.

Finally, as mentioned above, we have checked that the correct calculation of the capture rate by nucleons (mainly for SI interactions), i.e., including the form factor in the $R_i^-(w \to v)$ factors, only represents a decrease of $\lesssim 10\%$ with respect to the results shown here.

For completeness, the capture rate of DM for scattering off individual elements in the Sun is depicted in Figs. 5.3, 5.4 and 5.5 for SI interactions, and Figs. 5.6, 5.7, 5.8 for SD interactions

with nucleons for all the cases considered here.

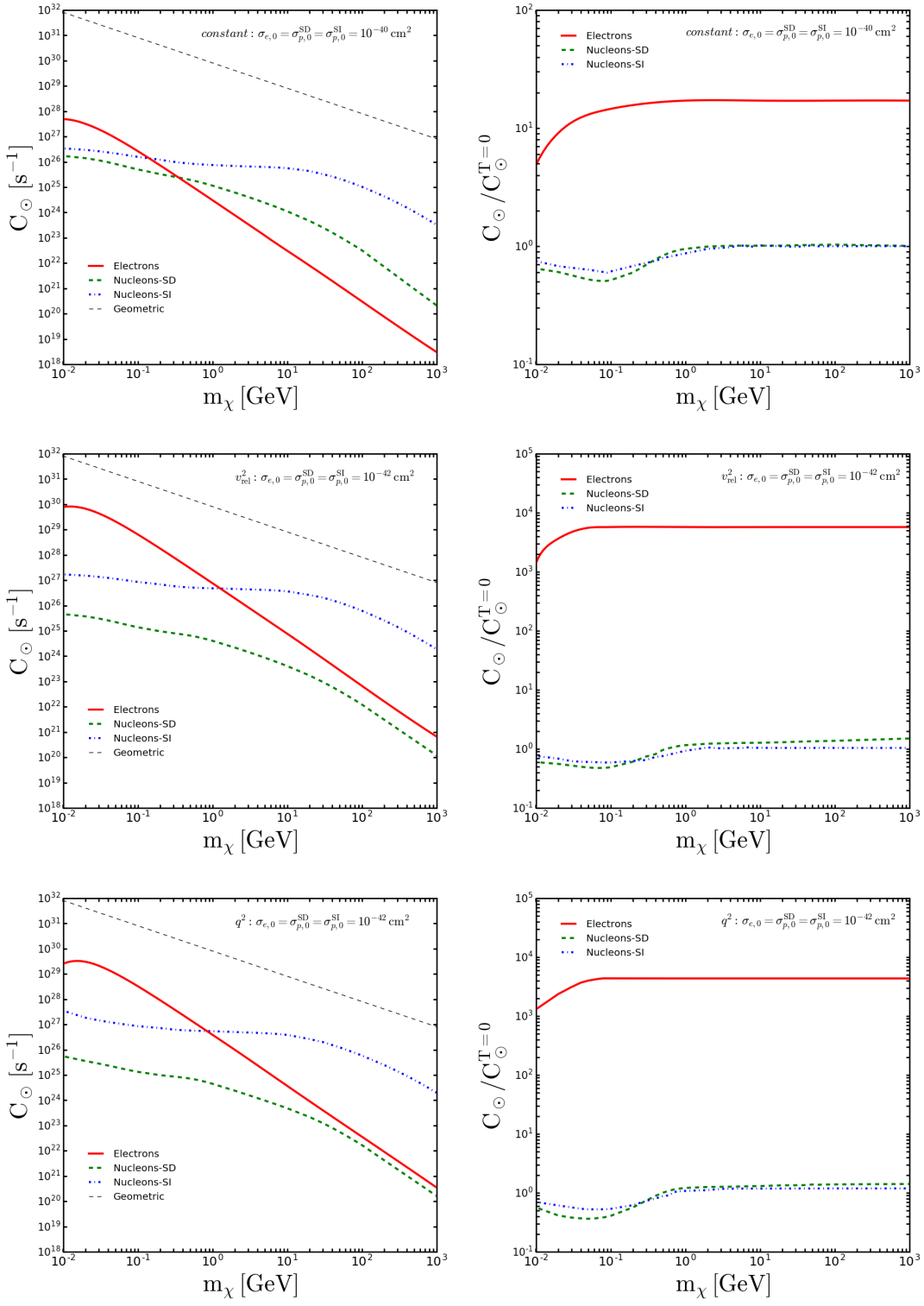

Figure 5.2: ***Capture rates as a function of the DM mass***, for DM-electron interactions (solid red curves), DM-nucleon SD interactions (dashed green curves) and DM-nucleon SI interactions (dot-dashed blue curves). *Left panels*: capture rates for the three types of interactions. The geometric capture rate is also shown (dashed black curves.) *Right panels*: ratio of capture rates with respect to the limit of targets at rest ($T_\odot(r) = 0$). *Top panels*: constant (velocity-independent and isotropic) scattering cross section with $\sigma_{i,0} = 10^{-40}$ cm^2. *Middle panels*: $v^2_{\rm rel}$-dependent scattering cross section with $\sigma_{i,0} = 10^{-42}$ cm^2. *Bottom panels*: q^2-dependent scattering cross section with $\sigma_{i,0} = 10^{-42}$ cm^2.

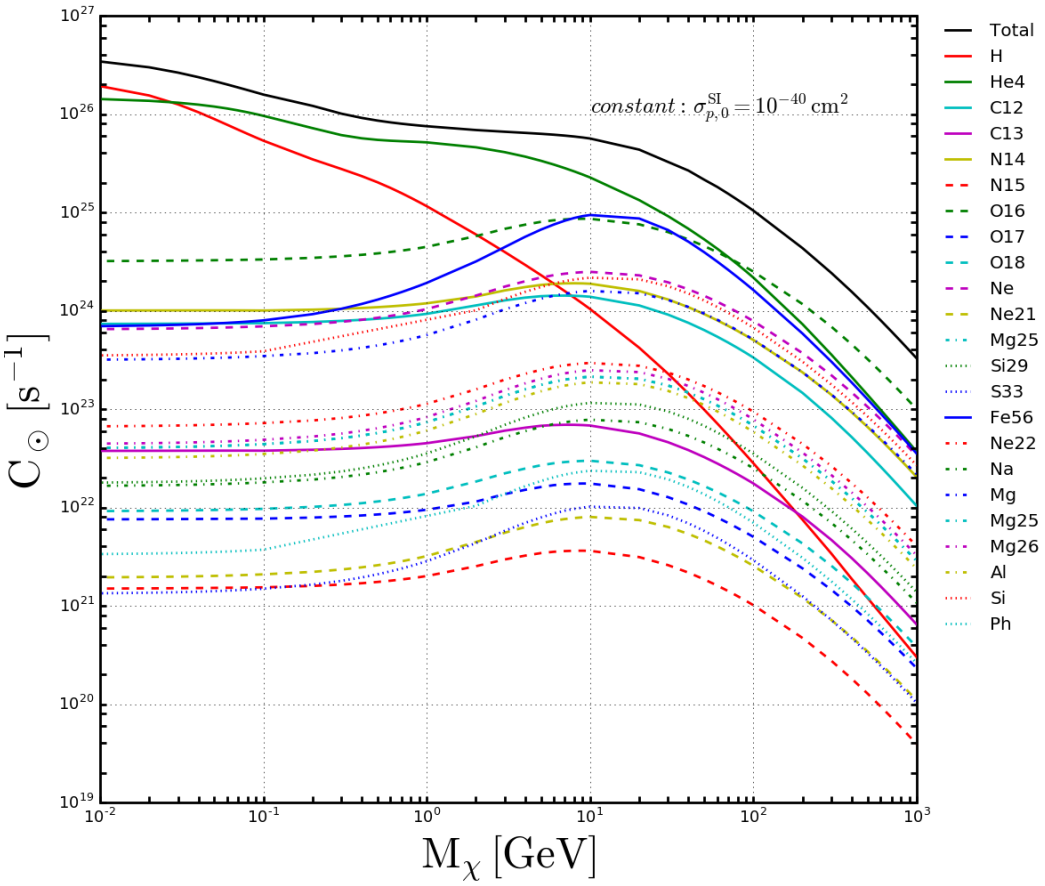

Figure 5.3: ***Capture Rate per individual element for constant cross section, SI:*** The legend corresponds to only the dominant target elements considered.

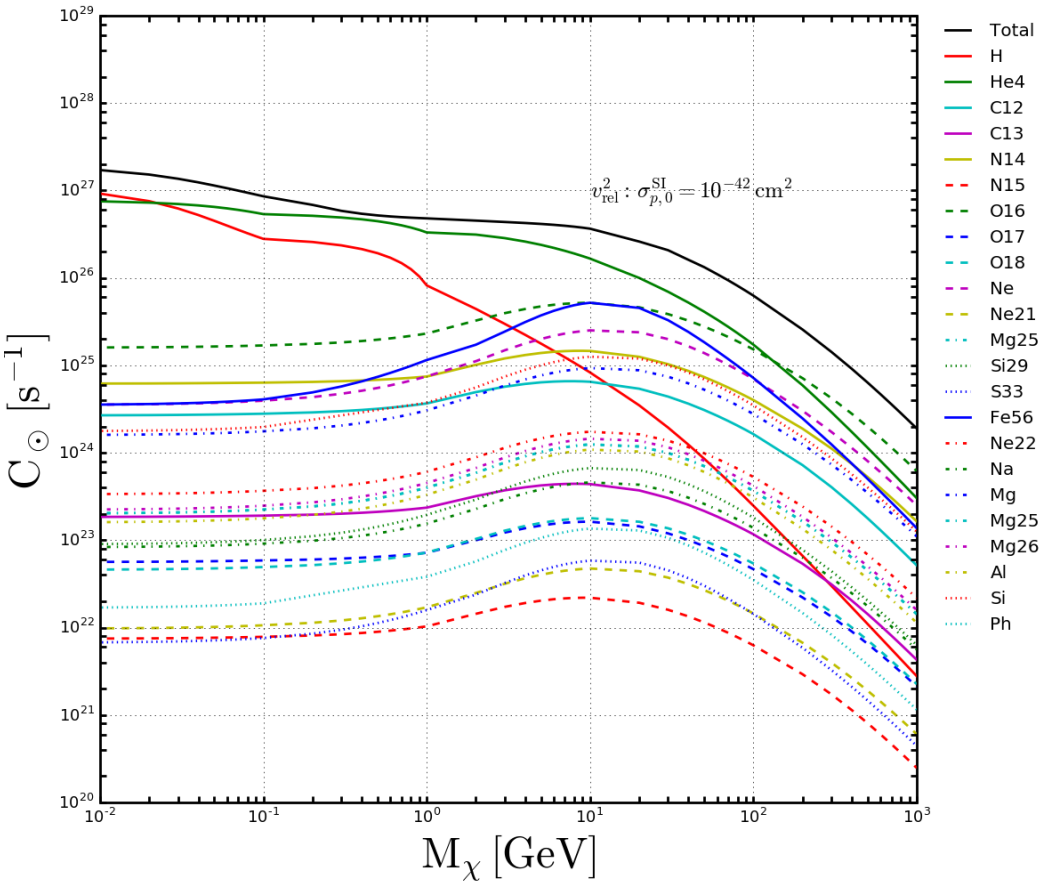

Figure 5.4: ***Capture Rate per individual element for velocity dependent isotropic cross section, SI:*** The legend corresponds to only the dominant target elements considered.

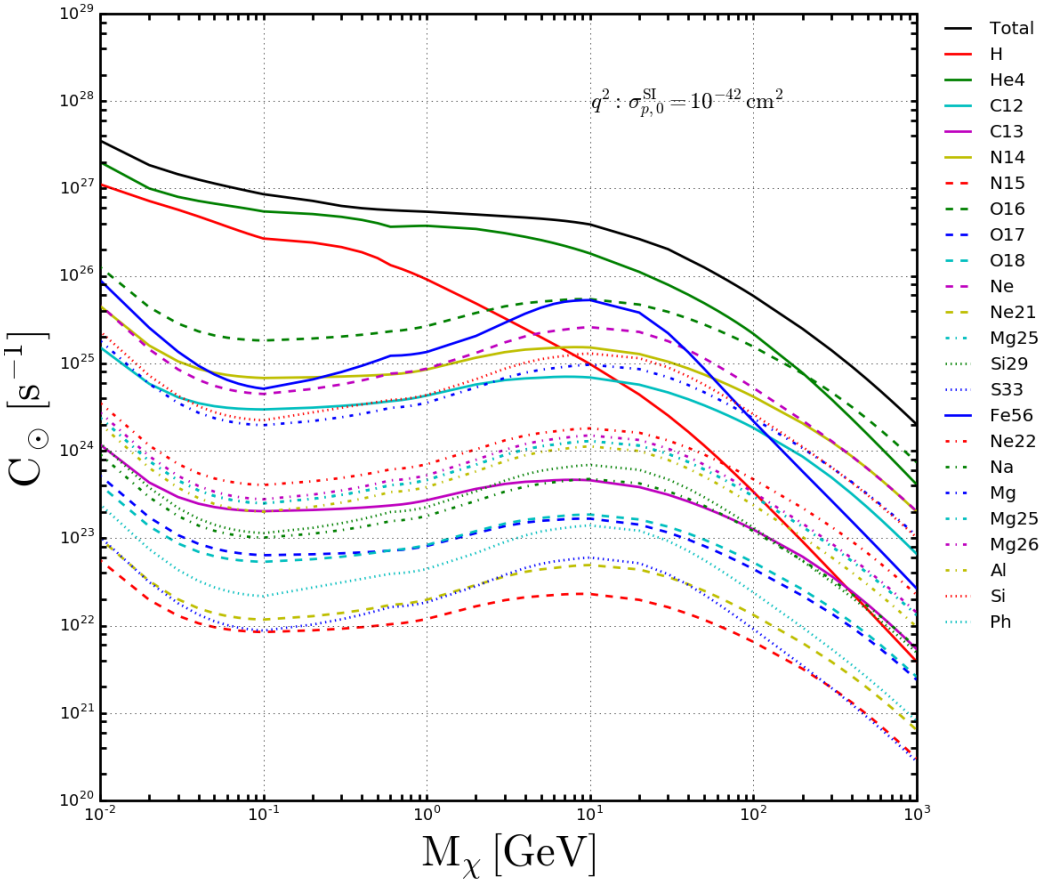

Figure 5.5: ***Capture Rate per individual element for momentum dependent cross section, SI:*** The legend corresponds to only the dominant target elements considered.

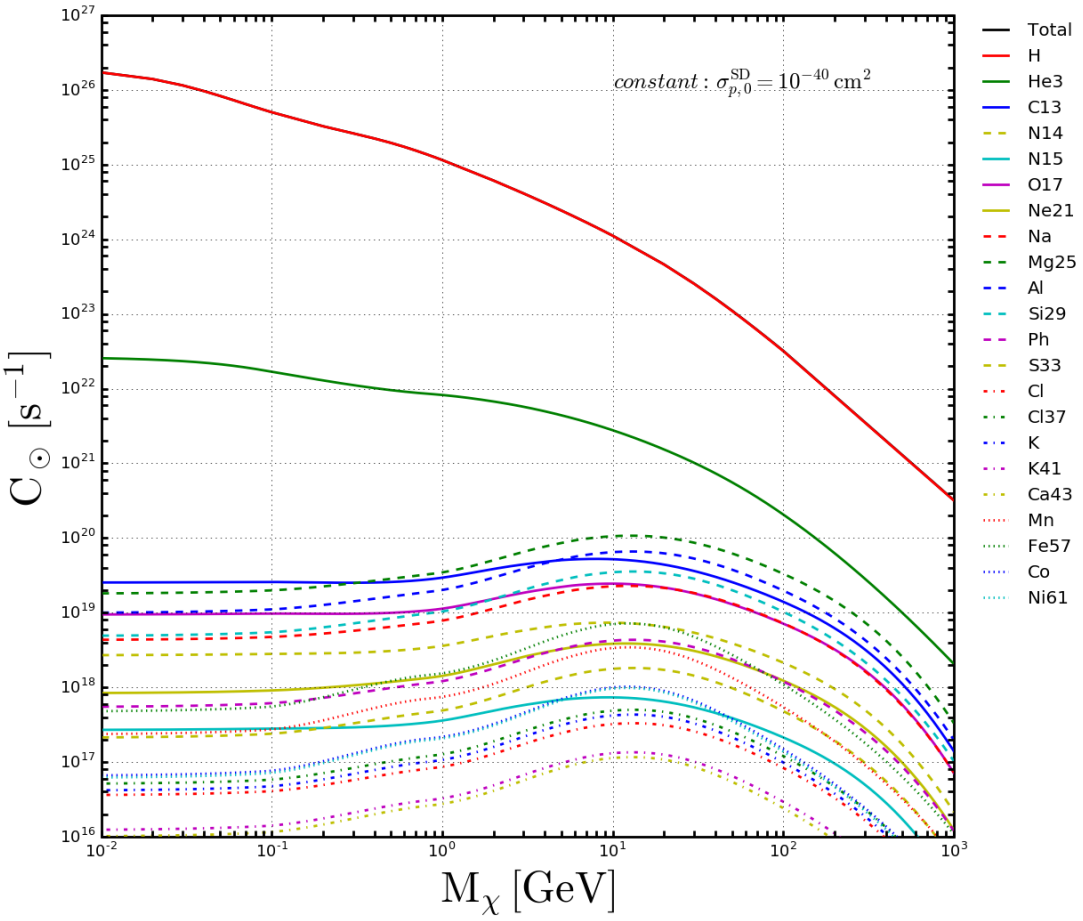

Figure 5.6: ***Capture Rate per individual element for constant cross section, SD:*** The legend corresponds to only the dominant target elements considered.

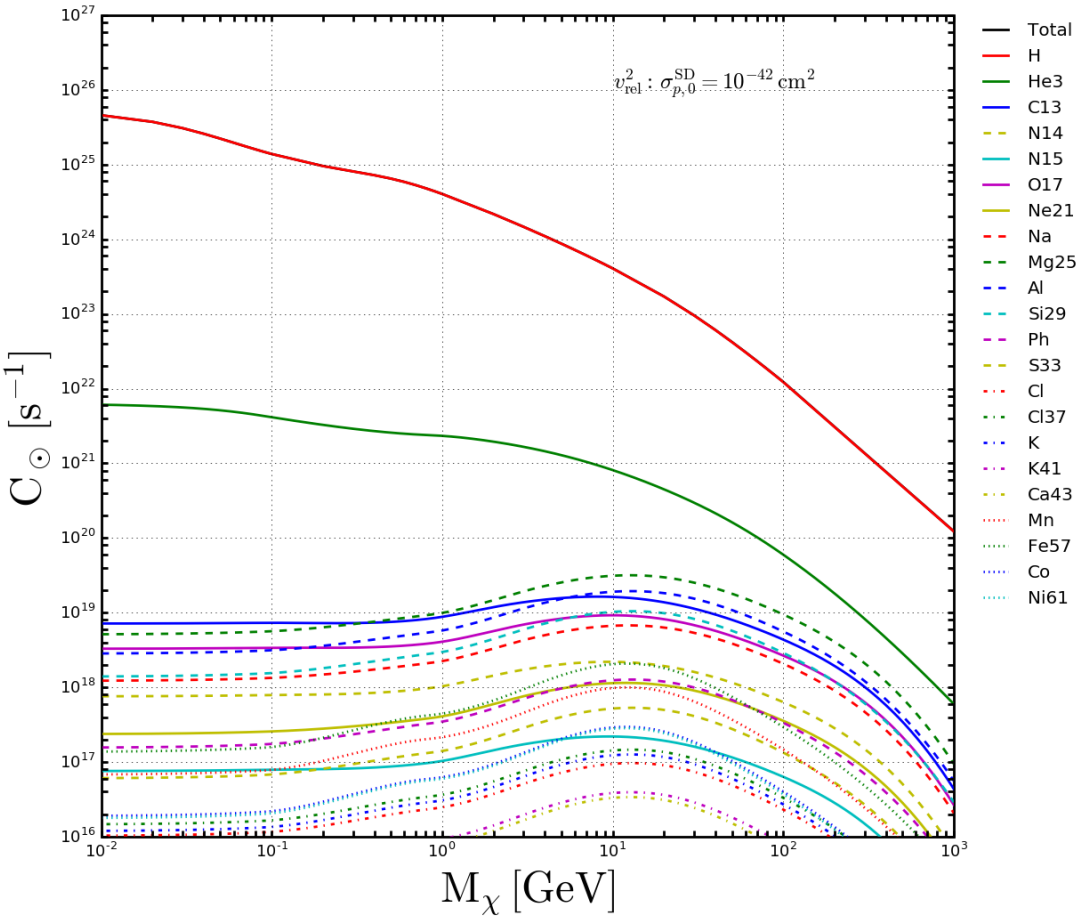

Figure 5.7: ***Capture Rate per individual element for velocity dependent isotropic cross section, SD:*** The legend corresponds to only the dominant target elements considered.

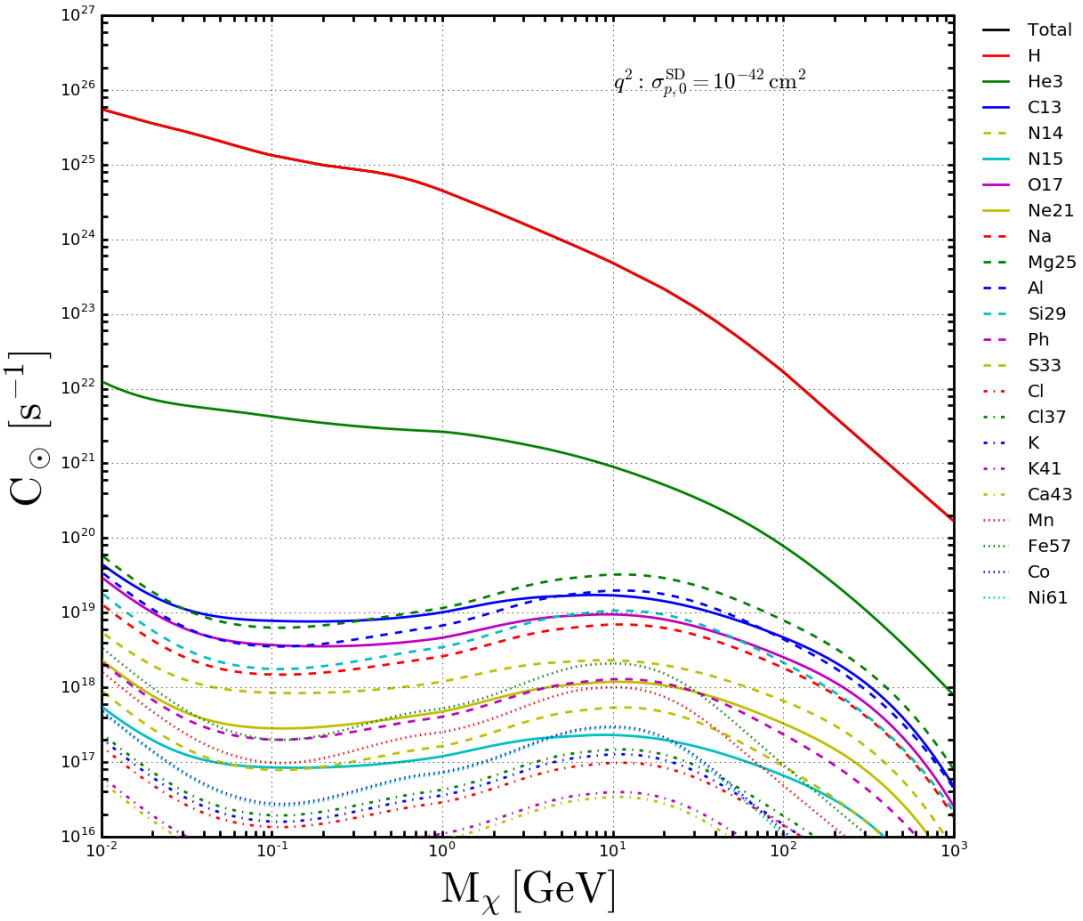

Figure 5.8: ***Capture Rate per individual element for momentum dependent cross section, SD:*** The legend corresponds to only the dominant target elements considered.

5.4 Dark Matter Distribution and Annihilation rate in the Sun

After DM particles are trapped inside the Sun, successive scatterings with the target material (nuclei and electrons), which is in local thermodynamic equilibrium (LTE), would thermalize them at a temperature $T_\chi(r)$. Therefore, the velocity distributions of target and DM particles can be assumed to have a M-B form,

$$f_i(\boldsymbol{u}, r) = \frac{1}{\sqrt{\pi^3}} \left(\frac{m_i}{2\,T_\odot(r)}\right)^{3/2} e^{-\frac{m_i u^2}{2\,T_\odot(r)}} , \tag{5.19}$$

$$f_\chi(\boldsymbol{w}, r) = \frac{e^{-w^2/v_\chi^2(r)}\ \Theta(v_c(r) - w)}{\sqrt{\pi^3}\ v_\chi^3(r) \left(\mathrm{Erf}\left(\frac{v_c(r)}{v_\chi(r)}\right) - \frac{2}{\sqrt{\pi}} \frac{v_c(r)}{v_\chi(r)}\, e^{-v_c^2(r)/v_\chi^2(r)}\right)} , \tag{5.20}$$

where $T_\odot(r)$ and $v_\chi(r) \equiv \sqrt{2\,T_\chi(r)/m_\chi}$ are the solar temperature and the thermal DM velocity at a distance r from the center of the Sun, respectively. Whereas in the case of large scattering cross sections (conduction limit or optically thick regime), DM particles would also be in LTE with the solar medium, i.e., $T_\chi(r) = T_\odot(r)$, in the case of weak cross sections (Knudsen limit or optically thin regime), the DM distribution could be approximated as being isothermal, i.e., with a single temperature, T_χ.

Note that we have included a cutoff in the DM velocity distribution, $v_c(r)$, which in general depends on the position (a valid assumption for circular orbits) and it is usually assumed to be equal to the escape velocity at a distance r from the center of the Sun, $v_c(r) = v_e(r)$, but we also consider another possibility, $v_c(r) = 0.9\,v_e(r)$. The last choice is motivated by the fact that the bulk of evaporation and annihilation takes place in the solar core and for DM particles only passing through the core such a cutoff is a reasonable approximation to the actual distribution function [128]. As apparent from the comparison of the results of this approximation with those of Refs. [128, 231], the actual non-thermal distribution (obtained by solving the collisional Boltzmann equation numerically) cannot be accurately mimicked by the approximate radial and truncated velocity distributions assumed in this work (and in most works in the literature). This has already been noted long ago, as the distribution function is locally non-isotropic with radial orbits always dominating and the local temperature in the Knudsen limit is not uniform [230].

As we will assume, in the case of weak cross sections, after DM particles are captured by the Sun, they would thermalize non-locally by multiple interactions, with a single isothermal (iso) distribution. In this limit (Knudsen limit), their radial distribution can be written as [88, 125, 126]

$$n_{\chi,\mathrm{iso}}(r,t) = N_\chi(t)\, \frac{e^{-m_\chi \phi(r)/T_\chi}}{\int_0^{R_\odot} e^{-m_\chi \phi(r)/T_\chi}\, 4\pi r^2\, \mathrm{d}r} , \tag{5.21}$$

which corresponds to an isothermal sphere following the law of atmospheres, with a radial dependence set by the gravitational potential $\phi(r) = \int_0^r G M_\odot(r')/r'^2\, \mathrm{d}r'$, with G the gravitational constant and $M_\odot(r)$ the solar mass at radius r, and where $N_\chi(t)$ is the total population of DM particles at a given time t.

A relatively simple semi-analytical method to treat the problem in the Knudsen limit was proposed in Ref. [125]. By assuming a Maxwell-Boltzmann velocity distribution for the DM and target particles, one can obtain a solution to the isothermal assumption by requiring the DM distribution to satisfy its first energy moment and solving for T_χ. By imposing that there is no net heat transferred between the two gases, the equation to be solved reads [125]

$$\sum_i \int_0^{R_\odot} \epsilon_i(r, T_\chi, v_c)\, 4\pi r^2\, \mathrm{d}r = 0 , \tag{5.22}$$

where

$$\epsilon_i(r, T_\chi, v_c) \equiv \int \mathrm{d}^3\boldsymbol{w}\, n_{\chi,\mathrm{iso}}(r, t_\odot)\, f_{\chi,\mathrm{iso}}(\boldsymbol{w}, r) \int \mathrm{d}^3\boldsymbol{u}\, n_i(r)\, f_i(\boldsymbol{u}, r)\, \sigma_{i,0}\, |\boldsymbol{w} - \boldsymbol{u}|\, \langle \Delta E_i \rangle \,, \tag{5.23}$$

is the energy transfer per unit volume and time, with $\langle \Delta E_i \rangle$ being the energy transfer per collision averaged over the scattering angle and $n_{\chi,\mathrm{iso}}(r, t_\odot)$ (see Eq. (5.21)) and $n_i(r)$ being the radial distributions of DM particles and targets i, respectively. As we mentioned above, this approximation relies on the assumption of a uniform and locally isotropic Maxwell-Boltzmann distribution for the DM particles, conditions which do not hold in a realistic situation [128, 230, 231]. Indeed, the above approximation overestimates the efficiency of energy transfer by a factor of a few, which depends on the DM and target mass ratio [230, 316, 317]. Baring in mind the approximated nature of this approach, which is the usual one followed in the literature, we also compute the DM distribution function in the Knudsen limit in this way. However, we implement two semi-analytical corrections. First, we perform the calculation with a cutoff in the DM velocity distribution, in order to be consistent with the inputs used for the computation of the annihilation and evaporation rates. Second, we also include the energy flow in the form of evaporated DM particles that escape the Sun, which is relevant for DM masses of a few GeV and below, so that the final equation we solve is

$$\sum_i \int_0^{R_\odot} \epsilon_i(r, T_\chi, v_c)\, 4\pi r^2\, \mathrm{d}r = \sum_i \int_0^{R_\odot} \epsilon_{\mathrm{evap},i}(r, T_\chi, v_c)\, 4\pi r^2\, \mathrm{d}r \,, \tag{5.24}$$

where $\epsilon_{\mathrm{evap},i}(r, T_\chi, v_c)$ is defined in Sec. 4.2. Indeed, when there is a velocity cutoff, in the case of interactions with electrons, unless this correction is included, wrong solutions are found for $m_\chi \lesssim 1.1$ GeV and $m_\chi \lesssim 1.5$ GeV and there are no solutions for $m_\chi \lesssim 0.4$ GeV and $m_\chi \lesssim 0.5$ GeV, for $v_c(r) = v_e(r)$ and $v_c(r) = 0.9\, v_e(r)$, respectively. All the relevant expressions for different types of cross sections (velocity-independent and isotropic, velocity-dependent and isotropic and momentum-dependent) and with a generic cutoff in the DM velocity distribution are provided in Sec. 4.2.

In Fig. 5.9 we show the results for the temperature as a function of the DM mass in the one-zone model or isothermal approximation for electrons (red curves), nucleons with SD (green curves) and SI (blue curves) interactions, for the case of no cutoff, $v_c(r) = \infty$, (solid curves), $v_c(r) = v_e(r)$ (dashed curves) and $v_c(r) = 0.9\, v_e(r)$ (dotted curves). We show the temperatures for constant (top panel), v_{rel}^2-dependent (bottom-left panel) and q^2-dependent (bottom-right panel) cross sections. For $m_\chi \gtrsim 2$ GeV, the temperatures for the three velocity distributions are practically equal, i.e., the cutoff has no effect. This can be understood by the fact that the larger the mass the lower the typical velocities of the DM particles and thus, the high-velocity tail of the distribution is less important. Notice also that all results converge in the large mass limit. For $m_\chi \lesssim 2$ GeV, the lower the cutoff velocity, the lower the temperature, but the differences are never larger than 10% for all shown cases. For these low masses, the temperature in the case of interactions off electrons is slightly larger than that obtained when DM interacts with nucleons, being relatively larger for v_{rel}^2-dependent and q^2-dependent cross sections. Notice also that, in the case of interactions with nucleons, the temperatures for the three cross section dependencies are very similar. In the case of thermalization with electrons, constant cross sections result in a bit lower temperatures than the other two cases (up to $\sim 10\%$), the differences getting reduced for low-cutoff velocities. Whereas for the no-cutoff case, for which the correction due to evaporation is negligible, the temperatures for v_{rel}^2-dependent and q^2-dependent cross sections (as defined in this work) are exactly equal (see Sec. 4.2), for the case with cutoff, v_{rel}^2-dependent cross sections result in slightly larger temperatures. Overall, the differences in the temperatures for the cases under consideration are small for the relevant range of masses and have a small impact on the final neutrino fluxes.

On the other hand, in the case of large scattering cross sections (conduction limit or optically

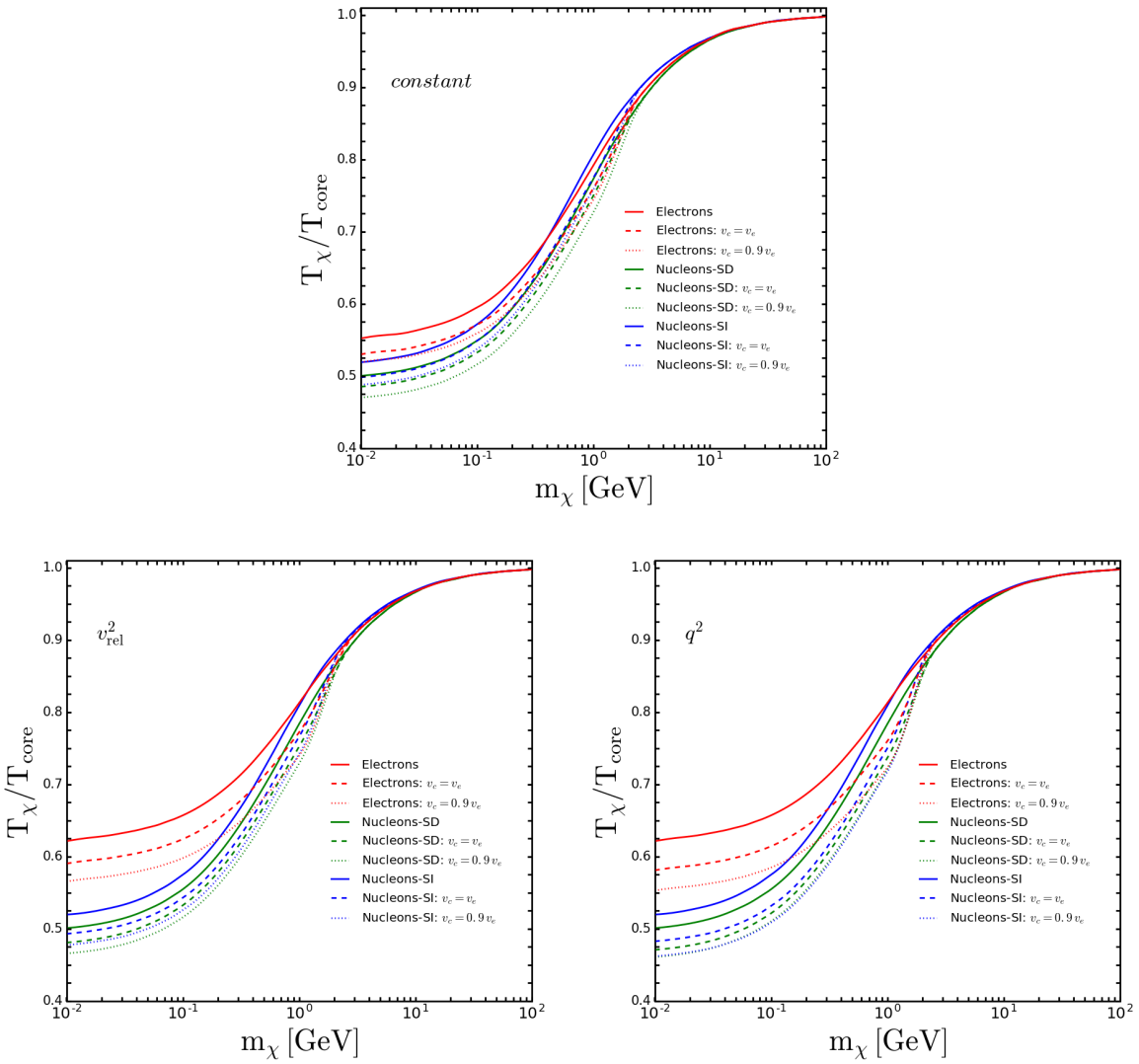

Figure 5.9: ***DM temperature as a function of the DM mass in the isothermal approximation***, in units of the solar core temperature, $T_{\rm core} \equiv T_\odot(0)$, for DM scattering off electrons (red curves), off nucleons via SD interactions (green curves) and off nucleons via SI interactions (blue curves), and for three DM velocity distributions: without cutoff (solid curves), with a cutoff at $v_c(r) = v_e(r)$ (dashed curves) and with a cutoff at $v_c(r) = 0.9\,v_e(r)$ (dotted curves). *Top panel*: constant (velocity-independent and isotropic) scattering cross sections. *Bottom-left panel*: $v_{\rm rel}^2$-dependent scattering cross sections. *Bottom-right panel:* q^2-dependent scattering cross sections.

thick regime), DM particles thermalize locally, i.e., $T_\chi = T_\odot(r)$, and the DM radial distribution can be approximated as [229, 317]

$$n_{\chi,\rm LTE}(r,t) = n_{\chi,\rm LTE,0}(t)\left(\frac{T_\odot(r)}{T_\odot(0)}\right)^{3/2} \exp\left(-\int_0^r \frac{\alpha(r')\frac{{\rm d}T_\odot(r',t)}{{\rm d}r'} + m_\chi\frac{{\rm d}\phi(r')}{{\rm d}r'}}{T_\odot(r')}\,{\rm d}r'\right), \tag{5.25}$$

where $n_{\chi,\rm LTE,0}(t)$ is set by the normalization $\int_0^{R_\odot} n_{\chi,\rm LTE}(r)\,4\pi r^2\,{\rm d}r = N_\chi(t)$. For an admixture of targets, a good approximation for the dimensionless thermal diffusivity $\alpha(r)$ is represented by

the weighted mean of the single-target solutions [229, 232],

$$\alpha(r) = \ell(r) \sum_i \ell_i^{-1}(r)\, \alpha_0(\mu_i) \,, \tag{5.26}$$

where $\alpha_0(\mu_i)$ is the thermal diffusivity for a single target and it is tabulated as a function of $\mu_i \equiv m_\chi/m_i$ in Ref. [229] for constant cross sections and in Ref. [262] for velocity-dependent and momentum-dependent cross sections. The total mean free path of DM particles in the solar medium is defined as $\ell^{-1}(r) = \sum_i \ell_i^{-1}(r)$, where $\ell_i(r) = (\langle\sigma_i\rangle(r)\, n_i(r))^{-1}$ is the partial mean free path for DM interactions at a distance r from the center of the Sun with a thermal averaged scattering cross section $\langle\sigma_i\rangle(r)$ off targets i with density $n_i(r)$. This thermal average is performed over the DM and target velocity distributions and is given by

$$\langle\sigma_i\rangle(r) = \int \mathrm{d}^3\boldsymbol{w}\, f_\chi(\boldsymbol{w}, r) \int \mathrm{d}^3\boldsymbol{u}\, f_i(\boldsymbol{u}, r)\, \sigma_i(\boldsymbol{w}, \boldsymbol{u}) \,. \tag{5.27}$$

The expressions for this thermal average for different types of cross sections (constant, velocity-dependent and momentum-dependent) are given in Sec. 4.3.1.
The transition from one regime to the other is indicated by the so-called Knudsen number,

$$K \equiv \frac{\ell(0)}{r_\chi} \,, \qquad r_\chi = \sqrt{\frac{3\, T_\odot(0)}{2\pi G\, \rho_\odot(0)\, m_\chi}} \,, \tag{5.28}$$

where r_χ is the approximate scale height of the DM distribution, with $\rho_\odot(0)$ the density at the solar center. The Knudsen limit corresponds to $K = \infty$. Note that the definition of the Knudsen number should in principle be a function of the position in the Sun. Nevertheless, given that most of the DM would be concentrated in the center of the Sun, this is sufficient for our purposes and a more accurate definition is beyond the scope of this paper.
Although the actual solution of the problem can only be obtained by solving the collisional Boltzmann equation, however, an approximate solution can be considered by interpolating between the optically thin ($K \gg 1$) and the optically thick ($K \ll 1$) regimes. In order to do so, we follow Refs. [212, 315], which motivated by the results of Ref. [229], approximated the DM radial and velocity distribution as

$$n_\chi(r,t)\, f_\chi(\boldsymbol{w}, r) \;=\; \mathfrak{f}(K)\, n_{\chi,\mathrm{LTE}}(r,t)\, f_{\chi,\mathrm{LTE}}(\boldsymbol{w}, r) + (1 - \mathfrak{f}(K))\; n_{\chi,\mathrm{iso}}(r,t)\, f_{\chi,\mathrm{iso}}(\boldsymbol{w}, r) \,, \tag{5.29}$$

$$\mathfrak{f}(K) = \frac{1}{1 + (K/K_0)^2} \,, \tag{5.30}$$

where $K_0 = 0.4$ is the value of the Knudsen number for which DM particles transport energy most efficiently [229]. This value was obtained by assuming a spherical harmonic oscillator potential and keeping the mean free path as a constant throughout the entire star, which is also the reason why we used the position-independent definition in Eq. (5.28). Note that a given K_0, which marks the transition from one regime to the other, corresponds to different values of $\sigma_{i,0}$ for different types of cross sections [264] and targets.
Once the DM distribution is known, we can compute the annihilation rate $A_\odot$, defined as

$$A_\odot = \frac{\int \mathrm{d}^3\boldsymbol{w_1} \int \mathrm{d}^3\boldsymbol{w_2}\, \sigma_A v_{\chi\chi} \int_0^{R_\odot} n_\chi(r,t)\, f_\chi(\boldsymbol{w_1}, r)\, n_\chi(r,t)\, f_\chi(\boldsymbol{w_2}, r)\, 4\pi r^2\, \mathrm{d}r}{\left(\int_0^{R_\odot} n_\chi(r,t)\, 4\pi r^2\, \mathrm{d}r\right)^2} \,, \tag{5.31}$$

where we have used

$$\int \mathrm{d}^3\boldsymbol{w}\, n_\chi(r,t)\, f_\chi(\boldsymbol{w}, r) = n_\chi(r,t) = \mathfrak{f}(K)\, n_{\chi,\mathrm{LTE}}(r,t) + (1 - \mathfrak{f}(K))\; n_{\chi,\mathrm{iso}}(r,t) \tag{5.32}$$

in the denominator and where $\sigma_A v_{\chi\chi}$ is the DM annihilation cross section times the relative velocity of the two DM particles, $v_{\chi\chi} = |\boldsymbol{w_2} - \boldsymbol{w_1}|$. In general, $\sigma_A v_{\chi\chi} = a + b\, v_{\chi\chi}^2$, but in this work, our default case is that of an s-wave annihilation cross section corresponding to a thermal DM candidate, i.e., $\langle \sigma_A v_{\chi\chi} \rangle = 3 \times 10^{-26}\,\mathrm{cm}^3/\mathrm{s}$, where $\langle\,\rangle$ denotes thermal average over the two DM velocity distributions. In such a case, Eq. (5.31) simplifies as

$$A_\odot = \langle \sigma_A v_{\chi\chi} \rangle \frac{\int_0^{R_\odot} n_\chi^2(r,t)\, 4\pi r^2\, \mathrm{d}r}{\left(\int_0^{R_\odot} n_\chi(r,t)\, 4\pi r^2\, \mathrm{d}r\right)^2} \,. \tag{5.33}$$

Note that for p-wave annihilations, for $v_{\rm rel}^2$-dependent and q^2-dependent cross sections equilibrium would be attained for smaller values of $\sigma_{i,0}$ than for the constant case, but we will not discuss this possibility here.

5.5 Evaporation Rate of Dark Matter from the Sun

In general, for sufficiently small DM masses, below a few GeV, interactions with the targets of the solar medium would bring most of the DM particles to velocities above the escape velocity $v_e(r)$, so that they can evaporate from the Sun. The evaporation rate is given by

$$E_\odot = \sum_i \int_0^{R_\odot} s(r)\, n_\chi(r,t)\, 4\pi r^2\, \mathrm{d}r \int_0^{v_c(r)} f_\chi(\boldsymbol{w}, r)\, 4\pi w^2\, \mathrm{d}w \int_{v_e(r)}^{\infty} R_i^+(w \to v) \mathrm{d}v \,. \tag{5.34}$$

where the factor $s(r)$ accounts for the suppression of the fraction of DM particles that, even after acquiring a velocity larger than the escape velocity, would actually escape from the Sun due to further interactions in their way out, and can be written as [232]

$$s(r) = \eta_{\rm ang}(r)\, \eta_{\rm mult}(r)\, e^{-\tau(r)} \,, \tag{5.35}$$

where $\tau(r) = \int_r^{R_\odot} \ell^{-1}(r')\, \mathrm{d}r'$ is the optical depth at radius r. The factors $\eta_{\rm ang}(r)$ and $\eta_{\rm mult}(r)$, which take into account that DM particles travel in non-radial trajectories and that multiple scatterings are possible, are described in Sec. 4.3.2. Although the result for the factors in $s(r)$ is based on a calculation for a velocity-independent and isotropic cross section [232], lacking a better estimate, we also use it for the other cases under study. In the optically thin regime, the suppression factor $s(r)$ is nearly one, but we always included it in the calculations.

Note that, to keep it general, we should have considered a term with $R_i^-(w \to v)$ corresponding to down-scatterings to velocities above the escape velocity and hence, the limits for the $R_i^+(w \to v)$ and $R_i^-(w \to v)$ integrals would be $(v_e(r), w)$ and (w, ∞), respectively. Moreover, a priori, the nuclear form factor for the case of interactions off nuclei must be included too. Whereas in the $R_i^-(w \to v)$ term, the nuclear form factor can be factored out by computing it in the zero-temperature limit, in that limit, the contribution from the $R_i^+(w \to v)$ term is exactly zero. However, for non-zero temperatures, the form factor has to be included in the calculation of the $R_i^+(w \to v)$ term, so an analogous simplification to the one for the $R_i^-(w \to v)$ term cannot be made. Nevertheless, if the DM velocity distribution has a cutoff at $v_c(r) \leq v_e(r)$, the $R_i^-(w \to v)$ term is absent and, for the case of the Sun, the nuclear form factors can be approximated to one (at these velocities $q\, r_i \ll 1$). In such cases, which are the ones we consider in this work, the evaporation rate is given by the usual expression, Eq. (5.34).

In Fig. 5.10 we show the evaporation rates for constant (top panels), $v_{\rm rel}^2$-dependent (middle panels) and q^2-dependent (bottom panels) cross sections, in the case of DM-electron (red curves), DM-nucleon SD (green curves) and DM-nucleon SI (blue curves) interactions. We consider the same cases depicted in Fig. 5.2, i.e., cross sections in the optically thin regime (left panels), but

also show the results for large cross sections in the optically thick regime (right panels). In all the panels we show the results of a DM velocity distribution with a cutoff at $v_c(r) = v_e(r)$ (solid lines) and $v_c(r) = 0.9\, v_e(r)$ (dashed lines). The usual exponential fall off at large masses, due to the dependence of the evaporation rate per unit volume on $e^{-m_\chi v_e^2(r)/2T_\chi}$, is clearly visible. Besides this, there are a number of other features worth noticing.

In the case of interactions with electrons, the effect of the modification of the high-velocity tail of the DM distribution is striking, with a huge impact for masses above $O(0.1)$ GeV, for which evaporation is very suppressed in the case of $v_c(r) = 0.9\, v_e(r)$. On the other hand, in the case of interactions with nucleons, the evaporation rates are only moderately modified when a different cutoff in the DM velocity distribution is considered. This can be understood by the mass scales involved in the problem. Electrons, being light compared to the DM particles, carry little momentum, so that in the case of DM-electron interactions only DM particles with velocities close to the escape velocity are susceptible of gaining enough energy to escape after one interaction. In practice, the differential scattering rate $R_i^+(w \to v)$ for interactions with electrons peaks at DM velocities w close to the escape velocity, whereas for the case of scattering off nucleons it has a broader shape. Therefore, a maximum velocity smaller than the escape velocity significantly suppresses evaporation in the former case. This has important consequences on the available parameter space, as we will discuss below.

Moreover, whereas in the Knudsen limit the evaporation rate scales linearly with the scattering cross section, for large cross sections, the suppression of evaporation results in a slower-than-linear increase with the cross section. Therefore, although in the optically thin regime the evaporation rate for SI interactions is larger than for SD interactions due to the coherent enhancement of the cross section in the first case, this very same enhancement implies a shorter mean free path and hence, a larger suppression of the evaporation rate for SI cross sections in the optically thick regime. The relative suppression of the rate in the case of interactions with electrons is similar to the case of DM-nucleon SD interactions. We also note that the behavior of the evaporation rates in the case of $v_{\rm rel}^2$-dependent cross sections is very similar to that of q^2-dependent cross sections. We find that, in these two cases, the evaporation rates corresponding to DM interactions with electrons are larger than for scatterings off nucleons. In addition, although in general low masses enter the optically thick regime for smaller cross sections (see Eq. (5.28)), for $v_{\rm rel}^2$-dependent and q^2-dependent cross sections this effect is more pronounced (see Eqs. (4.76) and (4.80)).

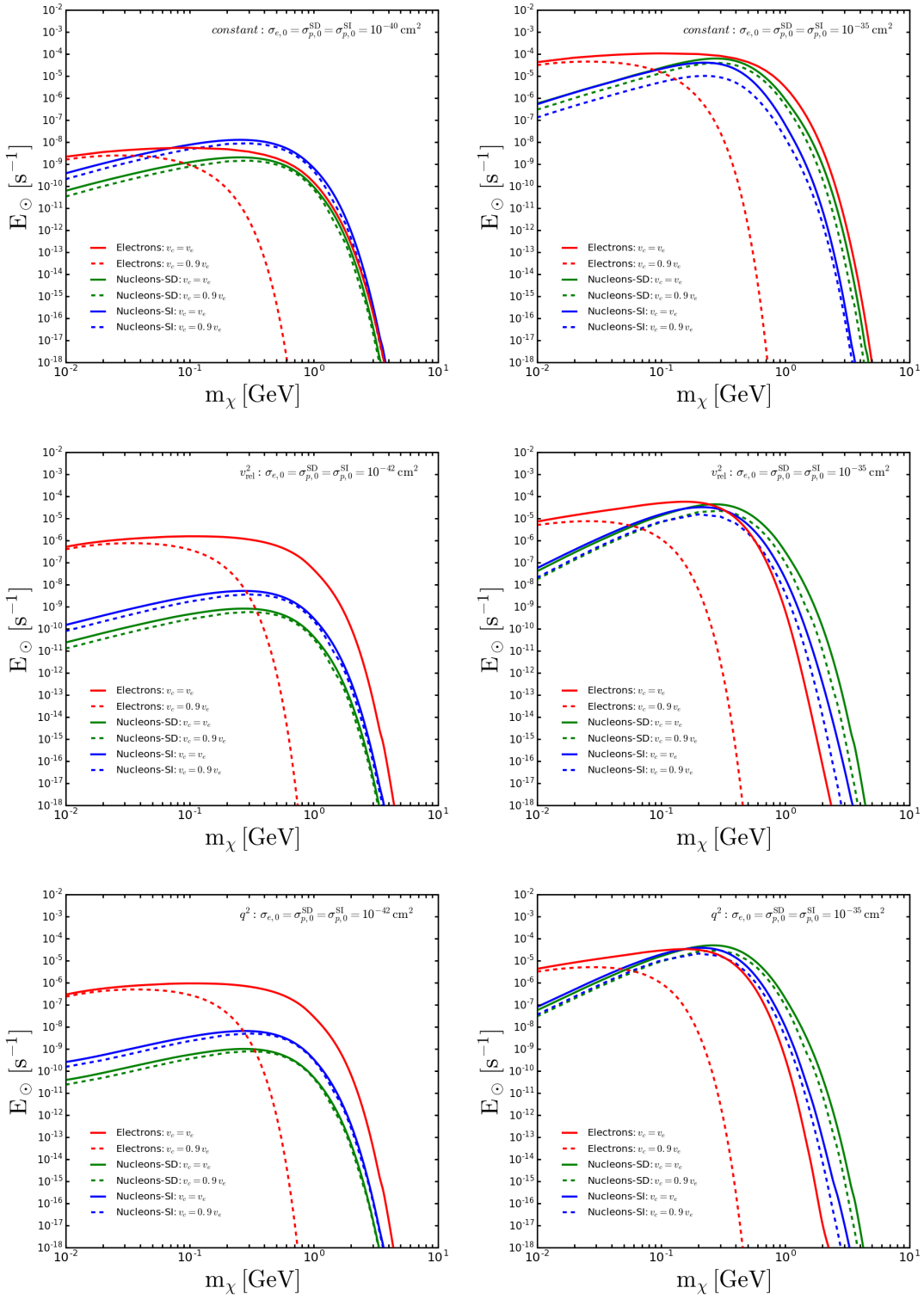

Figure 5.10: ***Evaporation rates as a function of the DM mass***, for DM-electron interactions (red curves), DM-nucleon SD interactions (green curves) and DM-nucleon SI interactions (blue curves), with a velocity cutoff at $v_c(r) = v_e(r)$ (solid curves) and at $v_c(r) = 0.9\,v_e(r)$ (dashed curves). *Left panels:* optically thin regime. *Right panels:* optically thick regime. *Top panels*: constant (velocity-independent and isotropic) scattering cross section for $\sigma_{i,0} = 10^{-40}$ cm^2 and $\sigma_{i,0} = 10^{-35}$ cm^2. *Middle panels*: $v_{\rm rel}^2$-dependent scattering cross section for $\sigma_{i,0} = 10^{-42}$ cm^2 and $\sigma_{i,0} = 10^{-35}$ cm^2. *Bottom panels*: q^2-dependent scattering cross section for $\sigma_{i,0} = 10^{-42}$ cm^2 and $\sigma_{i,0} = 10^{-35}$ cm^2.

5.6 Evaporation mass

Once all the ingredients are computed, we are interested in knowing what is the minimum DM mass which is testable,[6] i.e., which is the minimum DM mass for which DM particles are not evaporated. In order to determine this mass we first consider the evolution of the total number of DM particles in the Sun, which is governed by the following equation:

$$\frac{\mathrm{d}N_\chi(t)}{\mathrm{d}t} = C_\odot - A_\odot N_\chi^2(t) - E_\odot N_\chi(t) \,. \tag{5.36}$$

The solution of this equation, computed at the present time ($t = t_\odot = 4.57$ Gyr), is given by [86, 88]

$$N_\chi(t_\odot) = \sqrt{\frac{C_\odot}{A_\odot}} \frac{\tanh(\kappa\, t_\odot/\tau_{\rm eq})}{\kappa + \frac{1}{2}\, E_\odot\, \tau_{\rm eq}\, \tanh(\kappa\, t_\odot/\tau_{\rm eq})} \,, \tag{5.37}$$

where $\tau_{\rm eq} = 1/\sqrt{A_\odot C_\odot}$ is the equilibration time scale in the absence of evaporation and $\kappa = \sqrt{1 + (E_\odot\, \tau_{\rm eq}/2)^2}$. For the usual value assumed for the thermal annihilation cross section, $\langle \sigma_A v_{\chi\chi} \rangle = 3 \times 10^{-26}$ cm^3/s, and for $\sigma_{e,0} \gtrsim 10^{-42}$ cm^2, $\sigma_{p,0}^{\rm SD} \gtrsim 10^{-43}$ cm^2 and $\sigma_{p,0}^{\rm SI} \gtrsim 10^{-44}$ cm^2 for constant cross sections (much smaller for the other cases), equilibrium is reached ($\kappa\, t_\odot \gg \tau_{\rm eq}$, $\tanh(\kappa\, t_\odot/\tau_{\rm eq}) \simeq 1$). In the limit when evaporation is important, $\kappa \gg 1$, $N_\chi \simeq C_\odot/E_\odot$, and the number of accumulated DM particles decreases exponentially with decreasing mass (in the optically thin regime). In the limit when evaporation is negligible, $\kappa \simeq 1$, $N_\chi \simeq \sqrt{C_\odot/A_\odot}$, and the number of accumulated DM particles decreases with increasing mass (as $m_\chi^{-7/4}$ for large masses). Given these considerations, one can define the minimum testable mass or evaporation mass[7] as that for which the number of captured DM particles approaches $C_\odot/E_\odot$ at the 10% level [319]

$$\left| N_\chi(m_{\rm evap}) - \frac{C_\odot(m_{\rm evap})}{E_\odot(m_{\rm evap})} \right| = 0.1\, N_\chi(m_{\rm evap}) \,, \tag{5.38}$$

In the limit when equilibrium has been reached, i.e., $\kappa\, t_\odot \gg \tau_{\rm eq}$, it can be written as

$$E_\odot(m_{\rm evap})\, \tau_{\rm eq}(m_{\rm evap}) = \frac{1}{\sqrt{0.11}} \,. \tag{5.39}$$

In the optically thin regime, this results in the evaporation mass to increase with the scattering cross section and to decrease with the annihilation cross section. However, when the scattering cross section is large enough and the suppression factor $s(r)$ becomes important, the evaporation mass *decreases* with the scattering cross section, so the minimum testable DM mass attains a maximum value around the transition between the two regimes [189, 232]. Note that for very small scattering cross sections, equilibrium is not reached, the effects of evaporation are negligible and the number of DM particles scales as $N_\chi \simeq C_\odot\, t_\odot$. In this case, there is no evaporation mass, but the total number of DM particles in the Sun would be too small to give rise to any measurable signal.

In Fig. 5.11 we show (in reverse order) the evaporation mass as a function of the scattering cross section $\sigma_{i,0}$ for the same cases depicted in Fig. 5.10, i.e., interactions with electrons (red

[6] Note that the high-energy tail of the evaporating DM particles could also be used to probe masses below the evaporation mass [318].

[7] For the relevant range of scattering cross sections, other possible, equally good, definitions for the evaporation mass are: $\mathrm{d}N_\chi/\mathrm{d}m_\chi(m_{\rm evap}) = 0$; or $\left| N_\chi(m_{\rm evap}) - \sqrt{\frac{C_\odot(m_{\rm evap})}{A_\odot(m_{\rm evap})}}\, \tanh(t_\odot/\tau_{\rm eq}) \right| = \alpha\, N_\chi(m_{\rm evap})$, when the departure from the $E_\odot = 0$ limit is of a factor of α (it coincides with Eq. (5.39) for $\alpha = \sqrt{11} - 1$ and $t_\odot \gg \tau_{\rm eq}$).

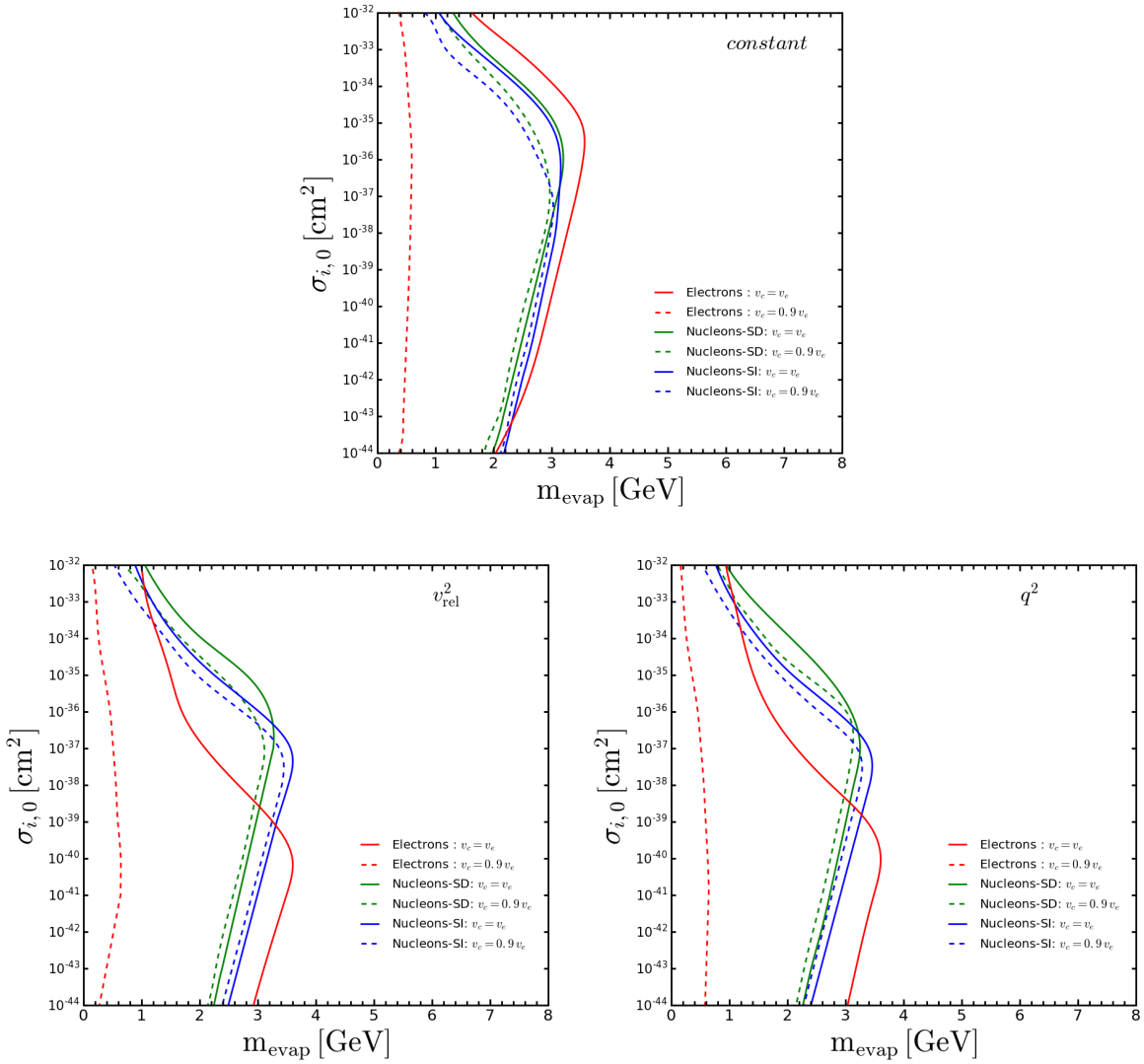

Figure 5.11: ***Evaporation mass as a function of the scattering cross section*** (in reverse order). Same cases as in Fig. 5.10, i.e., DM scattering off electrons (red curves), off nucleons via SD interactions (green curves) and off nucleons via SI interactions (blue curves) and for two DM velocity distributions: with a cutoff at $v_c(r) = v_e(r)$ (solid curves) and with a cutoff at $v_c(r) = 0.9\,v_e(r)$ (dashed curves). *Top panel*: constant (velocity-independent and isotropic) scattering cross sections. *Bottom-left panel*: $v_{\rm rel}^2$-dependent scattering cross sections. *Bottom-right panel:* q^2-dependent scattering cross sections.

curves), with nucleons via SD interactions (green curves) and with nucleons via SI interactions (blue curves), for a velocity cutoff at $v_c(r) = v_e(r)$ (solid curves) and with a cutoff at $v_c(r) = 0.9\,v_e(r)$ (dashed curves), and for constant (top panel), $v_{\rm rel}^2$-dependent (bottom-left panel) and q^2-dependent (bottom-right panel) cross sections.

For DM masses to the left of the curves, evaporation is very efficient and DM particles evaporate from the Sun. For a DM distribution with a cutoff at the escape velocity, the evaporation mass is slightly larger for interactions with electrons. This is always the case for constant cross sections. However, for $v_{\rm rel}^2$-dependent and q^2-dependent cross sections, the transition to the optically thick regime occurs for smaller values of $\sigma_{i,0}$ for DM-electron interactions than for DM-nucleon interactions, which has to do with the different mass dependence of the mean free path in each case. Whereas in the case of constant cross sections, the evaporation mass for DM-nucleon SD interactions is always slightly smaller than for SI interactions, for $v_{\rm rel}^2$-dependent

and q^2-dependent cross sections, this only happens in the optically thin regime. Nevertheless, the most interesting and new features appear for DM velocity distributions with a cutoff at $v_c(r) = 0.9\, v_e(r)$. While this velocity cutoff has a very small impact for DM interactions with nucleons, as could have been anticipated from the previous results, in the case of interactions with electrons, the evaporation mass can be substantially reduced below the GeV range, down to $m_{\rm evap} \sim (0.5 - 0.6)$ GeV for most values of the cross sections or even to $m_{\rm evap} \sim 0.2$ GeV for some extreme cases, which significantly opens this region of the parameter space, making it potentially testable with neutrino detectors. Therefore, in order to correctly assess the impact of this effect and given the importance of the high-velocity tail in the calculation of the evaporation mass, an accurate evaluation of the equilibrium DM distribution deserves a dedicated analysis.

5.6.1 Asymmetric DM

The time evolution of number density of ADM in the Sun has already been discussed in the previous chapter 4.0.1, here we recapitulate

$$\frac{\mathrm{dN}_\chi}{\mathrm{dt}} = C^\chi_\odot - E^\chi_\odot \mathrm{N}_\chi, \tag{5.40}$$

the solution for N_χ reads

$$N_\chi(t) = C^\chi_\odot t_\odot \left(\frac{1 - e^{-E^\chi_\odot t_\odot}}{E^\chi_\odot t_\odot} \right). \tag{5.41}$$

Since annihilation is absent in the ADM scenario, previous definition of the evaporation mass does not hold. For ADM, evaporation mass is defined as the minimum mass for which the capture process dominates over the evaporation process. Quantitatively, the minimum mass which satisfies the following condition[8] [320].

$$\frac{1 - e^{-E_\odot t_\odot}}{E_\odot t_\odot} > \frac{1}{2}, \tag{5.42}$$

is used to numerically evaluate the evaporation mass. In Fig. 5.12 we show the evaporation mass as a function of the scattering cross section $\sigma_{i,0}$ for the ADM scenario, for the same cases depicted in Fig. 5.11, i.e., interactions with electrons (red curves), with nucleons via SD interactions (green curves) and with nucleons via SI interactions (blue curves), for a velocity cutoff at $v_c(r) = v_e(r)$ (solid curves) and with a cutoff at $v_c(r) = 0.9\, v_e(r)$ (dashed curves), and for constant (top panel), $v^2_{\rm rel}$-dependent (bottom-left panel) and q^2-dependent (bottom-right panel) cross sections. Qualitatively, the results are very similar to the standard case, however few comments follow. The evaporation mass is approximately larger than the standard case by $\sim$ GeV in all cases, for $\sigma_{i,0} \sim 1$pb. Since the annihilation rate is 0, the rate of depletion of DM is lower than the standard case, this naturally leads to slightly larger evaporation masses. Features due to the cut-off dependence of the velocity distribution is also similar to the that of the standard case. Reference [320] provides evaporation mass for ADM scenario for various momentum and velocity dependent cross sections including re-scattering effects relevant for large cross sections $\sigma_{i,0} > 10^{-36}\,\mathrm{cm}^2$, however they do not consider the case of DM scattering off electrons.

[8] $\frac{\mathrm{d}N_\chi}{\mathrm{d}m_\chi} = 0$, is an equivalently good measure.

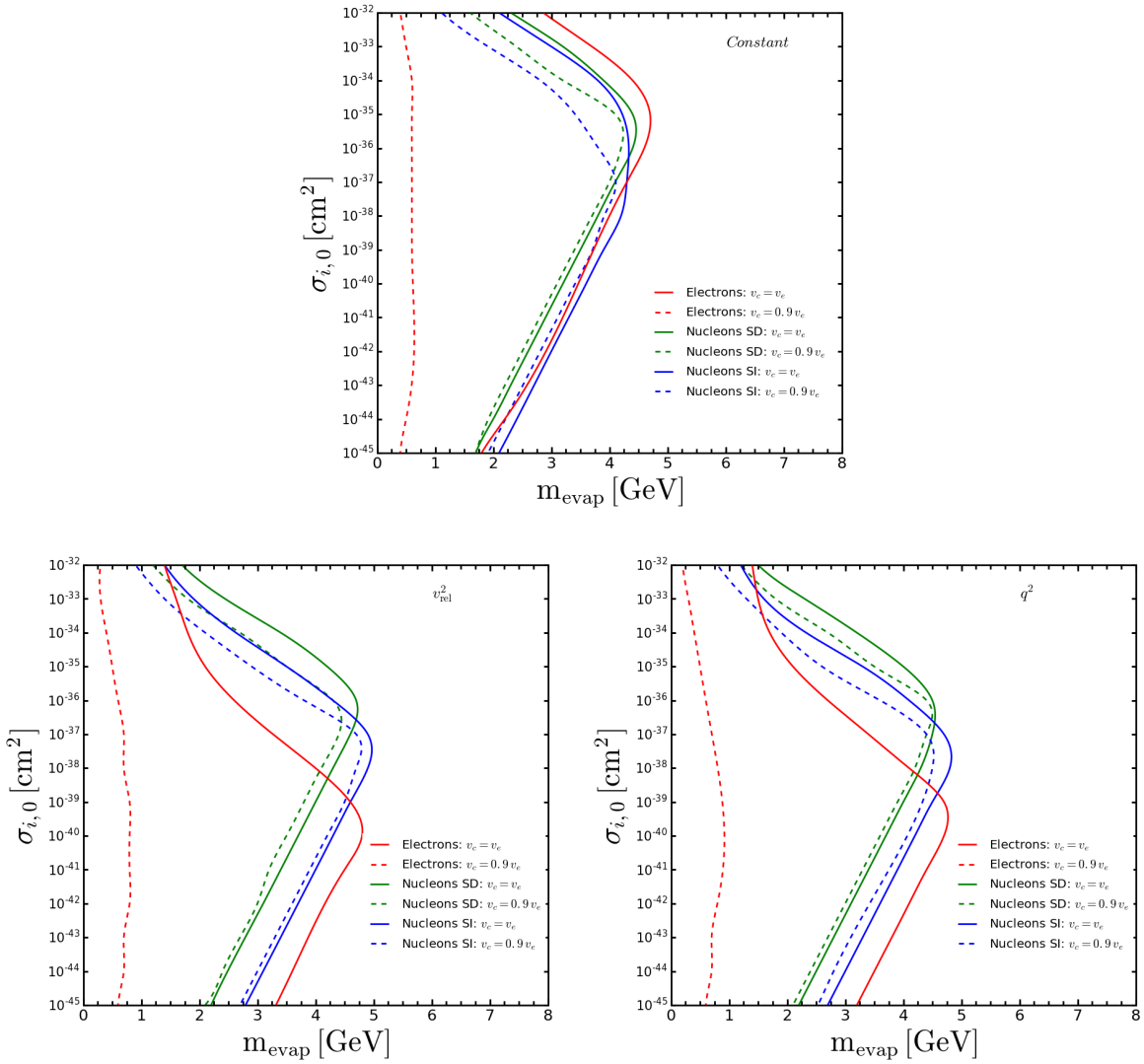

Figure 5.12: ***Asymmetric DM: Evaporation mass as a function of the scattering cross section*** (in reverse order). Same cases as in Fig. 5.10, i.e., DM scattering off electrons (red curves), off nucleons via SD interactions (green curves) and off nucleons via SI interactions (blue curves) and for two DM velocity distributions: with a cutoff at $v_c(r) = v_e(r)$ (solid curves) and with a cutoff at $v_c(r) = 0.9\,v_e(r)$ (dashed curves). *Top panel*: constant (velocity-independent and isotropic) scattering cross sections. *Bottom-left panel*: $v_{\rm rel}^2$-dependent scattering cross sections. *Bottom-right panel:* q^2-dependent scattering cross sections.

5.7 Neutrino Production Rates from DM Annihilations in the Sun

The neutrino production rate from DM annihilations in the Sun is proportional to the annihilation rate of the DM particles accumulated in the Sun and it is given by $\Gamma = A_\odot\, N_\chi^2/2$, which after the solution of Eq. (5.36), i.e., Eq. (5.37), results in

$$\Gamma(m_\chi, \sigma_{i,0}) = \frac{1}{2}\, C_\odot \left(\frac{\tanh(\kappa\, t_\odot/\tau_{\rm eq})}{\kappa + \frac{1}{2}\, E_\odot\, \tau_{\rm eq}\, \tanh(\kappa\, t_\odot/\tau_{\rm eq})} \right)^2 . \tag{5.43}$$

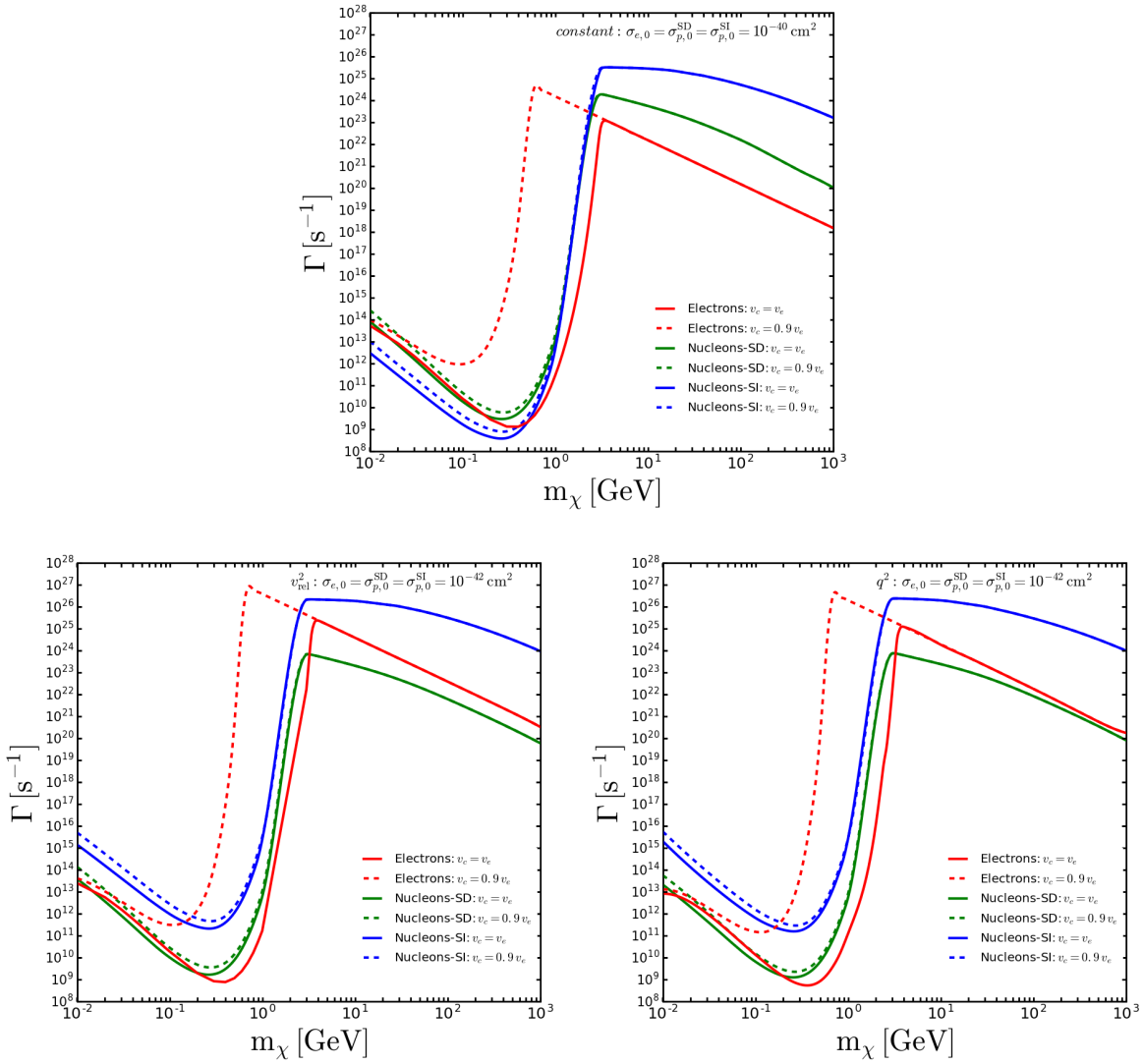

Figure 5.13: ***Neutrino production rates as a function of the DM mass***. Same cases as in the left panels of Fig. 5.10. Note the different values of $\sigma_{i,0}$ for the top and bottom panels.

It depends on the DM mass, the scattering cross section and on the annihilation cross section. Therefore, in the limit for which equilibration is attained, $\kappa\, t_\odot \gg \tau_{\rm eq}$, it reads

$$\Gamma(m_\chi, \sigma_{i,0}) = \frac{1}{2}\, \frac{C_\odot}{\left(\kappa + \frac{1}{2}\, E_\odot\, \tau_{\rm eq}\right)^2}\,, \tag{5.44}$$

although in our computations we keep the exact form of Eq. (5.43).
Once all the ingredients are at hand, we can compare the resulting neutrino rates at production for the case of capture by electrons and by nucleons in the Sun. As already mentioned, even if DM has only tree-level couplings to electrons, loop-induced processes could give rise to interactions with nucleons. Here we compare the relative importance of the different cases considered in this work. In Fig. 5.13 we show the neutrino production rates for the same cases depicted in the left panels of Fig. 5.10, i.e., interactions in the Knudsen limit with $\sigma_{i,0} = 10^{-40}$ cm^2 for constant cross sections (top panel) and $\sigma_{i,0} = 10^{-42}$ cm^2 for $v^2_{\rm rel}$-dependent cross sections (bottom-left panel) and for q^2-dependent cross sections (bottom-right panel).
For sufficiently large masses (above the evaporation mass), for which capture and annihilation

rates are in equilibrium, the neutrino production rates are proportional to the capture rates, $\Gamma = C_\odot/2$, and hence for all cases, the same behavior described for Fig. 5.2 is obtained. For low masses, equilibrium is attained between capture and evaporation and the neutrino production rate is suppressed by the large evaporation rate, $\Gamma = A_\odot \left(C_\odot/E_\odot\right)^2/2$. Notice that for very low masses, the suppression of the evaporation rate results in the increase of the neutrino production rates, so there is a minimum in the neutrino production rates,[9] which lies at $m_\chi \sim (0.3 - 0.5)$ GeV for the three types of cross sections we study if the DM velocity distribution extends up to $v_e(r)$. Although the form of the high-velocity tail does not have a strong impact when DM scatters off nucleons, in the case of interactions with electrons, this minimum shifts to $m_\chi \sim (0.1 - 0.2)$ GeV for $v_c(r) = 0.9\, v_e(r)$ and the neutrino production rate is significant for masses $m_\chi \gtrsim 0.4$ GeV for constant cross sections and $m_\chi \gtrsim 0.5$ GeV for $v_{\rm rel}^2$-dependent and q^2-dependent cross sections. This is to be compared to the minimum DM mass for which there could be a significant neutrino production rate in the case of interactions with nucleons (and with electrons with $v_c(r) = v_e(r)$), the commonly quoted lower limit $m_\chi \gtrsim 3$ GeV.
Above the evaporation mass, the neutrino production rates for DM-nucleon SI interactions are the largest for the three types of cross sections (for the normalizations used here). For constant DM-nucleon SD cross sections, these rates are larger than for scatterings off electrons. However, for $v_{\rm rel}^2$-dependent and q^2-dependent cross sections, the relative importance gets inverted, being the case of interactions with electrons the most favorable one, because of the larger enhancement due to thermal effects. This illustrates how, for some scenarios, interactions with electrons could give rise to the largest signals in neutrino detectors/telescopes [6].

We also provide the equilibration contours for all the cases considered: we plot the equilibration parameter $(\kappa\, t_\odot/\tau_{\rm eq})$ with respect to mass and the relevant cross section. The equilibration cross section can be read off from the plots by following the 0-line contour. In Fig. 5.14 we show the contours for the constant cross section case. In Fig. 5.15 we show the contours for the $v_{\rm rel}^2$-dependent cross section. In Fig. 5.16 we show the contours for the q^2-dependent cross section. In all of these Figs. the left column corresponds to the case $v_c(r) = v_e(r)$, the right columns correspond to the case $v_c(r) = 0.9\, v_e(r)$. The upper panels are for DM-electron scattering. The middle panels for DM-nucleon SD interactions, and the lower panels correspond to DM-nucleon SI interactions. From these plots we see that for constant isotropic cross sections, equilibrium is reached for $\sigma_{e,0} \gtrsim 10^{-42}$ cm^2, $\sigma_{p,0}^{\rm SD} \gtrsim 10^{-43}$ cm^2 and $\sigma_{p,0}^{\rm SI} \gtrsim 10^{-44}$ cm^2. For $v_{\rm rel}^2$-dependent cross sections, equilibrium is reached for $\sigma_{e,0} \gtrsim 10^{-46}$ cm^2, $\sigma_{p,0}^{\rm SD} \gtrsim 10^{-45}$ cm^2 and $\sigma_{p,0}^{\rm SI} \gtrsim 10^{-47}$ cm^2. Similarly, for q^2-dependent cross sections, equilibrium is reached for $\sigma_{e,0} \gtrsim 10^{-46}$ cm^2, $\sigma_{p,0}^{\rm SD} \gtrsim 10^{-45}$ cm^2 and $\sigma_{p,0}^{\rm SI} \gtrsim 10^{-47}$ cm^2.

[9] The rise of the flux at low masses, being much smaller than that at $m_\chi \gtrsim$ GeV, has no measurable effect.

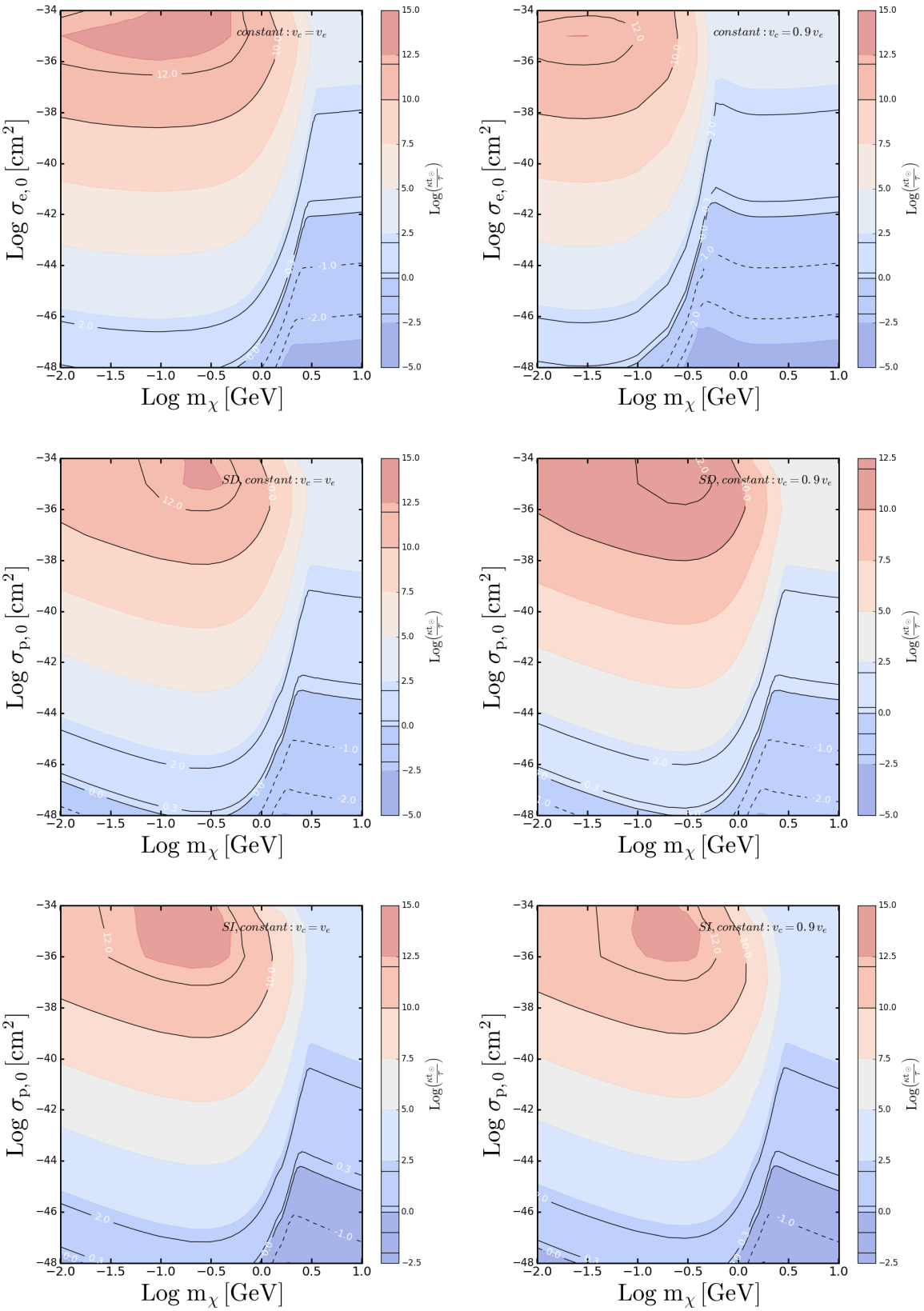

Figure 5.14: ***Equilibration contours as a function of the DM mass and constant elastic scattering cross section*:** The left column corresponds to the case $v_c(r) = v_e(r)$, the right columns correspond to the case $v_c(r) = 0.9\,v_e(r)$. The upper panels are for DM-electron scattering. The middle panels for DM-nucleon SD interactions, and the lower panels correspond to DM-nucleon SI interactions.

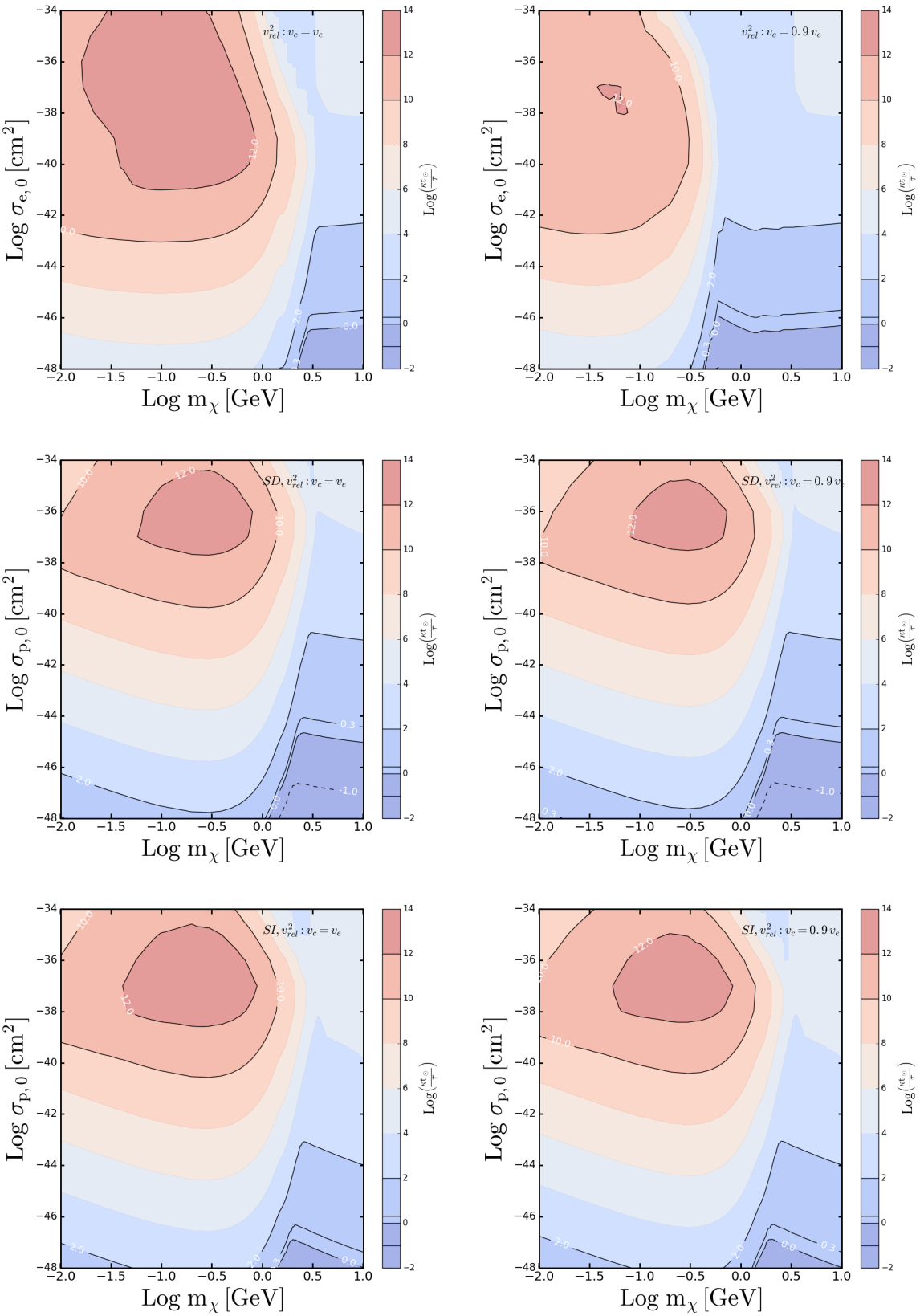

Figure 5.15: ***Equilibration contours as a function of the DM mass and velocity dependent elastic scattering cross section:*** The left column corresponds to the case $v_c(r) = v_e(r)$, the right columns correspond to the case $v_c(r) = 0.9\, v_e(r)$. The upper panels are for DM-electron scattering. The middle panels for DM-nucleon SD interactions, and the lower panels correspond to DM-nucleon SI interactions.

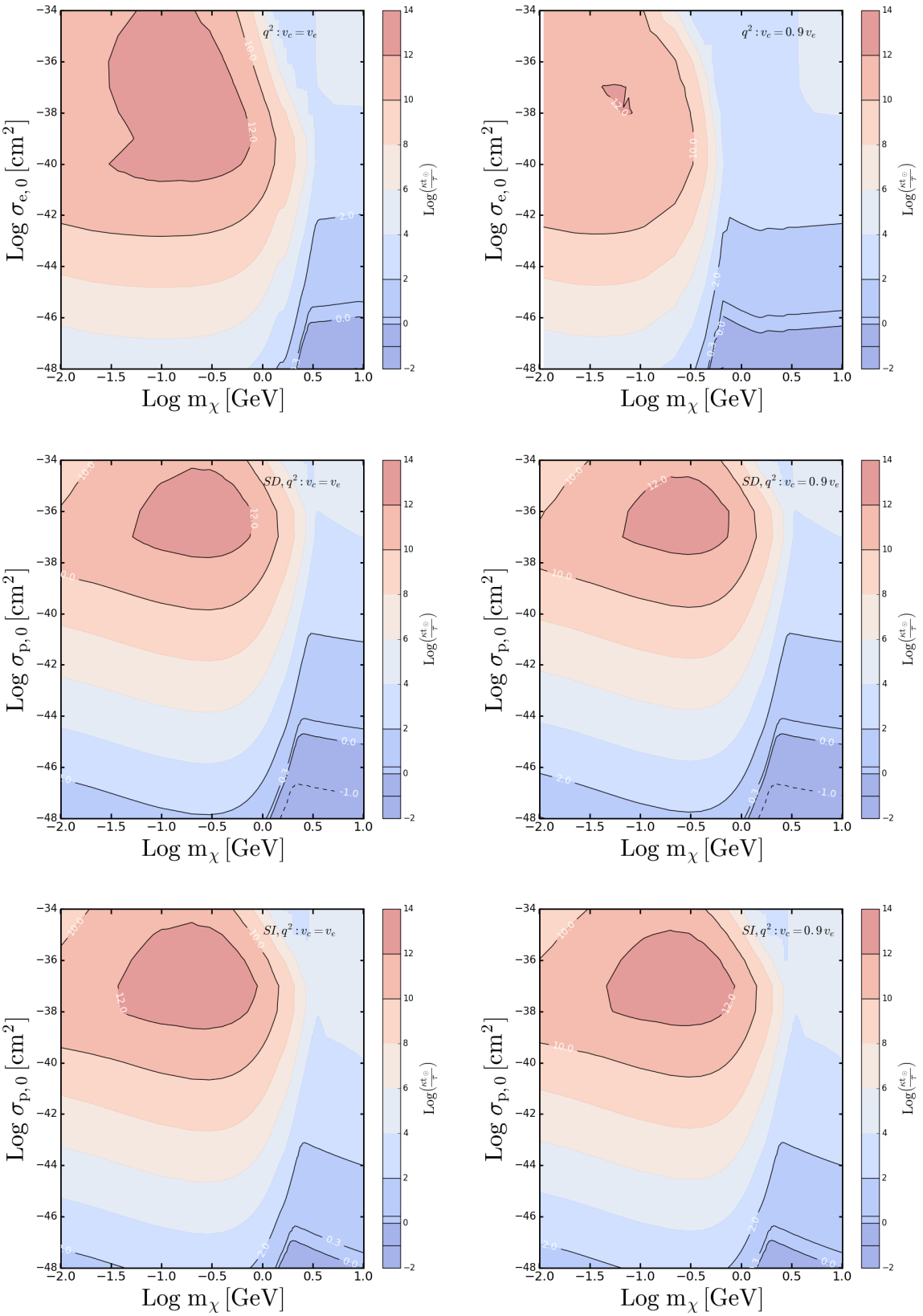

Figure 5.16: ***Equilibration contours as a function of the DM mass and momentum dependent elastic scattering cross section:*** The left column corresponds to the case $v_c(r) = v_e(r)$, the right columns correspond to the case $v_c(r) = 0.9\, v_e(r)$. The upper panels are for DM-electron scattering. The middle panels for DM-nucleon SD interactions, and the lower panels correspond to DM-nucleon SI interactions.

CHAPTER 6

Models

Predictions from well motivated UV theories such as the Minimal Supersymmetric Standard Model (MSSM) hint at the existence of DM at the electroweak scale. In recent years, several experiments have reported signals that may be interpreted as a hint for DM [36, 38–40, 43, 108, 321–324]. While some of these signals have lost significance [324], others have persisted in some tension with data from a plethora of other experiments [36]. However, none of these signals could be conveniently accommodated in the MSSM. In light of these null discoveries, there has been a renewed interest in studies of general DM models. A particular topic of recent interest is in the effective operator analysis [213, 269, 325], where the detailed UV structure of the underlying interactions between the dark sector and SM sector are abstracted away, leaving an effective 4-point contact interaction operators. Many studies approach the DM problem by constructing a list of 4–particle-interactions with Lorentz–invariant combinations of γ^μ, ∂^μ and spinor–/vector–indices up to mass dimension 5 or even 6, depending on the case. Generally, there is no explanation of how these operators may arise from a fundamental theory making it difficult to judge how exhaustive the lists of operators are, and how the effective model is connected to realistic fundamental theories and their couplings. Here, we follow a "simplified" approach presented in [23, 326, 327] and consider the scenario where DM couples universally to all leptons in SM (Leptophilic DM). In a simplified approach, renormalizable Lagrangian is constructed with only one DM candidate and a single mediator which connects DM and SM sectors. Of course, there exist limitations to this approach [26].

The discussion so far in this thesis has concentrated on model independent analysis of DM annihilation rate in the Sun for DM scattering off of electrons and nucleons. Now we will study realistic models. An important observation is that for $m_{DM} > 5\,\text{GeV}$, the total annihilation rate Γ is proportional to the elastic scattering cross section of DM and the target particles in the Sun. In this chapter we focus on the calculation of tree-level DM-electron [1] elastic scattering cross sections ($\sigma_{\chi e}$) and possible loop-level DM-nucleon elastic scattering cross sections in leptophilic DM models, in the non-relativistic limit. Since the three-momentum exchange in these processes is $O(keV)$, the effective theory analysis holds in the limit of large mediator mass ($\gg GeV$). Moreover, it is well recognized that the effective operator approximation can break down if the mediating particles are not heavy enough; however, there has been very few studies of the features of the effective operator analysis which are robust.

The goal of this chapter is to provide expressions for DM-target particle elastic scattering cross sections for leptonically interacting DM. In particular, we address the following questions: Are the matrix elements for DM-electron scattering unsuppressed, or suppressed by factors of the relative velocity or momentum transfer ? Given a leptophilic Lagrangian, does it generate sizable

[1] Contrary to direct detection experiments where electrons are bound to atoms or nuclei, electrons in the Sun can be treated as free particles; which inevitably results in significantly large $\sigma_{\chi e}$ for interactions in the Sun.

interactions with nucleons at loop level ?

Elements of the scattering matrix element can be suppressed by factors proportional to the relative velocity, or to the ratio of the momentum transfer to dark matter or target mass. For non-relativistic DM, these factors are all small. Thus it is common to focus on scattering matrix elements with no velocity or momentum suppression, since these terms will typically dominate the scattering cross section at leading order. However, velocity- or momentum-suppressed terms can dominate if the unsuppressed terms have very small coefficients. Given that thermal effects in the capture process results in enhanced annihilation rates when the target particles are electrons, we therefore provide a complete treatment of the velocity-and momentum-suppressed terms as well.

The subject of leptophilic models is vast and they are particularly rich in phenomenology and experimentally ill constrained. However, we do not consider all aspects of the subject matter. Particularly, we do not address the following issues: the exact origin of the interaction terms considered from UV complete theories (see Ref. [327] for a recent review), possible impact on CP violation in the lepton sector and the loop-induced CP violation in the quark sector and the possible interplay with DM; the neutrino spectra from DM annihilation and the phenomenology of the annihilation processes themselves is not considered. For example: one can induce model-independent loop level annihilation to quarks, which could be relevant for light DM with masses close to the evaporation mass, or when non-perturbative effects in the annihilation process become relevant [328]. The interplay between Indirect, Direct and Collider searches in leptophilic models is not studied. Given the topic of this study, we simply focus on DM-SM elastic scattering. This chapter is organized as follows: simplified models considered are presented in section 6.1. The resulting elastic scattering cross sections are tabulated in section 6.2.

6.1 Simplified Models

We have decided to limit the discussion to scalar, fermion and vector DM only, which can also lead to s-channel annihilation processes [2]. In the spirit of the simplified models, the smallest possible number of degrees of freedom should be added to the SM, i.e. the following prescription is used:

- The SM is extended by the addition of a DM particle, which is absolutely stable and a mediator which is assumed to be much heavier than DM.
- The new operators of the models are renormalizable and consistent with the symmetries of the theory, i.e. Lorentz invariance, $SU_c(3) \times U(1)_{\rm em}$ gauge invariance.
- In the SM, global symmetries such as baryon and lepton number are anomalous, but they can be treated as exact symmetries at the renormalizable level. So, we require that simplified models respect baryon and lepton number.

Using the above recipe, the simplified interaction Lagrangians considered here are tabulated in Tab. 6.1, with references to the resulting DM-target scattering cross sections listed in column 3. Irrespective of the case at hand, χ denotes DM particle, and l is the SM lepton field. We closely follow the notation and discussion provided in Ref. [325]. Some common definitions and variables used are described in Tab. 6.2.

A few comments regarding the calculation are in order:

[2] Models where interactions are of the Yukawa type inevitable lead to t-channel annihilation as well. We consider only two such examples.

DM	Mediator	Summary Table	$-\mathcal{L}_{int}$
Scalar (χ)	Scalar(ϕ)	6.3	$g_\chi \chi^\dagger \chi \phi + \bar{l}(g_s + g_p\gamma_5)l\phi$
Scalar (χ)	Fermion (η)	6.4	$\bar{\eta}(g_L P_L + g_R P_R)l\chi$ + h.c.
Scalar (χ)	Vector (ϕ^μ)	6.5	$g\chi^\dagger \overleftrightarrow{\partial_\mu} \chi \phi^\mu + \bar{l}\gamma_\mu(g_v + \gamma_5 g_{pv})l\phi^\mu$
Fermion (χ)	Scalar (ϕ)	6.6	$\bar{\chi}(g_s^\chi + g_p^\chi\gamma_5)\chi\phi + \bar{l}(g_s + g_p\gamma_5)l\phi$
Fermion (χ)	Vector (ϕ^μ)	6.7	$\bar{\chi}\gamma_\mu(g_V^\chi + g_A^\chi\gamma_5)\chi\phi^\mu +$ $\bar{l}\gamma_\mu(g_V + g_A\gamma_5)l\phi^\mu$
Vector (χ)	Scalar (ϕ)	6.8	$g\chi_\mu\chi^\mu\phi + \bar{l}(g_S + g_P\gamma_5)l\phi$
Vector (χ)	Fermion (η)	6.9	$\bar{\eta}\gamma_\mu(g_L P_L + g_R P_R)l\chi^\mu$ + h.c.

Table 6.1: ***Simplified Leptophilic Lagrangians:*** List of all considered leptophilic simplified models.

Quantity	Definition
k	Incoming DM 4-momenta
$k' = k - q$	Outgoing DM 4-momenta
p	4-momenta of the incoming target particle
$p + q$	4-momenta of the outgoing target particle
q^2	3-momentum transfer for the process
$\mu_{\chi N}$	Reduced mass of DM-nucleon system
Z	Atomic Number

Table 6.2: ***Notations:*** The relevant variable is listed in the first column, and the corresponding definition in the second column

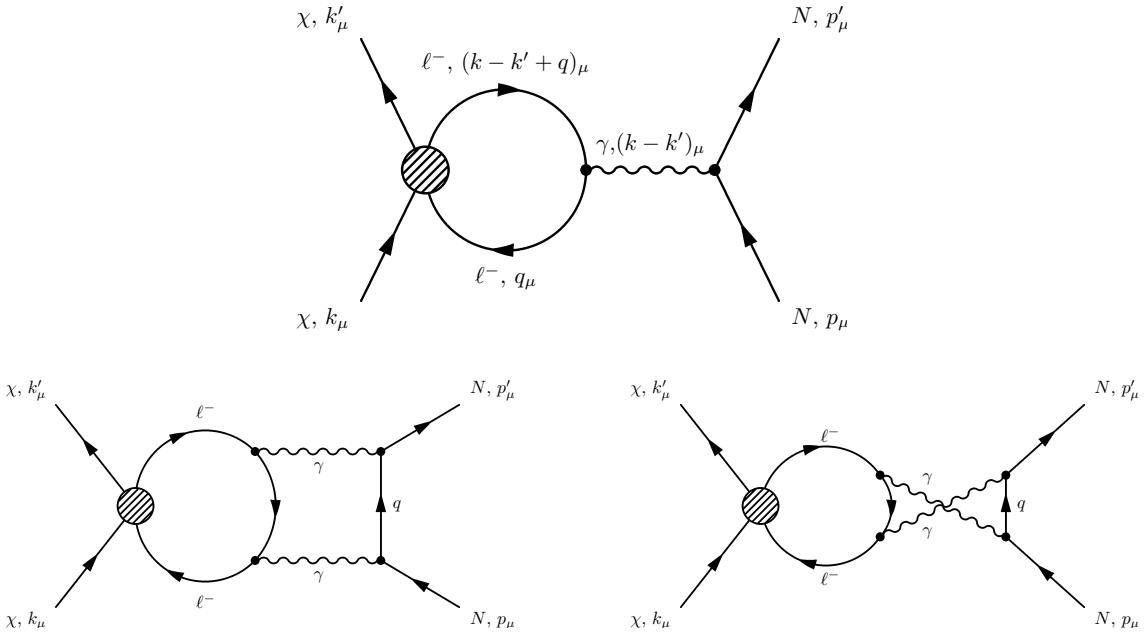

Figure 6.1: DM–nucleus interaction induced by a charged lepton loop and photon exchange at 1-loop (top) and 2-loop (bottom).

- We conservatively work in the limit of heavy mediator mass. We do not account for possible renormalization group flow and operator mixing.

- DM-electron scattering at tree-level: In all of the models considered here, tree-level DM-electron elastic scattering occurs through t-channel diagrams. All differential scattering cross sections that are listed in the summary tables 6.3, 6.4, 6.5, 6.6, 6.7, 6.8, and 6.9 , is the result of an expansion in m_e/m_χ. Phenomenologically we are interested only in DM mass $\geq O(GeV)$, hence the expansion is justified. As noted in the literature, many of the Lorentz structures considered here lead to momentum dependent elastic scattering cross sections.

- DM-nucleon scattering at 1-loop: Even in a leptophilic model, one does induce model independently, loop level couplings to quarks from photon exchange between virtual leptons and the quarks as shown in Fig. 6.1. The lepton running in the loop can be any charged lepton to which the DM couples. Diagrams with a photon replaced by a Z^0 or a Higgs boson are also possible, however they are power suppressed by either $(k-k')^2/M^2_{Z^0,H}$ or by the Yukawa couplings times the higgs propagator and thus negligible. In the context of leptophilic models considered here, models with vector mediators lead to 1-loop interactions with quarks. These models are scalar-DM with vector-mediator (see, Tab. 6.5), fermion-DM with vector-mediator (see, Tab. 6.7) and vector-DM with fermion-mediator (see, Tab. 6.9). To illustrate some general features, we consider the example of fermion-DM with a vector-mediator: the one loop contribution involves the integral over loop momenta of the form [228]

$$\int \frac{d^4q}{(4\pi)^4} \mathrm{Tr}\left[\Gamma_e \frac{\not{q}'+m_l}{q'^2-m_l^2}\gamma^\mu \frac{\not{q}+m_l}{q^2-m_l^2}\right], \tag{6.1}$$

with $q' = k-k'+q$ and k,k' the incoming momenta as denoted in Fig. 6.1 and $\Gamma_e \in \{1,\gamma_5,\gamma_\mu,\gamma_\mu\gamma_5,\gamma_\mu\gamma_\nu\}$ the possible Dirac structures obtained in the heavy mediator limit.

The one loop contribution is non-zero only for vector like interactions [3]. The calculation is straight forward, and performed in the minimal subtraction scheme ($\overline{\text{MS}}$) with the extensive use of computer packages FeynCalc [329] , PackageX [330] and LoopTools [331].

- No loop induced DM-nucleon scattering: Consider Fermion-DM and pseudo-scalar/axial-vector mediator (see, Tabs. 6.6, 6.7). Then, $\Gamma_e = \gamma_5$ or $\gamma_\mu\gamma_5$ in Eq. (6.1),respectively; the trace vanish to all loop orders. Thus, pseudo-scalar or axial vector coupling to leptons does not induce DM-quark interactions at loop-level.

- DM-nucleon scattering at 2-loop: Again, for the case of Fermion DM, when $\Gamma_e = 1$ in the above expression, the loop integral vanishes. Then, leading DM interaction with quarks is generated at 2-loops, see fig. 6.1. In this work, typical models with scalar mediators lead to 2-loop interactions with quarks. These models are scalar-DM with scalar mediator (see, Tab. 6.3), scalar-DM with fermion mediator (see, Tab. 6.4), fermion-DM with scalar mediator (see, Tab. 6.6), and vector-DM with scalar mediator (see, Tab. 6.8). In the following sub-section we discuss the model with scalar-DM and scalar mediator and estimate the 2-loop cross section using approximations. However, with the intention of deriving accurate 2-loop expression we have also performed the full 2-loop calculation including massive propagators using the Mellin-Barnes technique [332, 333]. Where we have extensively used the Mathematica package AMBRE [334, 335] and MBsums [336]. Due to the tedious nature of the involved expressions they are not presented here. Its important to note that technical workings of the Mellin-Barnes method deserve an entire chapter. Such techniques are often employed in higher order QCD calculations.

6.1.1 Example: Scalar DM and Scalar Mediator

In this simplified model we consider DM to be a complex scalar singlet χ, with a neutral real scalar singlet mediator ϕ which interacts with SM leptons l universally with scalar g_s and pseudo scalar g_p couplings. To simplify, the interactions between ϕ and SM higgs at tree level is forbidden and we disregard self interaction terms. The interaction part of the Lagrangian reads

$$-\mathcal{L}_{int} = g_\chi \chi^\dagger \chi \phi + \bar{l}(g_s + i g_p \gamma_5) l \phi, \tag{6.2}$$

For elastic scattering with leptons, the amplitude is given by

$$\mathcal{M} \sim \frac{g_\chi}{t - m_\phi^2} \bar{u}_2 (g_s + i g_p \gamma_5) u_1, \tag{6.3}$$

in the non relativistic limit, the bilinear $\bar{u}(g_s + i g_p \gamma_5)u \sim g_s m_e + g_p q \cdot S$, where S is the spin of the target particle. The differential scattering cross section in the CM reads

$$\frac{\mathrm{d}\sigma^{\chi e}}{\mathrm{d}\cos\theta^*} = \frac{g_\chi^2}{32\,\pi\, m_\phi^4} \left(g_s^2 \frac{m_e^2}{m_\chi^2} \left(1 + \frac{q^2}{4\, m_e^2} \right) + g_p^2 \frac{q^2}{4\, m_\chi^2} \right). \tag{6.4}$$

Turning to the case of loop induced elastic scattering with nucleons. Notice that the most dominant contribution to the scattering process only appears at 2-loop, involving an exchange of 2-photons, see Fig. 6.1. Instead of completely solving the 2-loop integrals, Ref. [228] evaluated the amplitude for DM-nucleon scattering by first constructing dimension 6 operator $\chi^\dagger \chi F_{\mu\nu} F^{\mu\nu}$ (through 1-loop diagrams with leptons running in the loop, evaluated in the limit $q^2 \ll m_l^2$; using the low energy theorem [337]) and then matching it onto the nucleon current. Thus solving two 1-loop integrals rather than a much complicated 2-loop integral. The amplitude for $\chi N \to \chi N$

[3] The statement is also true for tensor like interactions, but not considered in this work

reads

$$\mathcal{M} \sim \frac{1}{12}\alpha_{\rm em}^2 \frac{g_\chi g_s}{t-m_\phi^2}\frac{Q_0}{m_l} Z^2\, F_R(|q|)\left(\bar{u}_2^N \frac{(1+\gamma^0)}{2} u_1^N\right). \tag{6.5}$$

$Q_0 = \sqrt{6}\left(0.3+0.89\mathrm{A}^{1/3}\right)^{-1}$ fm^{-1} is the nuclear coherence scale [338], and $F_R(|q|)$ is the form factor that accounts for 2-photon exchange with the nucleon,

$$F_R(\tilde{q}) = \frac{4}{\pi}\int_0^1 dx \int_0^\infty d\tilde{l}\ \ \frac{\tilde{l}^2}{(\tilde{l}^2+(1-x)x\tilde{q}^2)^2} \times \exp\left(-\tilde{l}^2-\tilde{q}^2(\tfrac{1}{2}-x+x^2)\right) \times \left(\cosh\left((1-2x)\tilde{l}\tilde{q}\right) - \frac{\tilde{l}^2-(1-x)x\tilde{q}^2+1}{(1-2x)\tilde{l}\tilde{q}}\ \sinh\left((1-2x)\tilde{l}\tilde{q}\right)\right), \tag{6.6}$$

with dimensionless variables, $\tilde{l} = |\mathbf{l}|/Q_0$ and $\tilde{q} = |\mathbf{q}|/Q_0$.

Let us remark that the expression Eq. (6.5)is an excellent approximation when $l = \mu, \tau$, however, on comparison of the result of the full 2-loop integrals with that given above, differences of $\sim 100\%$ were found for the case when electrons were running in the loop. Thus the above approximation is a very good indicator of the order of magnitude and does not significantly change the results [4].

The differential cross section in the limit of large mediator mass reads,

$$\frac{\mathrm{d}\sigma^{\chi N}}{\mathrm{d}\cos\theta^*} = \frac{1}{4608\,\pi}\alpha_{\rm em}^4 Z^4 \frac{g_s^2 g_\chi^2}{m_\phi^4}\mu_{\chi N}^2 \frac{1}{m_\chi^2}\frac{Q_0^2}{m_l^2} F_R^2(|q|). \tag{6.7}$$

Notice that no loop level interactions with nucleons is possible when $g_s = 0$. The relevant figure of merit to estimate the relative importance of loop induced interactions, in the limit $g_p \to 0$ and $l = \tau$, is the ratio

$$R_{eN} = \frac{\mathrm{d}\sigma^{\chi e}}{\mathrm{d}\sigma^{\chi N}} \sim 8\times 10^6 \frac{1}{Z^4}\frac{1}{\mu_{\chi N}^2} F_R^{-2}(|q|). \tag{6.8}$$

For DM of mass $\sim 10\,GeV$, and $N = p$ (proton) the ratio $R_{ep} \sim 10^6$. For heavier nucleon targets such as Fe, the ratio can be $\sim O(1)$, hence could be important. For the case of constant cross section ($< 1\,pb$), this implies that the total annihilation rate $\Gamma^{\chi e} \sim 10^{-2}\cdot R_{eN}\cdot\Gamma^{\chi N}$. Where the superscript indicates χe indicates that the capture is through scattering off electrons, and χN scattering off nucleon N. In the end this results in competitive bounds on $\sigma_{\chi e}$ for DM around GeV and poorer bounds for TeV scale DM compared to bounds obtained by direct detection experiments.

6.2 Cross Sections for DM-Electron Elastic Scattering in Leptophilic Models

In Tab. 6.3 the relevant cross sections are listed for the model with a complex scalar DM (χ) and a real scalar mediator (ϕ). Interactions with nucleons only arise at 2-loop level.

In Tab. 6.4 the relevant cross sections are listed for the model with a scalar DM (χ) and a charged fermion mediator (η) (Yukawa like interactions with leptons). Interactions with nucleons arise at 2-loop level.

[4] The statement is qualitatively true for all the 2-loop results presented here

Model: Scalar DM - Scalar Mediator	$-\mathcal{L}_{int} = g_\chi \chi^\dagger \chi \phi + \bar{l}(g_s + i g_p \gamma_5) l \phi$
Elastic scattering $\chi - e$	$\frac{\mathrm{d}\sigma^{\chi e}}{\mathrm{d}\cos\theta^*} = \frac{g_\chi^2}{32\pi m_\phi^4}\left(g_s^2 \frac{m_e^2}{m_\chi^2}\left(1 + \frac{q^2}{4m_e^2}\right) + g_p^2 \frac{q^2}{4m_\chi^2}\right)$
Elastic scattering $\chi - N$ (2-loop)	$\frac{\mathrm{d}\sigma^{\chi N}}{\mathrm{d}\cos\theta^*} = \frac{1}{4608\pi}\alpha_{\mathrm{em}}^4 Z^4 \frac{g_s^2 g_\chi^2}{m_\phi^4}\frac{\mu_{\chi N}^2}{m_\chi^2}\frac{Q_0^2}{m_l^2}F_R^2(\lvert q\rvert)$
Comments	The 2-photon exchange form factor $F_R(\lvert q\rvert)$ is defined in Eq.(6.6).

Table 6.3: ***Scalar DM and Scalar Mediator:*** Cross sections for DM–electron elastic scattering, and DM–nucleon interactions at 2-loop in the heavy lepton limit.

Model: Scalar DM - Fermion Mediator	$-\mathcal{L}_{int} = \bar{\eta}(g_L P_L + g_R P_R) l \chi + \mathrm{h.c.}$
Elastic scattering $\chi - e$	$\frac{\mathrm{d}\sigma^{\chi e}}{\mathrm{d}\cos\theta^*} = \frac{\left(g_L^2 + g_R^2\right)^2}{64\pi m_\eta^2}\frac{m_e^2}{m_\chi^2}\left(1 + \frac{q^2}{2m_e^2}\right)$
Elastic scattering $\chi - N$ (2-loop)	$\frac{\mathrm{d}\sigma^{\chi N}}{\mathrm{d}\cos\theta^*} = \frac{1}{9216\pi}\alpha_{\mathrm{em}}^4 Z^4 \frac{\left(g_L^2 + g_R^2\right)^2}{m_\eta^2}\frac{\mu_{\chi N}^2}{m_\chi^2}\frac{Q_0^2}{m_l^2}F_R^2(\lvert q\rvert)$
Comments	Note that there are more terms $\propto g_L^2 \cdot g_R^2$, but are power suppressed in m_η^{-2}. The 2-photon exchange form factor $F_R(\lvert q\rvert)$ is defined in Eq.(6.6).

Table 6.4: ***Scalar DM and Fermion Mediator:*** Cross sections for DM–electron elastic scattering, and DM–nucleon interactions at 2-loop in the heavy lepton limit.

Model: Scalar DM - Vector Mediator	$-\mathcal{L}_{int} = g\chi^{\dagger}\overleftrightarrow{\partial_\mu}\chi\phi^\mu + \bar{l}\gamma_\mu(g_v + \gamma_5 g_{pv})l\phi^\mu$
Elastic scattering $\chi - e$	$\frac{\mathrm{d}\sigma^{\chi e}}{\mathrm{d}\cos\theta^*} = \frac{g^2 m_e^2}{8\pi m_\phi^4}\left(g_v^2\left(1+\frac{q^2}{2m_e^2}\right)+g_{pv}^2\frac{q^2}{m_e^2}\right)$
Elastic scattering $\chi - N$ (1-loop)	$\frac{\mathrm{d}\sigma^{\chi N}}{\mathrm{d}\cos\theta^*} = \frac{g^2 g_v^2 \mu_{\chi N}^2}{8\pi m_\phi^4} Z^2 F^2(\lvert q\rvert)\,\mathrm{L}_1^2\left(1-\frac{q^2}{2\mu_{\chi N}(m_\chi+m_N)}-\frac{q^2}{4m_N^2}\right)$
Comments	$\mathrm{L}_1 = \frac{\alpha_{em}}{\pi}\int_0^1 \mathrm{d}x\,(1-x)\,\mathrm{Log}\left[\frac{-x(1-x)q^2+m_l^2+i0}{\mu^2}\right]$ is the 1-loop integral, μ is chosen to be 100 GeV. $F(\lvert q\rvert)$ is the usual Helm form factor defined in Eq. 6.9. Notice that $\mathrm{d}\sigma^{\chi e}$ is independent of m_χ.

Table 6.5: ***Scalar DM and Vector Mediator:*** Cross sections for tree-level DM–electron elastic scattering, and DM–nucleon scattering at 1-loop.

In Tab. 6.5 the relevant cross sections are listed for the model with a complex scalar DM (χ) and a vector mediator (ϕ^μ). Interactions with nucleons arise at 1-loop level, proportional to the Helm form factor. For a real scalar DM the interactions with ϕ^μ vanish.

The Helm form factor is given by [339]

$$F(q) = 3e^{-\kappa^2 s^2/2}[\sin(\kappa r) - \kappa r\cos(\kappa r)]/(\kappa r)^3, \tag{6.9}$$

with $s = 1$ fm, $r = \sqrt{R^2 - 5s^2}$, $R = 1.2A^{1/3}$ fm, and $\kappa^2 \simeq q^2$.

In Tab. 6.6 the relevant cross sections are listed for the model with a fermion DM (χ) and a scalar mediator (ϕ). Interactions with nucleons arise at 2-loop level.

In Tab. 6.7 the relevant cross sections are listed for the model with a fermion DM (χ) and a vector mediator (ϕ^μ). Interactions with nucleons arise at 1-loop level for vector like interactions and they vanish for axial-vector type interactions.

In Tab. 6.8 the relevant cross sections are listed for the model with a vector DM (χ) and a neutral scalar mediator (ϕ). Interactions with nucleons arise at 2-loop level.

In Tab. 6.9 the relevant cross sections are listed for the model with a vector DM (χ) and a charged fermion mediator (η). Interactions with nucleons are tensor like and arise at 1-loop level.

Model: Fermion DM - Scalar Mediator	$-\mathcal{L}_{int} = \bar{\chi}(g_s^\chi + i\, g_p^\chi \gamma_5)\chi\phi + \bar{l}(g_s^l + i\, g_p^l \gamma_5) l\phi$
Elastic scattering $\chi - e$	$\frac{\mathrm{d}\sigma^{\chi e}}{\mathrm{d}\cos\theta^*} = \frac{m_e^2}{4\pi m_\phi^4}\left((g_s^l g_s^\chi)^2\left(1 + \frac{q^2}{4m_e^2}\right) + (g_s^l g_p^\chi)^2 \frac{q^2}{4m_e^2}\right) + \frac{m_e^2}{4\pi m_\phi^4}\left((g_p^l g_p^\chi)^2 \frac{m_e^2}{m_\chi^2}\frac{q^2}{4m_e^2}\right)$
Elastic scattering $\chi - N$ (2-loop)	$\frac{\mathrm{d}\sigma^{\chi N}}{\mathrm{d}\cos\theta^*} = \frac{1}{288\pi}\alpha_{\mathrm{em}}^4 Z^4 \frac{\mu_{\chi N}^2}{m_\phi^4}\frac{\mu_{\chi N}^2}{m_l^2}\frac{Q_0^2}{m_l^2} F_R^2(\lvert q\rvert)\left((g_s^l g_s^\chi)^2\left(\frac{q^2}{4m_N^2}\right)\right) + \frac{1}{288\pi}\alpha_{\mathrm{em}}^4 Z^4 \frac{\mu_{\chi N}^2}{m_\phi^4}\frac{\mu_{\chi N}^2}{m_l^2}\frac{Q_0^2}{m_l^2} F_R^2(\lvert q\rvert)\left((g_s^l g_p^\chi)^2 \frac{q^2}{4m_\chi^2}\right)$
Comments	$g_s^l = g_s^\chi = 0$ results in no interactions with nucleons at all loop orders. The 2-photon exchange form factor $F_R(\lvert q\rvert)$ is defined in Eq.(6.6).

Table 6.6: ***Fermion DM and Scalar Mediator:*** Cross sections for tree-level DM–electron elastic scattering, and DM–nucleon scattering at 2-loop in the heavy lepton limit.

Model: Fermion DM - Vector Mediator	$-\mathcal{L}_{int} = \bar{\chi}\gamma_\mu(g_V^\chi + g_A^\chi\gamma_5)\chi\phi^\mu + \bar{l}\gamma_\mu(g_V^l + g_A^l\gamma_5)l\phi^\mu$
Elastic scattering $\chi - e$	$\frac{\mathrm{d}\sigma^{\chi e}}{\mathrm{d}\cos\theta^*} = \frac{m_e^2}{4\pi m_\phi^4}\left((g_V^\chi g_V^l)^2 + 3(g_A^\chi g_A^l)^2\right) + \frac{m_e^2}{4\pi m_\phi^4}\left(\left((g_V^\chi g_A^l)^2 + 3(g_A^\chi g_V^l)^2\right)\frac{q^2}{4m_e^2}\right)$
Elastic scattering $\chi - N$ (1-loop)	$\frac{\mathrm{d}\sigma^{\chi N}}{\mathrm{d}\cos\theta^*} = \frac{\mu_{\chi N}^2}{8\pi m_\phi^4} Z^2 F^2(\lvert q\rvert)\,\mathrm{L}_1^2\left((g_V^\chi g_V^l)^2 + 3(g_A^\chi g_V^l)^2\left(\frac{q^2}{4m_N^2}\right)\right)$
Comments	$\mathrm{L}_1 = \frac{\alpha_{em}}{\pi}\int_0^1 \mathrm{d}x\,(1-x)\mathrm{Log}\left[\frac{-x(1-x)q^2 + m_l^2 + i\,0}{\mu^2}\right]$. $g_V^l = g_V^\chi = 0$ results in no interactions with nucleons. L_1 is the 1-loop integral, μ is chosen to be 100 GeV. $F(\lvert q\rvert)$ is the usual Helm form factor defined in Eq. 6.9.

Table 6.7: ***Fermion DM and Vector Mediator:*** Cross sections for tree-level DM–electron elastic scattering, and DM–nucleon scattering at 1-loop.

Model: Vector DM - Scalar Mediator	$-\mathcal{L}_{int} = g\chi_\mu\chi^\mu\phi + \bar{l}(g_S + i\,g_P\gamma_5)l\phi$
Elastic scattering $\chi - e$	$\frac{\mathrm{d}\sigma^{\chi e}}{\mathrm{d}\cos\theta^*} = \frac{g^2}{16\pi m_\phi^4}\left(g_S^2\frac{m_e^2}{m_\chi^2}\left(1 + \frac{q^2}{2m_e^2}\right) + g_p^2\frac{q^2}{4m_\chi^2}\right)$
Elastic scattering $\chi - N$ (2-loop)	$\frac{\mathrm{d}\sigma^{\chi N}}{\mathrm{d}\cos\theta^*} = \frac{1}{4608\pi}\alpha_{\mathrm{em}}^4 Z^4\frac{g^2 g_S^2}{m_\phi^4}\frac{\mu_{\chi N}^2}{m_\chi^2}\frac{Q_0^2}{m_l^2}F_R^2(\lvert q\rvert)$
Comments	The 2-photon exchange form factor $F_R(\lvert q\rvert)$ is defined in Eq.(6.6).

Table 6.8: ***Vector DM and Scalar Mediator:*** Cross sections for tree-level DM–electron elastic scattering, and DM–nucleon scattering at 2-loop in the heavy lepton limit

Model: Vector DM - Fermion Mediator	$-\mathcal{L}_{int} = \bar{\eta}\gamma_\mu(g_L P_L + g_R P_R) l \chi^\mu + \text{h.c.}$
Elastic scattering $\chi - e$	$\dfrac{\mathrm{d}\sigma^{\chi e}}{\mathrm{d}\cos\theta^*} = \dfrac{(g_L\, g_R)^2}{16\,\pi\, m_\eta^2}\, \dfrac{m_e^2}{m_\chi^2}\left(1 - \dfrac{q^2}{2m_e^2}\right)$
Elastic scattering $\chi - N$ (1-loop)	$\dfrac{\mathrm{d}\sigma^{\chi N}}{\mathrm{d}\cos\theta^*} = \dfrac{(g_L\, g_R)^2}{16\,\pi}\, \dfrac{\alpha_{em}^2}{\pi^2}\, Z^2\, F^2(\lvert q\rvert) \dfrac{m_l^2}{m_N^2}\, \dfrac{\mu_{\chi N}^2}{m_\chi^2}\, \dfrac{q^2}{m_N^2} B_0^2(q^2, m_l^2, m_l^2)$
Comments	$B_0(q^2, m_l^2, m_l^2)$ is the 2-point Passarino Veltman function. $F(\lvert q\rvert)$ is the Helm form factor defined in Eq. 6.9.

Table 6.9: ***Vector DM and Fermion Mediator:*** Cross sections for tree-level DM–electron elastic scattering, and DM–nucleon scattering at 1-loop.

CHAPTER 7

Summary and Outlook

There is undeniable evidence that DM exists in the present Universe [1]. Lack of an unambiguous, smoking-gun signal in experiments searching for a non-gravitational interaction of DM leaves the determination of its particle physics properties to be an open problem. There are several well motivated particle DM candidates [285], however the focus of this work has been the primarily WIMPs. The topic of this thesis has been to develop new techniques that could test the particle nature of DM with neutrino telescopes. We particularly study in detail how DM particles in the galactic halo could be brought into close orbits around the Sun after scattering off solar elements and be captured in the gravitational potential of the Sun. The annihilation of DM particles accumulated in the Sun can result in flux of neutrinos with energies of the order of the DM mass from decays of heavy hadrons, gauge bosons and tau leptons [82–88, 130–187] and with energies from tens to few hundred MeV from decays of stopped mesons and muons [188–191], which are potentially detectable with neutrino detectors/telescopes [192–205].

In chapter 2, creation of WIMPs in the early Universe through *thermal freeze-out* has been reviewed. Complementarity of the various detection methods for WIMPs and their present status has been briefly illustrated. We can conclude that the WIMP paradigm is in mild tension with current experimental results. In several well-motivated scenarios of WIMP dark matter, a significant part of the parameter space has already been excluded, but there is still a variety of interesting models which are consistent with all current constraints.

In chapter 3, the standard solar models are described, which serve as inputs for the calculations that follow in chapter 4 and chapter 5. The main results from chapter 4, 5 and 6 are summarized below. The process of capture in astrophysical objects like the Sun is commonly assumed to be due to interactions with nucleons. However, in leptophilic scenarios, in which only couplings to leptons are present at tree level, capture via interactions off electrons could be the only possibility to trap DM particles [228]. Moreover, scattering cross sections for DM-electron (and DM-nucleon) interactions, rather than being constant, could depend on the relative velocity ($v_{\rm rel}$) and the scattering angle ($\theta_{\rm cm}$) [213–227]. Indeed, even if loop-induced interactions with nucleons are, in general, possible, scatterings off electrons could be the dominant capture mechanism in models with scalar mediators and axial-vector mediators (chapter 6).

In this thesis, we have considered DM scatterings off electrons and have studied the different ingredients (capture, annihilation and evaporation) entering the calculation of the neutrino production rates from DM annihilations in the Sun for three type of generic interactions: constant (velocity-independent and isotropic), $v_{\rm rel}^2$-dependent (and isotropic) and q^2-dependent cross sections (Section 5.2). To the best of our knowledge, the possibility of capture via DM-electron interactions had only been considered for the case of constant cross sections and for masses for which evaporation can be neglected ($m_\chi > 10$ GeV) [228]. Here, we have presented detailed

analytical and numerical results for the differential scattering rates for three different types of cross sections and generic target particles (Sec. 4.1), which enter the calculation of the capture (Sec. 5.3) and evaporation (Sec. 5.5) rates; we have presented refinements in the calculation of the temperature in the isothermal approximation (Sec. 4.2), which slightly modify the DM distribution in the Sun with respect to the standard case (Sec. 5.4) and thus, could affect the annihilation and evaporation rates; and we have also computed the mean free path of DM particles for each type of cross section in generic terms (Sec. 4.3.1), which is relevant for the computation of the DM distribution in the Sun and for the suppression factor appearing in the evaporation rate (Sec. 4.3.2). Moreover, we have also investigated the effects of the truncation of the DM distribution at a velocity smaller than the escape velocity.

Given that for leptophilic DM models loop-induced interactions with nucleons would, in general, be present, we compare all our results on DM capture by electrons to those obtained for DM capture by nuclei. All our computations of capture rates take into account thermal effects (left panels of Fig. 5.2), which are very important for interactions off electrons [228], but are usually neglected for scatterings off nucleons (here presented for the first time for $v_{\rm rel}^2$-dependent and q^2-dependent cross sections). Indeed, for DM-electron scatterings the enhancement of the capture rate with respect to the zero-temperature limit could be up to three orders of magnitude for $v_{\rm rel}^2$-dependent and q^2-dependent cross sections. On the other hand, we confirm the well-known fact that, in the case of constant cross sections, thermal effects are negligible for capture by nucleons, but we note that for $v_{\rm rel}^2$-dependent and q^2-dependent cross sections, these effects could be significant (see the right panels of Fig. 5.2).

For low DM masses (typically of a few GeV), evaporation is a very effective process to reduce the number of DM particles accumulated in the Sun [83, 88, 124–126, 128, 232, 316, 317], so we have also evaluated the evaporation mass as a function of the scattering cross section, i.e., the minimum mass for which DM could remained trapped in the Sun (Section 5.6). Whereas for the case of nucleons the evaporation mass does not depend much on the cutoff (comparing $v_c(r) = v_e(r)$ and $v_c(r) = 0.9\, v_e(r)$) of the DM velocity distribution (Fig. 5.11), for interactions with electrons, the presence of a cutoff $v_c(r) < v_e(r)$ could have important implications, shifting the evaporation mass below the GeV range, down to few-hundred MeV, and opening up a new region in the parameter space suitable to be tested in the future. A definite answer regarding this possibility would require the use of the correct DM distribution and thus, solving the collisional Boltzmann equation, which is beyond the scope of this thesis.

In chapter 6, we have considered elementary leptophilic simplified models and illustrated that q^2 and $v_{\rm rel}^2$-dependent DM-electron elastic scattering cross sections naturally arise in these models, we have also shown that DM-nucleon elastic scattering is generally loop suppressed. Nevertheless, 1-loop DM-nucleon interactions can dominate over DM-electron interactions for certain choice of model and their parameters. Whereas, in some models considered here DM-electron interactions always dominate over 2-loop DM-nucleon interactions. We have summarized the obtained cross sections in a list of tables; for a model with scalar DM with a scalar mediator see Tab. 6.3, scalar DM with a fermion mediator in Tab. 6.4, scalar DM with vector mediator in Tab. 6.5. Similarly, fermion DM with a scalar mediator in Tab. 6.6, fermion DM with vector mediator in Tab. 6.7. For vector DM with scalar mediator in Tab. 6.8 and vector DM with fermion mediator in Tab. 6.9.

Finally, we have compared the neutrino rates at production resulting from (s-wave) annihilations of DM particles after being captured either by solar electrons or nuclei for constant, $v_{\rm rel}^2$-dependent and q^2-dependent scattering cross sections (Fig. 5.13). We have found that, for the normalizations of the cross sections considered in this work, capture by electrons would result in neutrino rates about two orders of magnitude smaller than those obtained in the case of

DM-nucleon SD interactions for constant cross sections, whereas in the case of $v_{\rm rel}^2$-dependent and q^2-dependent cross sections, interactions off electrons result in a larger neutrino production rate. For the three type of cross sections, the most efficient process is via DM-nucleon SI interactions, although stronger limits exist in this case [45, 47–49, 241–245].

So far, there is no conclusive evidence of the existence of DM, other than from its gravitational interactions. Therefore, investigating different and complementary techniques to search for DM is of crucial importance. Here, we have studied one of the existing strategies to indirectly detect DM, which is in turn complementary to DM direct searches. Indeed, the phenomenological approach discussed in much detail in this work represents the first step in evaluating the relevance of DM capture in leptophilic scenarios and of their potential signals at neutrino detectors/telescopes [6]. In the coming decade, we expect more data and increased experimental sensitivities: ton-scale direct detection experiments such as XENONnT, LZ or DARWIN will further push the sensitivity to the scattering cross section of dark matter with nucleons all the way to the neutrino floor; indirect detection experiments such as HyperKamiokande, Juno, IceCube, which is sensitive to Spin-Dependent scattering of nucleons in the Sun will also greatly improve in sensitivity. Experiments such as CTA or AMS-02 will probe even smaller values of the annihilation cross section of dark matter. We end with the hope that the discussion provided in this thesis can help in effectively constraining DM-electron cross section independent of Direct detection and Collider experiments.

References

Bibliography

[1] C. Patrignani et al., *Review of Particle Physics*, Chin. Phys. **C40** (2016) 100001 (cit. on pp. 1, 40, 83).

[2] J. de Swart, G. Bertone and J. van Dongen, *How Dark Matter Came to Matter*, (2017), [Nature Astron.1,0059(2017)], arXiv: 1703.00013 [astro-ph.CO] (cit. on p. 1).

[3] M. Drees and M. M. Nojiri, *The Neutralino relic density in minimal N = 1 supergravity*, Phys. Rev. **D47** (1993) 376, arXiv: hep-ph/9207234 [hep-ph] (cit. on p. 1).

[4] K. Benakli, J. R. Ellis and D. V. Nanopoulos, *Natural candidates for superheavy dark matter in string and M theory*, Phys. Rev. **D59** (1999) 047301, arXiv: hep-ph/9803333 [hep-ph] (cit. on p. 1).

[5] R. Garani and S. Palomares-Ruiz, *Dark matter in the Sun: scattering off electrons vs nucleons*, JCAP **1705** (2017) 007, arXiv: 1702.02768 [hep-ph] (cit. on pp. 2, 10).

[6] Dark matter in the Sun: the Leptophilic Case, R. Garani and S. Palomares-Ruiz, in preparation (cit. on pp. 3, 40, 45, 66, 85).

[7] J. R. Primack, D. Seckel and B. Sadoulet, *Detection of Cosmic Dark Matter*, Ann. Rev. Nucl. Part. Sci. **38** (1988) 751 (cit. on p. 5).

[8] C. Alcock et al., *The MACHO Project: Microlensing Results from 5.7 Years of Large Magellanic Cloud Observations*, **542** (2000) 281, eprint: astro-ph/0001272 (cit. on p. 5).

[9] B. Fields and S. Sarkar, *Big-Bang nucleosynthesis (Particle Data Group mini-review)*, ArXiv Astrophysics e-prints (2006), eprint: astro-ph/0601514 (cit. on p. 5).

[10] K. Kadota, T. Sekiguchi and H. Tashiro, *A new constraint on millicharged dark matter from galaxy clusters*, ArXiv e-prints (2016), arXiv: 1602.04009 (cit. on p. 5).

[11] N. Aghanim et al., *Planck 2015 results. XI. CMB power spectra, likelihoods, and robustness of parameters*, Astron. Astrophys. **594** (2016) A11, arXiv: 1507.02704 [astro-ph.CO] (cit. on p. 5).

[12] R. Cowsik and J. McClelland, *An Upper Limit on the Neutrino Rest Mass*, Physical Review Letters **29** (1972) 669 (cit. on p. 5).

[13] S. Tremaine and J. E. Gunn, *Dynamical Role of Light Neutral Leptons in Cosmology*, Phys. Rev. Lett. **42** (1979) 407 (cit. on p. 5).

[14] E. W. Kolb and M. S. Turner, *The Early Universe*, Front.Phys. **69** (1990) 1 (cit. on pp. 5, 7).

[15] M. Srednicki, R. Watkins and K. A. Olive, *Calculations of Relic Densities in the Early Universe*, Nucl.Phys. **B310** (1988) 693 (cit. on p. 6).

[16] K. A. Olive, D. N. Schramm and G. Steigman, *Limits on New Superweakly Interacting Particles from Primordial Nucleosynthesis*, Nucl.Phys. **B180** (1981) 497 (cit. on p. 6).

[17] M. Drees, F. Hajkarim and E. Rossi Schmitz,
The effects of QCD equation of state on the relic density of WIMP dark matter,
6, 025 (2015) 025, arXiv: 1503.03513 [hep-ph] (cit. on p. 6).

[18] P. Gondolo and G. Gelmini, *Cosmic abundances of stable particles: Improved analysis*,
Nucl.Phys. **B360** (1991) 145 (cit. on p. 7).

[19] J. Edsjo and P. Gondolo, *Neutralino relic density including coannihilations*,
Phys.Rev. **D56** (1997) 1879, arXiv: hep-ph/9704361 [hep-ph] (cit. on p. 7).

[20] T. R. Slatyer, N. Padmanabhan and D. P. Finkbeiner, *CMB Constraints on WIMP Annihilation: Energy Absorption During the Recombination Epoch*,
Phys. Rev. **D80** (2009) 043526, arXiv: 0906.1197 [astro-ph.CO] (cit. on p. 7).

[21] R. Diamanti et al.,
Constraining Dark Matter Late-Time Energy Injection: Decays and P-Wave Annihilations,
JCAP **1402** (2014) 017, arXiv: 1308.2578 [astro-ph.CO] (cit. on p. 7).

[22] S. A. Malik et al., *Interplay and Characterization of Dark Matter Searches at Colliders and in Direct Detection Experiments*, Phys. Dark Univ. **9-10** (2015) 51,
arXiv: 1409.4075 [hep-ex] (cit. on p. 8).

[23] J. Abdallah et al., *Simplified Models for Dark Matter Searches at the LHC*,
Phys. Dark Univ. **9-10** (2015) 8, arXiv: 1506.03116 [hep-ph] (cit. on pp. 8, 71).

[24] D. Abercrombie et al., *Dark Matter Benchmark Models for Early LHC Run-2 Searches: Report of the ATLAS/CMS Dark Matter Forum*, (2015), ed. by A. Boveia et al.,
arXiv: 1507.00966 [hep-ex] (cit. on p. 8).

[25] A. Choudhury et al.,
Less-simplified models of dark matter for direct detection and the LHC,
JHEP **04** (2016) 182, arXiv: 1509.05771 [hep-ph] (cit. on p. 8).

[26] F. Kahlhoefer et al.,
Implications of unitarity and gauge invariance for simplified dark matter models,
JHEP **02** (2016) 016, arXiv: 1510.02110 [hep-ph] (cit. on pp. 8, 71).

[27] C. Englert, M. McCullough and M. Spannowsky,
S-Channel Dark Matter Simplified Models and Unitarity, Phys. Dark Univ. **14** (2016) 48,
arXiv: 1604.07975 [hep-ph] (cit. on p. 8).

[28] V. Khachatryan et al., *Search for new phenomena in monophoton final states in proton-proton collisions at $\sqrt{s} = 8$ TeV*, Phys. Lett. **B755** (2016) 102,
arXiv: 1410.8812 [hep-ex] (cit. on p. 8).

[29] G. Aad et al., *Search for dark matter in events with a hadronically decaying W or Z boson and missing transverse momentum in pp collisions at $\sqrt{s} = 8$ TeV with the ATLAS detector*,
Phys. Rev. Lett. **112** (2014) 041802, arXiv: 1309.4017 [hep-ex] (cit. on p. 8).

[30] G. Aad et al., *Search for dark matter in events with a Z boson and missing transverse momentum in pp collisions at $\sqrt{s}$=8 TeV with the ATLAS detector*,
Phys. Rev. **D90** (2014) 012004, arXiv: 1404.0051 [hep-ex] (cit. on p. 8).

[31] I. M. Shoemaker and L. Vecchi,
Unitarity and Monojet Bounds on Models for DAMA, CoGeNT, and CRESST-II,
Phys. Rev. **D86** (2012) 015023, arXiv: 1112.5457 [hep-ph] (cit. on p. 8).

[32] D. Barducci et al., *Monojet searches for momentum-dependent dark matter interactions*,
JHEP **01** (2017) 078, arXiv: 1609.07490 [hep-ph] (cit. on p. 8).

[33] M. Aaboud et al., *Search for dark matter in association with a Higgs boson decaying to b-quarks in pp collisions at $\sqrt{s} = 13$ TeV with the ATLAS detector*,
Phys. Lett. **B765** (2017) 11, arXiv: 1609.04572 [hep-ex] (cit. on p. 8).

[34] A. M. Sirunyan et al., *Search for associated production of dark matter with a Higgs boson decaying to $b\bar{b}$ or $\gamma\gamma$ at $\sqrt{s} = 13$ TeV*, (2017), arXiv: 1703.05236 [hep-ex] (cit. on p. 8).

[35] G. Bertone, D. Hooper and J. Silk, *Particle dark matter: Evidence, candidates and constraints*, Phys.Rept. **405** (2005) 279, arXiv: hep-ph/0404175 [hep-ph] (cit. on p. 9).

[36] R. Bernabei et al., *New results from DAMA/LIBRA*, Eur. Phys. J. **C67** (2010) 39, arXiv: 1002.1028 [astro-ph.GA] (cit. on pp. 9, 71).

[37] R. Bernabei et al., *Final model independent result of DAMA/LIBRA-phase1*, Eur. Phys. J. **C73** (2013) 2648, arXiv: 1308.5109 [astro-ph.GA] (cit. on pp. 9, 39).

[38] C. E. Aalseth et al., *Results from a Search for Light-Mass Dark Matter with a P-type Point Contact Germanium Detector*, Phys. Rev. Lett. **106** (2011) 131301, arXiv: 1002.4703 [astro-ph.CO] (cit. on pp. 9, 71).

[39] C. E. Aalseth et al., *Search for an Annual Modulation in a P-type Point Contact Germanium Dark Matter Detector*, Phys. Rev. Lett. **107** (2011) 141301, arXiv: 1106.0650 [astro-ph.CO] (cit. on pp. 9, 71).

[40] C. E. Aalseth et al., *CoGeNT: A Search for Low-Mass Dark Matter using p-type Point Contact Germanium Detectors*, Phys. Rev. **D88** (2013) 012002, arXiv: 1208.5737 [astro-ph.CO] (cit. on pp. 9, 71).

[41] C. E. Aalseth et al., *Search for An Annual Modulation in Three Years of CoGeNT Dark Matter Detector Data*, (2014), arXiv: 1401.3295 [astro-ph.CO] (cit. on p. 9).

[42] C. E. Aalseth et al., *Maximum Likelihood Signal Extraction Method Applied to 3.4 years of CoGeNT Data*, (2014), arXiv: 1401.6234 [astro-ph.CO] (cit. on p. 9).

[43] R. Agnese et al., *Silicon Detector Dark Matter Results from the Final Exposure of CDMS II*, Phys. Rev. Lett. **111** (2013) 251301, arXiv: 1304.4279 [hep-ex] (cit. on pp. 9, 71).

[44] E. Aprile et al., *Dark Matter Results from 100 Live Days of XENON100 Data*, Phys. Rev. Lett. **107** (2011) 131302, arXiv: 1104.2549 [astro-ph.CO] (cit. on p. 9).

[45] R. Agnese et al., *New Results from the Search for Low-Mass Weakly Interacting Massive Particles with the CDMS Low Ionization Threshold Experiment*, Phys. Rev. Lett. **116** (2016) 071301, arXiv: 1509.02448 [astro-ph.CO] (cit. on pp. 9, 39, 85).

[46] D. S. Akerib et al., *Improved Limits on Scattering of Weakly Interacting Massive Particles from Reanalysis of 2013 LUX Data*, Phys. Rev. Lett. **116** (2016) 161301, arXiv: 1512.03506 [astro-ph.CO] (cit. on p. 9).

[47] A. Tan et al., *Dark Matter Results from First 98.7 Days of Data from the PandaX-II Experiment*, Phys. Rev. Lett. **117** (2016) 121303, arXiv: 1607.07400 [hep-ex] (cit. on pp. 9, 10, 39, 85).

[48] D. S. Akerib et al., *Results from a search for dark matter in the complete LUX exposure*, Phys. Rev. Lett. **118** (2017) 021303, arXiv: 1608.07648 [astro-ph.CO] (cit. on pp. 9, 10, 39, 85).

[49] E. Aprile et al., *XENON100 Dark Matter Results from a Combination of 477 Live Days*, Phys. Rev. **D94** (2016) 122001, arXiv: 1609.06154 [astro-ph.CO] (cit. on pp. 9, 39, 85).

[50] E. Aprile et al., *First Dark Matter Search Results from the XENON1T Experiment*, (2017), arXiv: 1705.06655 [astro-ph.CO] (cit. on p. 9).

[51] C. Amole et al., *Dark Matter Search Results from the PICO-60 C_3F_8 Bubble Chamber*, Phys. Rev. Lett. **118** (2017) 251301, arXiv: 1702.07666 [astro-ph.CO] (cit. on p. 10).

[52] D. S. Akerib et al., *Limits on spin-dependent WIMP-nucleon cross section obtained from the complete LUX exposure*, Phys. Rev. Lett. **118** (2017) 251302, arXiv: 1705.03380 [astro-ph.CO] (cit. on p. 10).

[53] E. Behnke et al., *Final Results of the PICASSO Dark Matter Search Experiment*, Astropart. Phys. **90** (2017) 85, arXiv: 1611.01499 [hep-ex] (cit. on p. 10).

[54] D. S. Akerib et al., *LUX-ZEPLIN (LZ) Conceptual Design Report*, (2015), arXiv: 1509.02910 [physics.ins-det] (cit. on p. 10).

[55] M. Szydagis, *The Present and Future of Searching for Dark Matter with LUX and LZ*, PoS **ICHEP2016** (2016) 220, arXiv: 1611.05525 [astro-ph.CO] (cit. on p. 10).

[56] M. Schumann et al., *Dark matter sensitivity of multi-ton liquid xenon detectors*, JCAP **1510** (2015) 016, arXiv: 1506.08309 [physics.ins-det] (cit. on p. 10).

[57] P. Agnes et al., *Results from the first use of low radioactivity argon in a dark matter search*, Phys. Rev. **D93** (2016) 081101, [Addendum: Phys. Rev.D95,no.6,069901(2017)], arXiv: 1510.00702 [astro-ph.CO] (cit. on p. 10).

[58] S. Davini, P. Agnes and D. Franco, *The DarkSide awakens*, J. Phys. Conf. Ser. **718** (2016) 042016 (cit. on p. 10).

[59] A. Pullia, *Searches for Dark Matter with Superheated Liquid Techniques*, Adv. High Energy Phys. **2014** (2014) 387493 (cit. on p. 10).

[60] R. Agnese et al., *Projected Sensitivity of the SuperCDMS SNOLAB experiment*, Phys. Rev. **D95** (2017) 082002, arXiv: 1610.00006 [physics.ins-det] (cit. on p. 10).

[61] J. Alexander et al., "Dark Sectors 2016 Workshop: Community Report", 2016, arXiv: 1608.08632 [hep-ph], URL: http://inspirehep.net/record/1484628/files/arXiv:1608.08632.pdf (cit. on p. 10).

[62] R. Essig et al., *Direct Detection of sub-GeV Dark Matter with Semiconductor Targets*, JHEP **05** (2016) 046, arXiv: 1509.01598 [hep-ph] (cit. on pp. 10, 39).

[63] D. Green and S. Rajendran, *The Cosmology of Sub-MeV Dark Matter*, (2017), arXiv: 1701.08750 [hep-ph] (cit. on p. 10).

[64] T. Emken, C. Kouvaris and I. M. Shoemaker, *Terrestrial Effects on Dark Matter-Electron Scattering Experiments*, Phys. Rev. **D96** (2017) 015018, arXiv: 1702.07750 [hep-ph] (cit. on p. 10).

[65] R. Essig, T. Volansky and T.-T. Yu, *New Constraints and Prospects for sub-GeV Dark Matter Scattering off Electrons in Xenon*, (2017), arXiv: 1703.00910 [hep-ph] (cit. on p. 10).

[66] F. Kadribasic et al., *Directional Sensitivity In Light-Mass Dark Matter Searches With Single-Electron Resolution Ionization Detectors*, (2017), arXiv: 1703.05371 [physics.ins-det] (cit. on p. 10).

[67] P. W. Graham et al., *Semiconductor Probes of Light Dark Matter*, Phys. Dark Univ. **1** (2012) 32, arXiv: 1203.2531 [hep-ph] (cit. on p. 10).

[68] Y. Hochberg, T. Lin and K. M. Zurek, *Absorption of light dark matter in semiconductors*, Phys. Rev. **D95** (2017) 023013, arXiv: 1608.01994 [hep-ph] (cit. on p. 10).

[69] Y. Hochberg, Y. Zhao and K. M. Zurek,
Superconducting Detectors for Superlight Dark Matter,
Phys. Rev. Lett. **116** (2016) 011301, arXiv: 1504.07237 [hep-ph] (cit. on p. 10).

[70] Y. Hochberg et al., *Detecting Superlight Dark Matter with Fermi-Degenerate Materials*,
JHEP **08** (2016) 057, arXiv: 1512.04533 [hep-ph] (cit. on p. 10).

[71] Y. Hochberg, T. Lin and K. M. Zurek,
Detecting Ultralight Bosonic Dark Matter via Absorption in Superconductors,
Phys. Rev. **D94** (2016) 015019, arXiv: 1604.06800 [hep-ph] (cit. on p. 10).

[72] S. Derenzo et al., *Direct Detection of sub-GeV Dark Matter with Scintillating Targets*,
Phys. Rev. **D96** (2017) 016026, arXiv: 1607.01009 [hep-ph] (cit. on p. 10).

[73] K. Schutz and K. M. Zurek, *Detectability of Light Dark Matter with Superfluid Helium*,
Phys. Rev. Lett. **117** (2016) 121302, arXiv: 1604.08206 [hep-ph] (cit. on p. 10).

[74] S. Knapen, T. Lin and K. M. Zurek,
Light Dark Matter in Superfluid Helium: Detection with Multi-excitation Production,
Phys. Rev. **D95** (2017) 056019, arXiv: 1611.06228 [hep-ph] (cit. on p. 10).

[75] R. Essig et al.,
Detection of sub-GeV Dark Matter and Solar Neutrinos via Chemical-Bond Breaking,
Phys. Rev. **D95** (2017) 056011, arXiv: 1608.02940 [hep-ph] (cit. on p. 10).

[76] L. M. Capparelli et al., *Directional Dark Matter Searches with Carbon Nanotubes*,
Phys. Dark Univ. **9-10** (2015) 24, [Erratum: Phys. Dark Univ.11,79(2016)],
arXiv: 1412.8213 [physics.ins-det] (cit. on p. 10).

[77] Y. Hochberg et al., *Directional detection of dark matter with two-dimensional targets*,
Phys. Lett. **B772** (2017) 239, arXiv: 1606.08849 [hep-ph] (cit. on p. 10).

[78] G. Cavoto, F. Luchetta and A. D. Polosa,
Sub-GeV Dark Matter Detection with Electron Recoils in Carbon Nanotubes, (2017),
arXiv: 1706.02487 [hep-ph] (cit. on p. 10).

[79] R. Budnik et al., *Direct Detection of Light Dark Matter and Solar Neutrinos via Color Center Production in Crystals*, (2017), arXiv: 1705.03016 [hep-ph] (cit. on p. 10).

[80] C. Kouvaris and J. Pradler, *Probing sub-GeV Dark Matter with conventional detectors*,
Phys. Rev. Lett. **118** (2017) 031803, arXiv: 1607.01789 [hep-ph] (cit. on p. 10).

[81] C. McCabe,
New constraints and discovery potential of sub-GeV dark matter with xenon detectors,
(2017), arXiv: 1702.04730 [hep-ph] (cit. on p. 10).

[82] J. Silk, K. A. Olive and M. Srednicki, *The photino, the Sun and high-energy neutrinos*,
Phys. Rev. Lett. **55** (1985) 257 (cit. on pp. 11, 21, 83).

[83] L. M. Krauss, M. Srednicki and F. Wilczek,
Solar System Constraints and Signatures for Dark Matter Candidates,
Phys. Rev. **D33** (1986) 2079 (cit. on pp. 11, 21, 83, 84).

[84] K. Freese, *Can Scalar Neutrinos Or Massive Dirac Neutrinos Be the Missing Mass?*,
Phys. Lett. **B167** (1986) 295 (cit. on pp. 11, 21, 83).

[85] J. S. Hagelin, K. Ng and K. A. Olive,
A high-energy neutrino signature from supersymmetric relics, Phys.Lett. **B180** (1986) 375
(cit. on pp. 11, 21, 83).

[86] T. Gaisser, G. Steigman and S. Tilav,
Limits on cold dark matter candidates from deep underground detectors,
Phys. Rev. **D34** (1986) 2206 (cit. on pp. 11, 21, 22, 61, 83).

[87] M. Srednicki, K. A. Olive and J. Silk,
High-energy neutrinos from the Sun and cold dark matter, Nucl. Phys. **B279** (1987) 804 (cit. on pp. 11, 21, 83).

[88] K. Griest and D. Seckel, *Cosmic asymmetry, neutrinos and the Sun*,
Nucl. Phys. **B283** (1987) 681 (cit. on pp. 11, 21, 22, 31, 54, 61, 83, 84).

[89] L. Goodenough and D. Hooper, *Possible Evidence For Dark Matter Annihilation In The Inner Milky Way From The Fermi Gamma Ray Space Telescope*, (2009),
arXiv: 0910.2998 [hep-ph] (cit. on p. 11).

[90] T. Linden et al., *High-energy tail of the Galactic Center gamma-ray excess*,
Phys. Rev. **D94** (2016) 103013, arXiv: 1604.01026 [astro-ph.HE] (cit. on p. 11).

[91] F. Calore et al., *Diffuse gamma-ray emission from galactic pulsars*,
Astrophys. J. **796** (2014) 1, arXiv: 1406.2706 [astro-ph.HE] (cit. on p. 11).

[92] I. Cholis, D. Hooper and T. Linden,
Challenges in Explaining the Galactic Center Gamma-Ray Excess with Millisecond Pulsars,
JCAP **1506** (2015) 043, arXiv: 1407.5625 [astro-ph.HE] (cit. on p. 11).

[93] J. Petrović, P. D. Serpico and G. Zaharijas, *Millisecond pulsars and the Galactic Center gamma-ray excess: the importance of luminosity function and secondary emission*,
JCAP **1502** (2015) 023, arXiv: 1411.2980 [astro-ph.HE] (cit. on p. 11).

[94] I. Cholis et al.,
The Galactic Center GeV Excess from a Series of Leptonic Cosmic-Ray Outbursts,
JCAP **1512** (2015) 005, arXiv: 1506.05119 [astro-ph.HE] (cit. on p. 11).

[95] O. Macias et al.,
Discovery of Gamma-Ray Emission from the X-shaped Bulge of the Milky Way, (2016),
arXiv: 1611.06644 [astro-ph.HE] (cit. on p. 11).

[96] F. Calore et al., *A Tale of Tails: Dark Matter Interpretations of the Fermi GeV Excess in Light of Background Model Systematics*, Phys. Rev. **D91** (2015) 063003,
arXiv: 1411.4647 [hep-ph] (cit. on p. 11).

[97] G. Bertone et al., *Global analysis of the pMSSM in light of the Fermi GeV excess: prospects for the LHC Run-II and astroparticle experiments*, JCAP **1604** (2016) 037,
arXiv: 1507.07008 [hep-ph] (cit. on p. 11).

[98] A. Albert et al., *Searching for Dark Matter Annihilation in Recently Discovered Milky Way Satellites with Fermi-LAT*, Astrophys. J. **834** (2017) 110,
arXiv: 1611.03184 [astro-ph.HE] (cit. on p. 11).

[99] L. Struder et al.,
The European Photon Imaging Camera on XMM-Newton: The pn-CCD camera,
Astron. Astrophys. **365** (2001) L18 (cit. on p. 11).

[100] M. J. L. Turner et al.,
The European Photon Imaging Camera on XMM-Newton: The MOS cameras,
Astron. Astrophys. **365** (2001) L27, arXiv: astro-ph/0011498 [astro-ph]
(cit. on p. 11).

[101] E. Bulbul et al., *Detection of An Unidentified Emission Line in the Stacked X-ray spectrum of Galaxy Clusters*, Astrophys. J. **789** (2014) 13, arXiv: 1402.2301 [astro-ph.CO]
(cit. on p. 11).

[102] O. Ruchayskiy et al., *Searching for decaying dark matter in deep XMM–Newton observation of the Draco dwarf spheroidal*, Mon. Not. Roy. Astron. Soc. **460** (2016) 1390,
arXiv: 1512.07217 [astro-ph.HE] (cit. on p. 11).

[103] J. Franse et al., *Radial Profile of the 3.55 keV line out to R_{200} in the Perseus Cluster*, Astrophys. J. **829** (2016) 124, arXiv: 1604.01759 [astro-ph.CO] (cit. on p. 11).

[104] O. Urban et al., *A Suzaku Search for Dark Matter Emission Lines in the X-ray Brightest Galaxy Clusters*, Mon. Not. Roy. Astron. Soc. **451** (2015) 2447, arXiv: 1411.0050 [astro-ph.CO] (cit. on p. 11).

[105] F. A. Aharonian et al., *Hitomi constraints on the 3.5 keV line in the Perseus galaxy cluster*, Astrophys. J. **837** (2017) L15, arXiv: 1607.07420 [astro-ph.HE] (cit. on p. 11).

[106] N. Cappelluti et al., *Searching for the 3.5 keV Line in the Deep Fields with Chandra: the 10 Ms observations*, (2017), arXiv: 1701.07932 [astro-ph.CO] (cit. on p. 11).

[107] T. E. Jeltema and S. Profumo, *Discovery of a 3.5 keV line in the Galactic Centre and a critical look at the origin of the line across astronomical targets*, Mon. Not. Roy. Astron. Soc. **450** (2015) 2143, arXiv: 1408.1699 [astro-ph.HE] (cit. on p. 11).

[108] O. Adriani et al., *An anomalous positron abundance in cosmic rays with energies 1.5-100 GeV*, Nature **458** (2009) 607, arXiv: 0810.4995 [astro-ph] (cit. on pp. 11, 39, 71).

[109] M. Aguilar et al., *First Result from the Alpha Magnetic Spectrometer on the International Space Station: Precision Measurement of the Positron Fraction in Primary Cosmic Rays of 0.5–350 GeV*, Phys. Rev. Lett. **110** (2013) 141102 (cit. on p. 11).

[110] M. Di Mauro et al., *Interpretation of AMS-02 electrons and positrons data*, JCAP **1404** (2014) 006, arXiv: 1402.0321 [astro-ph.HE] (cit. on p. 11).

[111] J. N. Bahcall, M. H. Pinsonneault and S. Basu, *Solar models: Current epoch and time dependences, neutrinos, and helioseismological properties*, Astrophys. J. **555** (2001) 990, arXiv: astro-ph/0010346 [astro-ph] (cit. on pp. 13, 16).

[112] A. Serenelli, *Alive and well: a short review about standard solar models*, Eur. Phys. J. **A52** (2016) 78, arXiv: 1601.07179 [astro-ph.SR] (cit. on pp. 13, 17).

[113] A. Cox, W. Livingston and M. Matthews, *Solar interior and atmosphere*, Space science series, University of Arizona Press, 1991, ISBN: 9780816512294, URL: https://books.google.de/books?id=GZXvAAAAMAAJ (cit. on pp. 13, 16).

[114] M. Asplund et al., *The chemical composition of the Sun*, Ann. Rev. Astron. Astrophys. **47** (2009) 481, arXiv: 0909.0948 [astro-ph.SR] (cit. on pp. 13, 14, 16, 17, 43).

[115] E. Caffau et al., *Solar Chemical Abundances Determined with a CO5BOLD 3D Model Atmosphere*, Solar Phys. **268** (2011) 255, arXiv: 1003.1190 [astro-ph.SR] (cit. on p. 13).

[116] J. Engel and P. Vogel, *Spin dependent cross-sections of weakly interacting massive particles on nuclei*, Phys. Rev. **D40** (1989) 3132 (cit. on pp. 14, 42, 43).

[117] K. Lodders, H. Palme and H.-P. Gail, *Abundances of the Elements in the Solar System*, Landolt Börnstein (2009), arXiv: 0901.1149 [astro-ph.EP] (cit. on p. 14).

[118] R. B. Leighton, R. W. Noyes and G. W. Simon, *Velocity Fields in the Solar Atmosphere. I. Preliminary Report.*, **135** (1962) 474 (cit. on p. 15).

[119] J. W. Leibacher and R. F. Stein, *A New Description of the Solar Five-Minute Oscillation*, **7** (1971) 191 (cit. on p. 15).

[120] R. K. Ulrich, *The Five-Minute Oscillations on the Solar Surface*, **162** (1970) 993 (cit. on p. 15).

[121] J. N. Bahcall et al., *Standard solar models and the uncertainties in predicted capture rates of solar neutrinos*, Reviews of Modern Physics **54** (1982) 767 (cit. on p. 16).

[122] J. N. Bahcall and R. K. Ulrich, *Solar models, neutrino experiments, and helioseismology*, Reviews of Modern Physics **60** (1988) 297 (cit. on p. 16).

[123] W. C. Haxton, R. G. Hamish Robertson and A. M. Serenelli, *Solar Neutrinos: Status and Prospects*, Ann. Rev. Astron. Astrophys. **51** (2013) 21, arXiv: 1208.5723 [astro-ph.SR] (cit. on p. 16).

[124] G. Steigman et al., *Dynamical interactions and astrophysical effects of stable heavy neutrinos*, Astron. J. **83** (1978) 1050 (cit. on pp. 21, 84).

[125] D. N. Spergel and W. H. Press, *Effect of hypothetical, weakly interacting, massive particles on energy transport in the solar interior*, Astrophys. J. **294** (1985) 663 (cit. on pp. 21, 31, 32, 54, 84).

[126] J. Faulkner and R. L. Gilliland, *Weakly interacting, massive particles and the solar neutrino flux*, Astrophys. J. **299** (1985) 994 (cit. on pp. 21, 31, 54, 84).

[127] W. H. Press and D. N. Spergel, *Capture by the sun of a galactic population of weakly interacting massive particles*, Astrophys. J. **296** (1985) 679 (cit. on p. 21).

[128] A. Gould, *WIMP Distribution in and Evaporation From the Sun*, Astrophys. J. **321** (1987) 560 (cit. on pp. 21, 26, 28, 29, 31, 54, 55, 84).

[129] A. Gould, *Resonant Enhancements in WIMP Capture by the Earth*, Astrophys. J. **321** (1987) 571 (cit. on p. 21).

[130] M. Kamionkowski, *Energetic neutrinos from heavy neutralino annihilation in the Sun*, Phys. Rev. **D44** (1991) 3021 (cit. on pp. 21, 83).

[131] A. Bottino et al., *Indirect search for neutralinos at neutrino telescopes*, Phys.Lett. **B265** (1991) 57 (cit. on pp. 21, 83).

[132] F. Halzen, T. Stelzer and M. Kamionkowski, *Signatures of dark matter in underground detectors*, Phys. Rev. **D45** (1992) 4439 (cit. on pp. 21, 83).

[133] R. Gandhi et al., *Scrutinizing supergravity models through neutrino telescopes*, Phys. Rev. **D49** (1994) 3691, arXiv: astro-ph/9309048 [astro-ph] (cit. on pp. 21, 83).

[134] A. Bottino et al., *Signals of neutralino dark matter from earth and sun*, Astropart. Phys. **3** (1995) 65, arXiv: hep-ph/9408391 [hep-ph] (cit. on pp. 21, 83).

[135] L. Bergström, J. Edsjö and P. Gondolo, *Indirect neutralino detection rates in neutrino telescopes*, Phys. Rev. **D55** (1997) 1765, arXiv: hep-ph/9607237 [hep-ph] (cit. on pp. 21, 83).

[136] L. Bergström, J. Edsjö and P. Gondolo, *Indirect detection of dark matter in km size neutrino telescopes*, Phys. Rev. **D58** (1998) 103519, arXiv: hep-ph/9806293 [hep-ph] (cit. on pp. 21, 83).

[137] V. D. Barger et al., *Indirect search for neutralino dark matter with high-energy neutrinos*, Phys. Rev. **D65** (2002) 075022, arXiv: hep-ph/0105182 [hep-ph] (cit. on pp. 21, 83).

[138] V. Bertin, E. Nezri and J. Orloff, *Neutrino indirect detection of neutralino dark matter in the CMSSM*, Eur. Phys. J. **C26** (2002) 111, arXiv: hep-ph/0204135 [hep-ph] (cit. on pp. 21, 83).

[139] D. Hooper and G. D. Kribs, *Probing Kaluza-Klein dark matter with neutrino telescopes*, Phys. Rev. **D67** (2003) 055003, arXiv: hep-ph/0208261 [hep-ph] (cit. on pp. 21, 83).

[140] A. Bueno et al., *Indirect detection of dark matter WIMPs in a liquid argon TPC*, JCAP **0501** (2005) 001, arXiv: hep-ph/0410206 [hep-ph] (cit. on pp. 21, 83).

[141] M. Cirelli et al., *Spectra of neutrinos from dark matter annihilations*, Nucl. Phys. **B727** (2005) 99, arXiv: hep-ph/0506298 [hep-ph] (cit. on pp. 21, 83).

[142] F. Halzen and D. Hooper, *Prospects for detecting dark matter with neutrino telescopes in light of recent results from direct detection experiments*, Phys. Rev. **D73** (2006) 123507, arXiv: hep-ph/0510048 [hep-ph] (cit. on pp. 21, 83).

[143] O. Mena, S. Palomares-Ruiz and S. Pascoli, *Reconstructing WIMP properties with neutrino detectors*, Phys.Lett. **B664** (2008) 92, arXiv: 0706.3909 [hep-ph] (cit. on pp. 21, 83).

[144] R. Lehnert and T. J. Weiler, *Neutrino flavor ratios as diagnostic of solar WIMP annihilation*, Phys. Rev. **D77** (2008) 125004, arXiv: 0708.1035 [hep-ph] (cit. on pp. 21, 83).

[145] V. Barger et al., *High energy neutrinos from neutralino annihilations in the Sun*, Phys. Rev. **D76** (2007) 095008, arXiv: 0708.1325 [hep-ph] (cit. on pp. 21, 83).

[146] V. D. Barger, W.-Y. Keung and G. Shaughnessy, *Monochromatic Neutrino Signals from Dark Matter Annihilation*, Phys. Lett. **B664** (2008) 190, arXiv: 0709.3301 [astro-ph] (cit. on pp. 21, 83).

[147] M. Blennow, J. Edsjö and T. Ohlsson, *Neutrinos from WIMP annihilations using a full three-flavor Monte Carlo*, JCAP **0801** (2008) 021, arXiv: 0709.3898 [hep-ph] (cit. on pp. 21, 83).

[148] J. Liu, P.-f. Yin and S.-h. Zhu, *Neutrino Signals from Solar Neutralino Annihilations in Anomaly Mediated Supersymmetry Breaking Model*, Phys. Rev. **D77** (2008) 115014, arXiv: 0803.2164 [hep-ph] (cit. on pp. 21, 83).

[149] D. Hooper et al., *The New DAMA Dark-Matter Window and Energetic-Neutrino Searches*, Phys. Rev. **D79** (2009) 015010, arXiv: 0808.2464 [hep-ph] (cit. on pp. 21, 83).

[150] G. Wikström and J. Edsjö, *Limits on the WIMP-nucleon scattering cross-section from neutrino telescopes*, JCAP **0904** (2009) 009, arXiv: 0903.2986 [astro-ph.CO] (cit. on pp. 21, 83).

[151] S. Nussinov, L.-T. Wang and I. Yavin, *Capture of Inelastic Dark Matter in the Sun*, JCAP **0908** (2009) 037, arXiv: 0905.1333 [hep-ph] (cit. on pp. 21, 83).

[152] A. Menon et al., *Capture and Indirect Detection of Inelastic Dark Matter*, Phys. Rev. **D82** (2010) 015011, arXiv: 0905.1847 [hep-ph] (cit. on pp. 21, 83).

[153] M. R. Buckley et al., *High-Energy Neutrino Signatures of Dark Matter Decaying into Leptons*, Phys. Rev. **D81** (2010) 016006, arXiv: 0907.2385 [astro-ph.HE] (cit. on pp. 21, 83).

[154] A. R. Zentner, *High-Energy Neutrinos From Dark Matter Particle Self-Capture Within the Sun*, Phys. Rev. **D80** (2009) 063501, arXiv: 0907.3448 [astro-ph.HE] (cit. on pp. 21, 24, 83).

[155] J. Ellis et al., *Neutrino Fluxes from CMSSM LSP Annihilations in the Sun*, Phys. Rev. **D81** (2010) 085004, arXiv: 0912.3137 [hep-ph] (cit. on pp. 21, 83).

[156] A. Esmaili and Y. Farzan, *On the Oscillation of Neutrinos Produced by the Annihilation of Dark Matter inside the Sun*, Phys. Rev. **D81** (2010) 113010, arXiv: 0912.4033 [hep-ph] (cit. on pp. 21, 83).

[157] J. Ellis et al., *Neutrino Fluxes from NUHM LSP Annihilations in the Sun*, Phys. Rev. **D83** (2011) 085023, arXiv: 1102.1988 [hep-ph] (cit. on pp. 21, 83).

[158] N. F. Bell and K. Petraki, *Enhanced neutrino signals from dark matter annihilation in the Sun via metastable mediators*, JCAP **1104** (2011) 003, arXiv: 1102.2958 [hep-ph] (cit. on pp. 21, 83).

[159] R. Kappl and M. W. Winkler, *New limits on dark matter from Super-Kamiokande*, Nucl. Phys. **B850** (2011) 505, arXiv: 1104.0679 [hep-ph] (cit. on pp. 21, 83).

[160] S. K. Agarwalla et al., *Neutrino Probes of the Nature of Light Dark Matter*, JCAP **1109** (2011) 004, arXiv: 1105.4077 [hep-ph] (cit. on pp. 21, 83).

[161] S.-L. Chen and Y. Zhang, *Isospin-Violating Dark Matter and Neutrinos From the Sun*, Phys. Rev. **D84** (2011) 031301, arXiv: 1106.4044 [hep-ph] (cit. on pp. 21, 83).

[162] S. Kundu and P. Bhattacharjee, *Neutrinos from WIMP annihilation in the Sun : Implications of a self-consistent model of the Milky Way's dark matter halo*, Phys. Rev. **D85** (2012) 123533, arXiv: 1106.5711 [astro-ph.GA] (cit. on pp. 21, 44, 83).

[163] C. Rott, T. Tanaka and Y. Itow, *Enhanced sensitivity to dark matter self-annihilations in the Sun using neutrino spectral information*, JCAP **1109** (2011) 029, arXiv: 1107.3182 [astro-ph.HE] (cit. on pp. 21, 83).

[164] C. R. Das et al., *Determining the Dark Matter Mass with DeepCore*, Phys. Lett. **B725** (2013) 297, arXiv: 1110.5095 [hep-ph] (cit. on pp. 21, 83).

[165] J. Kumar et al., *Tools for Studying Low-Mass Dark Matter at Neutrino Detectors*, Phys. Rev. **D86** (2012) 073002, arXiv: 1204.5120 [hep-ph] (cit. on pp. 21, 39, 83).

[166] N. F. Bell, A. J. Brennan and T. D. Jacques, *Neutrino signals from electroweak bremsstrahlung in solar WIMP annihilation*, JCAP **1210** (2012) 045, arXiv: 1206.2977 [hep-ph] (cit. on pp. 21, 83).

[167] H. Silverwood et al., *Sensitivity of IceCube-DeepCore to neutralino dark matter in the MSSM-25*, JCAP **1303** (2013) 027, arXiv: 1210.0844 [hep-ph] (cit. on pp. 21, 83).

[168] M. Blennow, M. Carrigan and E. Fernández-Martinez, *Probing the Dark Matter mass and nature with neutrinos*, JCAP **1306** (2013) 038, arXiv: 1303.4530 [hep-ph] (cit. on pp. 21, 83).

[169] C. Arina, G. Bertone and H. Silverwood, *Complementarity of direct and indirect Dark Matter detection experiments*, Phys. Rev. **D88** (2013) 013002, arXiv: 1304.5119 [hep-ph] (cit. on pp. 21, 83).

[170] Z.-L. Liang and Y.-L. Wu, *Direct detection and solar capture of spin-dependent dark matter*, Phys. Rev. **D89** (2014) 013010, arXiv: 1308.5897 [hep-ph] (cit. on pp. 21, 39, 83).

[171] A. Ibarra, M. Totzauer and S. Wild, *High-energy neutrino signals from the Sun in dark matter scenarios with internal bremsstrahlung*, JCAP **1312** (2013) 043, arXiv: 1311.1418 [hep-ph] (cit. on pp. 21, 83).

[172] I. F. M. Albuquerque, C. Pérez de los Heros and D. S. Robertson, *Constraints on self interacting dark matter from IceCube results*, JCAP **1402** (2014) 047, arXiv: 1312.0797 [astro-ph.CO] (cit. on pp. 21, 83).

[173] P. Baratella et al., *PPPC 4 DMv: a Poor Particle Physicist Cookbook for Neutrinos from Dark Matter annihilations in the Sun*, JCAP **1403** (2014) 053, arXiv: 1312.6408 [hep-ph] (cit. on pp. 21, 83).

[174] W.-L. Guo, Z.-L. Liang and Y.-L. Wu, *Direct detection and solar capture of dark matter with momentum and velocity dependent elastic scattering*, Nucl. Phys. **B878** (2014) 295, arXiv: 1305.0912 [hep-ph] (cit. on pp. 21, 39, 83).

[175] A. Ibarra, M. Totzauer and S. Wild, *Higher order dark matter annihilations in the Sun and implications for IceCube*, JCAP **1404** (2014) 012, arXiv: 1402.4375 [hep-ph] (cit. on pp. 21, 83).

[176] C.-S. Chen et al., *Probing Dark Matter Self-Interaction in the Sun with IceCube-PINGU*, JCAP **1410** (2014) 049, arXiv: 1408.5471 [hep-ph] (cit. on pp. 21, 24, 83).

[177] J. Blumenthal et al., *Effective field theory interpretation of searches for dark matter annihilation in the Sun with the IceCube Neutrino Observatory*, Phys. Rev. **D91** (2015) 035002, arXiv: 1411.5917 [astro-ph.HE] (cit. on pp. 21, 83).

[178] R. Catena, *Dark matter signals at neutrino telescopes in effective theories*, JCAP **1504** (2015) 052, arXiv: 1503.04109 [hep-ph] (cit. on pp. 21, 83).

[179] J. Chen et al., *Long-range self-interacting dark matter in the Sun*, JCAP **1512** (2015) 021, arXiv: 1505.04031 [hep-ph] (cit. on pp. 21, 83).

[180] G. Bélanger et al., *Limits on dark matter proton scattering from neutrino telescopes using micrOMEGAs*, JCAP **1512** (2015) 036, arXiv: 1507.07987 [hep-ph] (cit. on pp. 21, 83).

[181] J. Heisig et al., *Constraints on Majorana Dark Matter from the LHC and IceCube*, Phys. Rev. **D93** (2016) 055029, arXiv: 1509.07867 [hep-ph] (cit. on pp. 21, 83).

[182] M. Danninger and C. Rott, *Solar WIMPs unravelled: Experiments, astrophysical uncertainties, and interactive tools*, Phys. Dark Univ. **5-6** (2014) 35, arXiv: 1509.08230 [astro-ph.HE] (cit. on pp. 21, 44, 83).

[183] M. Blennow, S. Clementz and J. Herrero-Garcia, *Pinning down inelastic dark matter in the Sun and in direct detection*, JCAP **1604** (2016) 004, arXiv: 1512.03317 [hep-ph] (cit. on pp. 21, 83).

[184] K. Murase and I. M. Shoemaker, *Detecting Asymmetric Dark Matter in the Sun with Neutrinos*, Phys. Rev. **D94** (2016) 063512, arXiv: 1606.03087 [hep-ph] (cit. on pp. 21, 83).

[185] J. Lopes and I. Lopes, *New Limits on Thermally annihilating Dark Matter from Neutrino Telescopes*, Astrophys. J. **827** (2016) 130, arXiv: 1607.08672 [astro-ph.CO] (cit. on pp. 21, 83).

[186] S. Baum et al., *Dark matter capture, subdominant WIMPs, and neutrino observatories*, Phys. Rev. **D95** (2017) 043007, arXiv: 1611.09665 [astro-ph.CO] (cit. on pp. 21, 83).

[187] R. Allahverdi et al., *Indirect Signals from Solar Dark Matter Annihilation to Long-lived Right-handed Neutrinos*, Phys. Rev. **D95** (2017) 075001, arXiv: 1612.03110 [hep-ph] (cit. on pp. 21, 83).

[188] C. Rott, J. Siegal-Gaskins and J. F. Beacom, *New Sensitivity to Solar WIMP Annihilation using Low-Energy Neutrinos*, Phys. Rev. **D88** (2013) 055005, arXiv: 1208.0827 [astro-ph.HE] (cit. on pp. 21, 83).

[189] N. Bernal, J. Martin-Albo and S. Palomares-Ruiz, *A novel way of constraining WIMPs annihilations in the Sun: MeV neutrinos*, JCAP **1308** (2013) 011, arXiv: 1208.0834 [hep-ph] (cit. on pp. 21, 36, 44, 61, 83).

[190] C. Rott et al., *Dark Matter Searches for Monoenergetic Neutrinos Arising from Stopped Meson Decay in the Sun*, JCAP **1511** (2015) 039, arXiv: 1510.00170 [hep-ph] (cit. on pp. 21, 83).

[191] C. Rott et al., *Directional Searches at DUNE for Sub-GeV Monoenergetic Neutrinos Arising from Dark Matter Annihilation in the Sun*, JCAP **1701** (2017) 016, arXiv: 1609.04876 [hep-ph] (cit. on pp. 21, 83).

[192] S. Desai et al., *Search for dark matter WIMPs using upward through-going muons in Super-Kamiokande*, Phys. Rev. **D70** (2004) 083523, [Erratum: Phys. Rev.D70,109901(2004)], arXiv: hep-ex/0404025 [hep-ex] (cit. on pp. 21, 83).

[193] S. Desai et al., *Study of TeV neutrinos with upward showering muons in Super-Kamiokande*, Astropart. Phys. **29** (2008) 42, arXiv: 0711.0053 [hep-ex] (cit. on pp. 21, 83).

[194] R. Abbasi et al., *Limits on a muon flux from neutralino annihilations in the Sun with the IceCube 22-string detector*, Phys. Rev. Lett. **102** (2009) 201302, arXiv: 0902.2460 [astro-ph.CO] (cit. on pp. 21, 83).

[195] R. Abbasi et al., *Limits on a muon flux from Kaluza-Klein dark matter annihilations in the Sun from the IceCube 22-string detector*, Phys. Rev. **D81** (2010) 057101, arXiv: 0910.4480 [astro-ph.CO] (cit. on pp. 21, 83).

[196] T. Tanaka et al., *An indirect search for WIMPs in the Sun using 3109.6 days of upward-going muons in Super-Kamiokande*, Astrophys. J. **742** (2011) 78, arXiv: 1108.3384 [astro-ph.HE] (cit. on pp. 21, 83).

[197] R. Abbasi et al., *Multi-year search for dark matter annihilations in the Sun with the AMANDA-II and IceCube detectors*, Phys. Rev. **D85** (2012) 042002, arXiv: 1112.1840 [astro-ph.HE] (cit. on pp. 21, 83).

[198] P. Scott et al., *Use of event-level neutrino telescope data in global fits for theories of new physics*, JCAP **1211** (2012) 057, arXiv: 1207.0810 [hep-ph] (cit. on pp. 21, 83).

[199] M. G. Aartsen et al., *Search for dark matter annihilations in the Sun with the 79-string IceCube detector*, Phys. Rev. Lett. **110** (2013) 131302, arXiv: 1212.4097 [astro-ph.HE] (cit. on pp. 21, 83).

[200] S. Adrián-Martinez et al., *First results on dark matter annihilation in the Sun using the ANTARES neutrino telescope*, JCAP **1311** (2013) 032, arXiv: 1302.6516 [astro-ph.HE] (cit. on pp. 21, 83).

[201] A. D. Avrorin et al., *Search for neutrino emission from relic dark matter in the Sun with the Baikal NT200 detector*, Astropart. Phys. **62** (2015) 12, arXiv: 1405.3551 [astro-ph.HE] (cit. on pp. 21, 83).

[202] K. Choi et al., *Search for neutrinos from annihilation of captured low-mass dark matter particles in the Sun by Super-Kamiokande*, Phys. Rev. Lett. **114** (2015) 141301, arXiv: 1503.04858 [hep-ex] (cit. on pp. 21, 83).

[203] M. G. Aartsen et al., *Improved limits on dark matter annihilation in the Sun with the 79-string IceCube detector and implications for supersymmetry*, JCAP **1604** (2016) 022, arXiv: 1601.00653 [hep-ph] (cit. on pp. 21, 83).

[204] S. Adrián-Martinez et al., *A search for Secluded Dark Matter in the Sun with the ANTARES neutrino telescope*, JCAP **1605** (2016) 016, arXiv: 1602.07000 [hep-ex] (cit. on pp. 21, 83).

[205] M. G. Aartsen et al.,
Search for annihilating dark matter in the Sun with 3 years of IceCube data,
Eur. Phys. J. **C77** (2017) 146, arXiv: 1612.05949 [astro-ph.HE] (cit. on pp. 21, 83).

[206] D. B. Kaplan, *A Single explanation for both the baryon and dark matter densities*,
Phys. Rev. Lett. **68** (1992) 741 (cit. on p. 23).

[207] D. E. Kaplan, M. A. Luty and K. M. Zurek, *Asymmetric Dark Matter*,
Phys. Rev. **D79** (2009) 115016, arXiv: 0901.4117 [hep-ph] (cit. on p. 23).

[208] T. Cohen et al., *Asymmetric Dark Matter from a GeV Hidden Sector*,
Phys. Rev. **D82** (2010) 056001, arXiv: 1005.1655 [hep-ph] (cit. on p. 23).

[209] M. T. Frandsen, S. Sarkar and K. Schmidt-Hoberg,
Light asymmetric dark matter from new strong dynamics, Phys. Rev. **D84** (2011) 051703,
arXiv: 1103.4350 [hep-ph] (cit. on p. 23).

[210] T. Cohen and K. M. Zurek, *Leptophilic Dark Matter from the Lepton Asymmetry*,
Phys. Rev. Lett. **104** (2010) 101301, arXiv: 0909.2035 [hep-ph] (cit. on pp. 23, 39).

[211] A. C. Vincent, P. Scott and A. Serenelli,
Possible Indication of Momentum-Dependent Asymmetric Dark Matter in the Sun,
Phys. Rev. Lett. **114** (2015) 081302, arXiv: 1411.6626 [hep-ph] (cit. on pp. 24, 39).

[212] P. Scott, M. Fairbairn and J. Edsjö, *Dark stars at the galactic centre - the main sequence*,
Mon. Not. Roy. Astron. Soc. **394** (2009) 82, arXiv: 0809.1871 [astro-ph]
(cit. on pp. 24, 57).

[213] J. Fan, M. Reece and L.-T. Wang,
Non-relativistic effective theory of dark matter direct detection, JCAP **1011** (2010) 042,
arXiv: 1008.1591 [hep-ph] (cit. on pp. 25, 39, 71, 83).

[214] A. L. Fitzpatrick et al., *The Effective Field Theory of Dark Matter Direct Detection*,
JCAP **1302** (2013) 004, arXiv: 1203.3542 [hep-ph] (cit. on pp. 25, 39, 83).

[215] N. Anand, A. L. Fitzpatrick and W. C. Haxton,
Weakly interacting massive particle-nucleus elastic scattering response,
Phys. Rev. **C89** (2014) 065501, arXiv: 1308.6288 [hep-ph] (cit. on pp. 25, 39, 43, 83).

[216] R. J. Hill and M. P. Solon, *WIMP-nucleon scattering with heavy WIMP effective theory*,
Phys. Rev. Lett. **112** (2014) 211602, arXiv: 1309.4092 [hep-ph]
(cit. on pp. 25, 39, 83).

[217] M. I. Gresham and K. M. Zurek,
Effect of nuclear response functions in dark matter direct detection,
Phys. Rev. **D89** (2014) 123521, arXiv: 1401.3739 [hep-ph] (cit. on pp. 25, 39, 83).

[218] P. Panci, *New Directions in Direct Dark Matter Searches*,
Adv. High Energy Phys. **2014** (2014) 681312, arXiv: 1402.1507 [hep-ph]
(cit. on pp. 25, 39, 83).

[219] R. Catena, *Prospects for direct detection of dark matter in an effective theory approach*,
JCAP **1407** (2014) 055, arXiv: 1406.0524 [hep-ph] (cit. on pp. 25, 39, 83).

[220] V. Gluscevic and A. H. G. Peter,
Understanding WIMP-baryon interactions with direct detection: A Roadmap,
JCAP **1409** (2014) 040, arXiv: 1406.7008 [astro-ph.CO] (cit. on pp. 25, 39, 83).

[221] R. Catena, *Analysis of the theoretical bias in dark matter direct detection*,
JCAP **1409** (2014) 049, arXiv: 1407.0127 [hep-ph] (cit. on pp. 25, 39, 83).

[222] V. Gluscevic et al., *Identifying the Theory of Dark Matter with Direct Detection*,
JCAP **1512** (2015) 057, arXiv: 1506.04454 [hep-ph] (cit. on pp. 25, 39, 83).

[223] J. B. Dent et al., *General analysis of direct dark matter detection: From microphysics to observational signatures*, Phys. Rev. **D92** (2015) 063515, arXiv: 1505.03117 [hep-ph] (cit. on pp. 25, 39, 83).

[224] R. Catena, *Dark matter directional detection in non-relativistic effective theories*, JCAP **1507** (2015) 026, arXiv: 1505.06441 [hep-ph] (cit. on pp. 25, 39, 83).

[225] B. J. Kavanagh, *New directional signatures from the nonrelativistic effective field theory of dark matter*, Phys. Rev. **D92** (2015) 023513, arXiv: 1505.07406 [hep-ph] (cit. on pp. 25, 39, 83).

[226] R. Catena and B. Schwabe, *Form factors for dark matter capture by the Sun in effective theories*, JCAP **1504** (2015) 042, arXiv: 1501.03729 [hep-ph] (cit. on pp. 25, 39, 43, 83).

[227] D. Gazda, R. Catena and C. Forssén, *Ab initio nuclear response functions for dark matter searches*, (2016), arXiv: 1612.09165 [hep-ph] (cit. on pp. 25, 39, 43, 83).

[228] J. Kopp et al., *DAMA/LIBRA and leptonically interacting Dark Matter*, Phys. Rev. **D80** (2009) 083502, arXiv: 0907.3159 [hep-ph] (cit. on pp. 26, 39, 45, 74, 75, 83, 84).

[229] A. Gould and G. Raffelt, *Thermal conduction by massive particles*, Astrophys. J. **352** (1990) 654 (cit. on pp. 26, 56, 57).

[230] A. Gould and G. Raffelt, *Cosmion Energy Transfer in Stars: The Knudsen Limit*, Astrophys. J. **352** (1990) 669 (cit. on pp. 31, 54, 55).

[231] Z.-L. Liang et al., *On the evaporation of solar dark matter: spin-independent effective operators*, JCAP **1609** (2016) 018, arXiv: 1606.02157 [hep-ph] (cit. on pp. 31, 54, 55).

[232] A. Gould, *Evaporation of WIMPs with arbitrary cross sections*, Astrophys. J. **356** (1990) 302 (cit. on pp. 35, 36, 57, 58, 61, 84).

[233] W. H. Press et al., *Numerical Recipes in FORTRAN: The Art of Scientific Computing*, (1992) (cit. on p. 37).

[234] R. Bernabei et al., *Investigating electron interacting dark matter*, Phys. Rev. **D77** (2008) 023506, arXiv: 0712.0562 [astro-ph] (cit. on p. 39).

[235] A. Dedes et al., *Searching for Secluded Dark Matter via Direct Detection of Recoiling Nuclei as well as Low Energy Electrons*, Nucl. Phys. **B826** (2010) 148, arXiv: 0907.0758 [hep-ph] (cit. on p. 39).

[236] B. Feldstein, P. W. Graham and S. Rajendran, *Luminous Dark Matter*, Phys. Rev. **D82** (2010) 075019, arXiv: 1008.1988 [hep-ph] (cit. on p. 39).

[237] S. Chang et al., *Leptophilic Effective WIMPs*, Phys. Rev. **D90** (2014) 015011, arXiv: 1402.7358 [hep-ph] (cit. on p. 39).

[238] N. F. Bell et al., *Leptophilic dark matter with Z prime interactions*, Phys. Rev. **D90** (2014) 035027, arXiv: 1407.3001 [hep-ph] (cit. on p. 39).

[239] R. Foot, *Can dark matter - electron scattering explain the DAMA annual modulation signal?*, Phys. Rev. **D90** (2014) 121302, arXiv: 1407.4213 [hep-ph] (cit. on p. 39).

[240] B. M. Roberts et al., *Dark matter scattering on electrons: Accurate calculations of atomic excitations and implications for the DAMA signal*, Phys. Rev. **D93** (2016) 115037, arXiv: 1604.04559 [hep-ph] (cit. on p. 39).

[241] M. Felizardo et al., *Final Analysis and Results of the Phase II SIMPLE Dark Matter Search*, Phys. Rev. Lett. **108** (2012) 201302, arXiv: 1106.3014 [astro-ph.CO] (cit. on pp. 39, 85).

[242] K. Abe et al., *Direct dark matter search by annual modulation in XMASS-I*, Phys. Lett. **B759** (2016) 272, arXiv: 1511.04807 [astro-ph.CO] (cit. on pp. 39, 85).

[243] C. Amole et al., *Improved dark matter search results from PICO-2L Run 2*, Phys. Rev. **D93** (2016) 061101, arXiv: 1601.03729 [astro-ph.CO] (cit. on pp. 39, 85).

[244] E. Aprile et al., *Low-mass dark matter search using ionization signals in XENON100*, Phys. Rev. **D94** (2016) 092001, arXiv: 1605.06262 [astro-ph.CO] (cit. on pp. 39, 85).

[245] E. Aprile et al., *Search for Electronic Recoil Event Rate Modulation with 4 Years of XENON100 Data*, Phys. Rev. Lett. **118** (2017) 101101, arXiv: 1701.00769 [astro-ph.CO] (cit. on pp. 39, 85).

[246] R. Essig, J. Mardon and T. Volansky, *Direct Detection of Sub-GeV Dark Matter*, Phys. Rev. **D85** (2012) 076007, arXiv: 1108.5383 [hep-ph] (cit. on p. 39).

[247] J.-W. Chen et al., *Electronic and nuclear contributions in sub-GeV dark matter scattering: A case study with hydrogen*, Phys. Rev. **D92** (2015) 096013, arXiv: 1508.03508 [hep-ph] (cit. on p. 39).

[248] S. K. Lee et al., *Modulation Effects in Dark Matter-Electron Scattering Experiments*, Phys. Rev. **D92** (2015) 083517, arXiv: 1508.07361 [hep-ph] (cit. on p. 39).

[249] P. J. Fox and E. Poppitz, *Leptophilic Dark Matter*, Phys. Rev. **D79** (2009) 083528, arXiv: 0811.0399 [hep-ph] (cit. on p. 39).

[250] Q.-H. Cao, E. Ma and G. Shaughnessy, *Dark Matter: The Leptonic Connection*, Phys. Lett. **B673** (2009) 152, arXiv: 0901.1334 [hep-ph] (cit. on p. 39).

[251] X.-J. Bi, X.-G. He and Q. Yuan, *Parameters in a class of leptophilic models from PAMELA, ATIC and FERMI*, Phys. Lett. **B678** (2009) 168, arXiv: 0903.0122 [hep-ph] (cit. on p. 39).

[252] A. Ibarra et al., *Cosmic Rays from Leptophilic Dark Matter Decay via Kinetic Mixing*, JCAP **0908** (2009) 017, arXiv: 0903.3625 [hep-ph] (cit. on p. 39).

[253] L. A. Cavasonza et al., *Constraints on leptophilic dark matter from the AMS-02 experiment*, (2016), arXiv: 1612.06634 [hep-ph] (cit. on p. 39).

[254] J. Chang et al., *An excess of cosmic ray electrons at energies of 300-800 GeV*, Nature **456** (2008) 362 (cit. on p. 39).

[255] O. Adriani et al., *PAMELA results on the cosmic-ray antiproton flux from 60 MeV to 180 GeV in kinetic energy*, Phys. Rev. Lett. **105** (2010) 121101, arXiv: 1007.0821 [astro-ph.HE] (cit. on p. 39).

[256] M. Ackermann et al., *Measurement of separate cosmic-ray electron and positron spectra with the Fermi Large Area Telescope*, Phys. Rev. Lett. **108** (2012) 011103, arXiv: 1109.0521 [astro-ph.HE] (cit. on p. 39).

[257] L. Accardo et al., *High Statistics Measurement of the Positron Fraction in Primary Cosmic Rays of 0.5–500 GeV with the Alpha Magnetic Spectrometer on the International Space Station*, Phys. Rev. Lett. **113** (2014) 121101 (cit. on p. 39).

[258] M. Aguilar et al., *Antiproton Flux, Antiproton-to-Proton Flux Ratio, and Properties of Elementary Particle Fluxes in Primary Cosmic Rays Measured with the Alpha Magnetic Spectrometer on the International Space Station*, Phys. Rev. Lett. **117** (2016) 091103 (cit. on p. 39).

[259] P. Agrawal, Z. Chacko and C. B. Verhaaren, *Leptophilic Dark Matter and the Anomalous Magnetic Moment of the Muon*, JHEP **08** (2014) 147, arXiv: 1402.7369 [hep-ph] (cit. on p. 39).

[260] F. D'Eramo, B. J. Kavanagh and P. Panci, *Probing Leptophilic Dark Sectors with Hadronic Processes*, (2017), arXiv: 1702.00016 [hep-ph] (cit. on p. 39).

[261] I. Lopes, K. Kadota and J. Silk, *Constraint on Light Dipole Dark Matter from Helioseismology*, Astrophys. J. Lett. **780** (2014) L15, arXiv: 1310.0673 [astro-ph.SR] (cit. on p. 39).

[262] A. C. Vincent and P. Scott, *Thermal conduction by dark matter with velocity and momentum-dependent cross-sections*, JCAP **1404** (2014) 019, arXiv: 1311.2074 [astro-ph.CO] (cit. on pp. 39, 57).

[263] I. Lopes, P. Panci and J. Silk, *Helioseismology with long range dark matter-baryon interactions*, Astrophys. J. **795** (2014) 162, arXiv: 1402.0682 [astro-ph.SR] (cit. on p. 39).

[264] A. C. Vincent, A. Serenelli and P. Scott, *Generalised form factor dark matter in the Sun*, JCAP **1508** (2015) 040, arXiv: 1504.04378 [hep-ph] (cit. on pp. 39, 57).

[265] A. C. Vincent, P. Scott and A. Serenelli, *Updated constraints on velocity and momentum-dependent asymmetric dark matter*, JCAP **1611** (2016) 007, arXiv: 1605.06502 [hep-ph] (cit. on p. 39).

[266] E. Massó, S. Mohanty and S. Rao, *Dipolar Dark Matter*, Phys. Rev. **D80** (2009) 036009, arXiv: 0906.1979 [hep-ph] (cit. on p. 39).

[267] S. Chang, A. Pierce and N. Weiner, *Momentum Dependent Dark Matter Scattering*, JCAP **1001** (2010) 006, arXiv: 0908.3192 [hep-ph] (cit. on p. 39).

[268] S. Chang, N. Weiner and I. Yavin, *Magnetic Inelastic Dark Matter*, Phys. Rev. **D82** (2010) 125011, arXiv: 1007.4200 [hep-ph] (cit. on p. 39).

[269] V. Barger, W.-Y. Keung and D. Marfatia, *Electromagnetic properties of dark matter: Dipole moments and charge form factor*, Phys. Lett. **B696** (2011) 74, arXiv: 1007.4345 [hep-ph] (cit. on pp. 39, 71).

[270] A. L. Fitzpatrick and K. M. Zurek, *Dark Moments and the DAMA-CoGeNT Puzzle*, Phys. Rev. **D82** (2010) 075004, arXiv: 1007.5325 [hep-ph] (cit. on p. 39).

[271] R. Foot, *Mirror and hidden sector dark matter in the light of new CoGeNT data*, Phys. Lett. **B703** (2011) 7, arXiv: 1106.2688 [hep-ph] (cit. on p. 39).

[272] T. Schwetz and J. Zupan, *Dark Matter attempts for CoGeNT and DAMA*, JCAP **1108** (2011) 008, arXiv: 1106.6241 [hep-ph] (cit. on p. 39).

[273] M. Farina et al., *Can CoGeNT and DAMA Modulations Be Due to Dark Matter?*, JCAP **1111** (2011) 010, arXiv: 1107.0715 [hep-ph] (cit. on p. 39).

[274] N. Fornengo, P. Panci and M. Regis, *Long-Range Forces in Direct Dark Matter Searches*, Phys. Rev. **D84** (2011) 115002, arXiv: 1108.4661 [hep-ph] (cit. on p. 39).

[275] E. Del Nobile et al., *Light Magnetic Dark Matter in Direct Detection Searches*, JCAP **1208** (2012) 010, arXiv: 1203.6652 [hep-ph] (cit. on p. 39).

[276] R. Foot, *Hidden sector dark matter explains the DAMA, CoGeNT, CRESST-II and CDMS/Si experiments*, Phys. Rev. **D88** (2013) 025032, arXiv: 1209.5602 [hep-ph] (cit. on p. 39).

[277] A. L. Fitzpatrick et al., *Model Independent Direct Detection Analyses*, (2012), arXiv: 1211.2818 [hep-ph] (cit. on p. 39).

[278] R. Catena and P. Gondolo, *Global fits of the dark matter-nucleon effective interactions*, JCAP **1409** (2014) 045, arXiv: 1405.2637 [hep-ph] (cit. on p. 39).

[279] G. Barello, S. Chang and C. A. Newby, *A Model Independent Approach to Inelastic Dark Matter Scattering*, Phys. Rev. **D90** (2014) 094027, arXiv: 1409.0536 [hep-ph] (cit. on p. 39).

[280] R. Catena and P. Gondolo, *Global limits and interference patterns in dark matter direct detection*, JCAP **1508** (2015) 022, arXiv: 1504.06554 [hep-ph] (cit. on p. 39).

[281] R. Catena, A. Ibarra and S. Wild, *DAMA confronts null searches in the effective theory of dark matter-nucleon interactions*, JCAP **1605** (2016) 039, arXiv: 1602.04074 [hep-ph] (cit. on p. 39).

[282] H. Rogers et al., *Multi-Dimensional Effective Field Theory Analysis for Direct Detection of Dark Matter*, (2016), arXiv: 1612.09038 [astro-ph.CO] (cit. on p. 39).

[283] J. Bovy and S. Tremaine, *On the local dark matter density*, Astrophys. J. **756** (2012) 89, arXiv: 1205.4033 [astro-ph.GA] (cit. on p. 40).

[284] R. Catena and P. Ullio, *A novel determination of the local dark matter density*, JCAP **1008** (2010) 004, arXiv: 0907.0018 [astro-ph.CO] (cit. on p. 40).

[285] J. Silk et al., *Particle Dark Matter: Observations, Models and Searches*, ed. by G. Bertone, Cambridge Univ. Press, 2010, ISBN: 9781107653924, URL: http://www.cambridge.org/uk/catalogue/catalogue.asp?isbn=9780521763684 (cit. on pp. 40, 83).

[286] N. Bernal et al., *Systematic uncertainties from halo asphericity in dark matter searches*, JCAP **1409** (2014) 004, arXiv: 1405.6240 [astro-ph.CO] (cit. on p. 40).

[287] M. Benito et al., *Particle Dark Matter Constraints: the Effect of Galactic Uncertainties*, JCAP **1702** (2017) 007, arXiv: 1612.02010 [hep-ph] (cit. on p. 40).

[288] N. Bozorgnia and G. Bertone, *Implications of hydrodynamical simulations for the interpretation of direct dark matter searches*, (2017), arXiv: 1705.05853 [astro-ph.CO] (cit. on pp. 40, 41).

[289] L. Wang et al., *NIHAO project – I. Reproducing the inefficiency of galaxy formation across cosmic time with a large sample of cosmological hydrodynamical simulations*, Mon. Not. Roy. Astron. Soc. **454** (2015) 83, arXiv: 1503.04818 [astro-ph.GA] (cit. on p. 40).

[290] J. Schaye et al., *The EAGLE project: Simulating the evolution and assembly of galaxies and their environments*, Mon. Not. Roy. Astron. Soc. **446** (2015) 521, arXiv: 1407.7040 [astro-ph.GA] (cit. on p. 40).

[291] G. Stinson et al., *Making Galaxies in a Cosmological Context: The Need for Early Stellar Feedback*, Mon. Not. Roy. Astron. Soc. **428** (2013) 129, arXiv: 1208.0002 [astro-ph.CO] (cit. on p. 40).

[292] J. D. Sloane et al., *Assessing Astrophysical Uncertainties in Direct Detection with Galaxy Simulations*, Astrophys. J. **831** (2016) 93, arXiv: 1601.05402 [astro-ph.GA] (cit. on p. 40).

[293] K. Choi, C. Rott and Y. Itow, *Impact of the dark matter velocity distribution on capture rates in the Sun*, JCAP **1405** (2014) 049, arXiv: 1312.0273 [astro-ph.HE] (cit. on pp. 41, 44).

[294] J. R. Ellis and R. Flores,
Realistic predictions for the detection of supersymmetric dark matter,
Nucl. Phys. **B307** (1988) 883 (cit. on p. 42).

[295] A. F. Pacheco and D. Strottman, *Nuclear Structure Corrections to Estimates of the Spin Dependent WIMP Nucleus Cross-section*, Phys. Rev. **D40** (1989) 2131 (cit. on p. 42).

[296] J. Engel, S. Pittel and P. Vogel, *Nuclear physics of dark matter detection*,
Int. J. Mod. Phys. **E1** (1992) 1 (cit. on pp. 42, 43).

[297] P. Divari et al.,
Shell model calculations for light supersymmetric particle scattering off light nuclei,
Phys. Rev. **C61** (2000) 054612 (cit. on p. 42).

[298] V. A. Bednyakov and F. Simkovic,
Nuclear spin structure in dark matter search: The Zero momentum transfer limit,
Phys. Part. Nucl. **36** (2005) 131, [Fiz. Elem. Chast. Atom. Yadra 36,257(2005)],
arXiv: hep-ph/0406218 [hep-ph] (cit. on p. 42).

[299] A. M. Serenelli, W. Haxton and C. Peña-Garay,
Solar models with accretion. I. Application to the solar abundance problem,
Astrophys. J. **743** (2011) 24, arXiv: 1104.1639 [astro-ph.SR] (cit. on p. 43).

[300] N. Vinyoles et al., *A new Generation of Standard Solar Models*,
Astrophys. J. **835** (2017) 202, arXiv: 1611.09867 [astro-ph.SR] (cit. on p. 43).

[301] G. Eder, *Nuclear forces*, Chapter 7, MIT Press, 1968 (cit. on p. 43).

[302] J. Engel, *Nuclear form-factors for the scattering of weakly interacting massive particles*,
Phys. Lett. **B264** (1991) 114 (cit. on p. 43).

[303] G. Bélanger et al.,
Dark matter direct detection rate in a generic model with micrOMEGAs 2.2,
Comput. Phys. Commun. **180** (2009) 747, arXiv: 0803.2360 [hep-ph] (cit. on p. 43).

[304] T. Piffl et al., *The RAVE survey: the Galactic escape speed and the mass of the Milky Way*,
Astron. Astrophys. **562** (2014) A91, arXiv: 1309.4293 [astro-ph.GA] (cit. on p. 44).

[305] A. Gould, *Direct and Indirect Capture of Wimps by the Earth*,
Astrophys. J. **328** (1988) 919 (cit. on p. 44).

[306] A. Gould, *Gravitational diffusion of Solar System WIMPs*, Astrophys. J. **368** (1991) 610 (cit. on p. 44).

[307] T. Damour and L. M. Krauss, *A New solar system population of WIMP dark matter*,
Phys. Rev. Lett. **81** (1998) 5726, arXiv: astro-ph/9806165 [astro-ph] (cit. on p. 44).

[308] T. Damour and L. M. Krauss,
A New WIMP population in the solar system and new signals for dark matter detectors,
Phys. Rev. **D59** (1999) 063509, arXiv: astro-ph/9807099 [astro-ph] (cit. on p. 44).

[309] A. Gould and S. M. Khairul Alam, *Can heavy WIMPs be captured by the earth?*,
Astrophys. J. **549** (2001) 72, arXiv: astro-ph/9911288 [astro-ph] (cit. on p. 44).

[310] J. Lundberg and J. Edsjö, *WIMP diffusion in the solar system including solar depletion and its effect on earth capture rates*, Phys. Rev. **D69** (2004) 123505,
arXiv: astro-ph/0401113 [astro-ph] (cit. on p. 44).

[311] A. H. G. Peter, *Dark matter in the solar system I: The distribution function of WIMPs at the Earth from solar capture*, Phys. Rev. **D79** (2009) 103531,
arXiv: 0902.1344 [astro-ph.HE] (cit. on p. 44).

[312] A. H. G. Peter, *Dark matter in the solar system III: The distribution function of WIMPs at the Earth from gravitational capture*, Phys. Rev. **D79** (2009) 103533,
arXiv: 0902.1348 [astro-ph.HE] (cit. on p. 44).

[313] A. H. G. Peter, *Dark matter in the solar system II: WIMP annihilation rates in the Sun*, Phys. Rev. **D79** (2009) 103532, arXiv: 0902.1347 [astro-ph.HE] (cit. on p. 44).

[314] S. Sivertsson and J. Edsjö, *WIMP diffusion in the solar system including solar WIMP-nucleon scattering*, Phys. Rev. **D85** (2012) 123514, arXiv: 1201.1895 [astro-ph.HE] (cit. on p. 44).

[315] A. Bottino et al., *Does solar physics provide constraints to weakly interacting massive particles?*, Phys. Rev. **D66** (2002) 053005, arXiv: hep-ph/0206211 [hep-ph] (cit. on pp. 44, 57).

[316] R. L. Gilliland et al., *Solar models with energy transport by weakly interacting particles*, Astrophys. J. **306** (1986) 703 (cit. on pp. 55, 84).

[317] M. Nauenberg, *Energy transport and evaporation of weakly interacting particles in the Sun*, Phys. Rev. **D36** (1987) 1080 (cit. on pp. 55, 56, 84).

[318] C. Kouvaris, *Probing Light Dark Matter via Evaporation from the Sun*, Phys. Rev. **D92** (2015) 075001, arXiv: 1506.04316 [hep-ph] (cit. on p. 61).

[319] G. Busoni, A. De Simone and W.-C. Huang, *On the Minimum Dark Matter Mass Testable by Neutrinos from the Sun*, JCAP **1307** (2013) 010, arXiv: 1305.1817 [hep-ph] (cit. on p. 61).

[320] G. Busoni et al., *Evaporation and scattering of momentum- and velocity-dependent dark matter in the Sun*, (2017), arXiv: 1703.07784 [hep-ph] (cit. on p. 63).

[321] G. Angloher et al., *Results from 730 kg days of the CRESST-II Dark Matter Search*, Eur. Phys. J. **C72** (2012) 1971, arXiv: 1109.0702 [astro-ph.CO] (cit. on p. 71).

[322] F. Aharonian et al., *The energy spectrum of cosmic-ray electrons at TeV energies*, Phys. Rev. Lett. **101** (2008) 261104, arXiv: 0811.3894 [astro-ph] (cit. on p. 71).

[323] F. Aharonian et al., *Probing the ATIC peak in the cosmic-ray electron spectrum with H.E.S.S*, Astron. Astrophys. **508** (2009) 561, arXiv: 0905.0105 [astro-ph.HE] (cit. on p. 71).

[324] T. Bringmann et al., *Fermi LAT Search for Internal Bremsstrahlung Signatures from Dark Matter Annihilation*, JCAP **1207** (2012) 054, arXiv: 1203.1312 [hep-ph] (cit. on p. 71).

[325] J. Kumar and D. Marfatia, *Matrix element analyses of dark matter scattering and annihilation*, Phys. Rev. **D88** (2013) 014035, arXiv: 1305.1611 [hep-ph] (cit. on pp. 71, 72).

[326] P. Agrawal et al., *A Classification of Dark Matter Candidates with Primarily Spin-Dependent Interactions with Matter*, (2010), arXiv: 1003.1912 [hep-ph] (cit. on p. 71).

[327] A. De Simone and T. Jacques, *Simplified models vs. effective field theory approaches in dark matter searches*, Eur. Phys. J. **C76** (2016) 367, arXiv: 1603.08002 [hep-ph] (cit. on pp. 71, 72).

[328] C. El Aisati et al., *Prospects for discovering a neutrino line induced by dark matter annihilation*, (2017), arXiv: 1706.06600 [hep-ph] (cit. on p. 72).

[329] V. Shtabovenko, R. Mertig and F. Orellana, *New Developments in FeynCalc 9.0*, Comput. Phys. Commun. **207** (2016) 432, arXiv: 1601.01167 [hep-ph] (cit. on p. 75).

[330] H. H. Patel,
Package-X 2.0: A Mathematica package for the analytic calculation of one-loop integrals,
Comput. Phys. Commun. **218** (2017) 66, arXiv: 1612.00009 [hep-ph] (cit. on p. 75).

[331] T. Hahn and M. Rauch, *News from FormCalc and LoopTools*,
Nucl. Phys. Proc. Suppl. **157** (2006) 236, [,236(2006)],
arXiv: hep-ph/0601248 [hep-ph] (cit. on p. 75).

[332] V. A. Smirnov, *Evaluating multiloop Feynman integrals by Mellin-Barnes representation*,
Nucl. Phys. Proc. Suppl. **135** (2004) 252, [,252(2004)],
arXiv: hep-ph/0406052 [hep-ph] (cit. on p. 75).

[333] A. V. Smirnov and V. A. Smirnov,
On the Resolution of Singularities of Multiple Mellin-Barnes Integrals,
Eur. Phys. J. **C62** (2009) 445, arXiv: 0901.0386 [hep-ph] (cit. on p. 75).

[334] J. Gluza, K. Kajda and T. Riemann, *AMBRE: A Mathematica package for the construction of Mellin-Barnes representations for Feynman integrals*,
Comput. Phys. Commun. **177** (2007) 879, arXiv: 0704.2423 [hep-ph] (cit. on p. 75).

[335] M. Czakon, *Automatized analytic continuation of Mellin-Barnes integrals*,
Comput. Phys. Commun. **175** (2006) 559, arXiv: hep-ph/0511200 [hep-ph]
(cit. on p. 75).

[336] M. Ochman and T. Riemann, *MBsums - a Mathematica package for the representation of Mellin-Barnes integrals by multiple sums*, Acta Phys. Polon. **B46** (2015) 2117,
arXiv: 1511.01323 [hep-ph] (cit. on p. 75).

[337] A. I. Vainshtein, V. I. Zakharov and M. A. Shifman, *Higgs Particles*,
Sov. Phys. Usp. **23** (1980) 429, [Usp. Fiz. Nauk131,537(1980)] (cit. on p. 75).

[338] N. Weiner and I. Yavin,
How Dark Are Majorana WIMPs? Signals from MiDM and Rayleigh Dark Matter,
Phys. Rev. **D86** (2012) 075021, arXiv: 1206.2910 [hep-ph] (cit. on p. 76).

[339] G. Jungman, M. Kamionkowski and K. Griest, *Supersymmetric dark matter*,
Phys. Rept. **267** (1996) 195, arXiv: hep-ph/9506380 [hep-ph] (cit. on p. 78).

List of Figures

List of Tables

List of Publications

1. “Phenomenology of WIMP Dark Matter interactions with electrons in the Sun”
   R. Garani and S. Palomares-Ruiz
   [*Work in preparation.*]

2. “Dark matter in the Sun: scattering off electrons vs nucleons”
   R. Garani and S. Palomares-Ruiz
   JCAP **1705** (2017) no.05, 007

3. “Sgoldstino searches at the LHC”
   M. Asano and R. Garani
   arXiv:1701.00829 [hep-ph].
   [*Submitted to PRD*]

4. “Systematic Uncertainties in Dark Matter Searches due to Halo Asphericity”
   N. Bernal, J. E. Forero-Romero, R. Garani and S. Palomares-Ruiz
   JCAP **1409** (2014) 004

5. “SuSeFLAV : A program for calculating supersymmetric spectra and lepton flavor violation”
   D. Chowdhury, R. Garani and S. K. Vempati
   Comput. Phys. Commun. **184**, 899 (2013)

6. “Flavored Co-annihilations”
   D. Chowdhury, R. Garani and S. K. Vempati
   JHEP **1206**, 014 (2012)